The Spatial Scaling Behaviour of Extreme Precipitation in an Atmospheric General Circulation Model and in Observational Data

D I P L O M A R B E I T

zur Erlangung des Grades
einer Diplom-Geoökologin
vorgelegt von:

Claudia Daniela Volosciuk

13. Februar 2012

Erstprüfer: Prof. Dr. Otto Richter, TU Braunschweig
Zweitprüfer: Prof. Dr. Douglas Maraun, GEOMAR Kiel

Technische Universität Braunschweig
Institut für Geoökologie
Abteilung für Umweltsystemanalyse

Eidesstattliche Erklärung

Ich erkläre eidesstattlich, dass ich diese Arbeit selbstständig angefertigt und die benutzten Quellen und Hilfsmittel sowie befragte Personen vollständig angegeben habe.

Braunschweig, 13. Februar 2012

Claudia Daniela Volosciuk

Abstract

Present-day simulations with the same boundary forcing but different resolutions (T213, T159, T106, T63, T42, T31) of the atmospheric general circulation model ECHAM5 were used to study the scaling behaviour of extreme precipitation in terms of return values, which are estimated quantiles of the generalised extreme value (GEV) distribution. Area-averaged return values of different regions in December, January, February (DJF) and June, July, August (JJA) of the highest resolution T213, averaged to coarser grids, were compared to area-averages of the coarser resolutions of ECHAM5. For the validation of return values, mean precipitation totals and the mean precipitation intensity of the different resolutions of ECHAM5 observational datasets of the UK and the USA were used. Additionally, the observational dataset E-OBS was validated in the UK. Different qualitative scaling behaviours were identified, depending on region and season. Extreme precipitation of different sources has to be compared with respect to spatial scale. However, mean precipitation totals do not show a scaling behaviour in the UK and the USA, indicating that for extreme precipitation in comparison to precipitation totals different processes and different spatial correlation lengths are responsible. T63 is the model resolution that is minimally necessary to represent extreme precipitation even though higher resolutions improve the result. The model ECHAM5 overestimates extreme precipitation and precipitation totals in the UK as well as in the USA. The bias varies in its amount and in the ratio of precipitation totals to return values. The qualitative scaling behaviours in the UK and the USA are captured by ECHAM5. The seasonal cycle of precipitation return values in the southeastern US is not well captured by the high resolutions of ECHAM5. The E-OBS dataset is not appropriate for the validation of climate models in the UK in JJA. Hence, in JJA the spatial correlation length of extreme precipitation is shorter than the distance between rain gauges included in the dataset. The responsible processes for return values in UK and US are on a considerably different spatial scale than those of precipitation totals.

Zusammenfassung

Um das Skalierungsverhalten von Extremniederschlag anhand von Wiederkehrwerten, die geschätzte Quantile der Extremwertverteilung sind, zu untersuchen, wurden Gegenwartssimulationen verschiedener Auflösungen (T213, T159, T106, T63, T42, T31) mit denselben Randbedingungen des atmosphärischen Zirkulationsmodells ECHAM5 verwendet. Flächenmittelwerte der Wiederkehrwerte verschiedener Regionen in Dezember, Januar, Februar (DJF) und Juni, Juli, August (JJA) der höchsten Auflösung, zu gröberen Auflösungen gemittelt, wurden mit Flächenmittelwerten der gröberen Auflösungen von ECHAM5 verglichen. Zur Validierung der Wiederkehrwerte, des mittleren Gesamtniederschlags und der mittleren Niederschlagsintensität der verschiedenen Auflösungen von ECHAM5 wurden Beobachtungsdatensätze des UK und der USA verwendet. Weiterhin wurde der Beobachtungsdatensatz E-OBS über dem UK validiert. Unterschiedliche qualitative Skalierungsverhalten wurden abhängig von Region und Jahreszeit gefunden. Extremniederschläge unterschiedlichen Ursprungs sollten nur unter Berücksichtigung der räumlichen Skala verglichen werden. Der mittlere Gesamtniederschlag zeigt hingegen kein Skalierungsverhalten im UK und in den USA. Dies weist darauf hin, dass für Extremniederschlag einerseits und für den mittleren Gesamtniederschlag andererseits verschiedene Prozesse sowie verschiedene räumliche Korrelationslängen verantwortlich sind. T63 ist die Mindestauflösung, um Extremniederschlag darzustellen. Dies wird durch höhere Auflösungen noch verbessert. Das Modell ECHAM5 überschätzt Extrem- und den mittleren Gesamtniederschlag über dem UK und den USA. Die Höhe des systematischen Fehlers sowie das Verhältnis zwischen Gesamt- und Extremniederschlag schwanken. ECHAM5 kann das qualitative Skalierungsverhalten im UK und in den USA wiedergeben. Die höchsten Auflösungen von ECHAM5 simulieren hingegen den jahreszeitlichen Zyklus der Wiederkehrwerte in den südöstlichen USA fehlerhaft. Zur Validierung von Klimamodellen im UK in JJA ist der E-OBS-Datensatz ungeeignet, da in JJA die räumliche Korrelationslänge des Extremniederschlags kürzer ist als der Abstand zwischen denen in E-OBS berücksichtigten Niederschlagsstationen. Der verantwortliche Prozess für Wiederkehrwerte im UK und in den USA ist auf einer deutlich anderen räumlichen Skala als derjenige des Gesamtniederschlags.

Contents

List of Figures

List of Tables

Acronyms

AGCM	Atmospheric General Circulation Model
AMSR	Advanced Microwave Scanning Radiometer
AOGCM	Atmosphere-Ocean coupled General Circulation Model
AR4	Fourth Assessment Report (IPCC)
AVHRR	Advanced Very High Resolution Radiometer
CCM3	Third generation Community Climate Model
CPC	Climate Prediction Center
DJF	December, January, February
ECHAM5	Fifth generation climate model originally evolved from the ECMWF with parameterisations of the MPIM Hamburg
ECMWF	European Centre for Medium Range Weather Forecasts
E-OBS	European Observational Dataset
EVT	Extreme Value Theory
FAR	First Assessment Report (IPCC)
FFT	Fast Fourier Transform
fvCAM2	Second generation finite volume dynamics version of the Community Atmospheric Model
GCM	General Circulation Model
GEV	Generalised Extreme Value (distribution)
HLRN	North-German Supercomputing Alliance (Norddeutscher Verbund für Hoch- und Höchstleistungsrechnen)

IPCC	Intergovernmental Panel on Climate Change
JJA	June, July, August
MPIM	Max-Planck Institute for Meteorology
NASA	National Aeronautics and Space Adminitration
NCAR	National Center for Atmospheric Research
NOAA	National Oceanic and Atmospheric Administration
OISST	Optimal Interpolation Sea Surface Temperature
SAR	second assessment report
SIC	Sea Ice Cover
SST	Sea Surface Temperature
TAR	Third Assessment Report (IPCC)
UK	United Kingdom of Great Britain
UKMO	United Kingdom Met Office observational dataset
USA	United States of America

1 Introduction

1.1 Extreme Precipitation Events

Extreme weather events can have serious impacts on human society as well as on ecosystems. Questions like whether new climatic records such as the European flood in summer 2002 are due to natural variability or anthropogenically influenced global warming or other non-stationary phenomena are not easy to answer. Extremes are hard to study as they are by definition rare and obey different statistical laws than averages, i.e. the study of extremes is the study of tails of distributions. Furthermore, it is harder to project changes in the hydrological cycle than in temperatures as physical constraints are weaker and observations are less complete (Allen and Ingram, 2002). Extreme value theory (EVT) is the only statistical discipline developing methods to describe the stochastic behaviour of a process at unusual large or small levels (Coles, 2004, p. 1).

Underlying Mechanisms in Changes in the Hydrological Cycle

Changes in the overall intensity of the hydrological cycle are mainly constrained by the energy budget, i.e. the energy balance between atmospheric radiative cooling and latent heating and hence, less than the increase in atmospheric moisture content (Allen and Ingram, 2002). However, the heaviest precipitation events are likely to occur when all moisture in a volume of air precipitates at once. This indicates the increase of the intensity of these events with enhanced moisture content of the atmosphere, following the Clausius-Clapeyron relationship (Trenberth, 1999). Emori and Brown (2005) found in six climate model experiments extreme precipitation worldwide increasing due to thermodynamic changes (i.e. enhanced atmospheric moisture content) whereas the response of mean precipitation to thermodynamic changes varies (Emori and Brown, 2005). The dynamic changes (i.e. changes in atmospheric motion) play a secondary role in the difference between mean and extreme precipitation and are limited to lower latitudes however (Emori and Brown,

2005). Meehl et al. (2005) found enhanced tropical precipitation intensity being related to water vapour increases whereas enhanced mid-latitude intensity was found to result from circulation changes affecting the distribution of increased water vapour in atmosphere-ocean coupled general circulation models (AOGCMs). Accordingly, Wehner (2004) found the correlations between the spatial pattern of return value changes and mean precipitation changes to be low. The changes in mean precipitation do not provide significant information about changes in precipitation extreme values (Wehner, 2004).

Recent and Projected Changes in Extreme Precipitation

Many regions show a positive trend of precipitation extremes over the recent decades (Alexander et al., 2006). The observed changes in heavy precipitation frequencies are greater than in precipitation totals. Even in regions with decreasing or unchanged precipitation totals an increase in heavy and/or very heavy precipitation was observed (Groisman et al., 2005).

Transient climate simulations show the changes in annual precipitation extremes substantially exceeding the changes in annual mean precipitation (Kharin and Zwiers, 2005). Increases in heavy precipitation were even found in regions where mean precipitation decreases (Semenov and Bengtsson, 2002). Semenov and Bengtsson (2002) found maxima of the increase in annual heavy precipitation over Europe and the eastern USA. Kharin et al. (2007) found an increase in return values of annual extremes of daily precipitation amounts of about 6 % with each Kelvin of global warming.

The magnitude and pattern of return values as well as projected changes in return values in transient climate change simulations were found to be dependent on the seasonal cycle (Wehner, 2004). Russo and Sterl (2012) found an increase in seasonal extreme precipitation in most of the Earth's regions. Seasonal precipitation means behave differently however. In many regions these are without increase or decreasing (Russo and Sterl, 2012).

1.2 Quality of Data

The reliability of the investigation of extreme precipitation is highly dependent on the quality of the underlying dataset. Regardless of the data source, the representation of extreme precipitation depends on the resolution of the dataset. Figure 1.1 shows that weather phenomena like thunderstorms happen on small spatial and temporal scales.

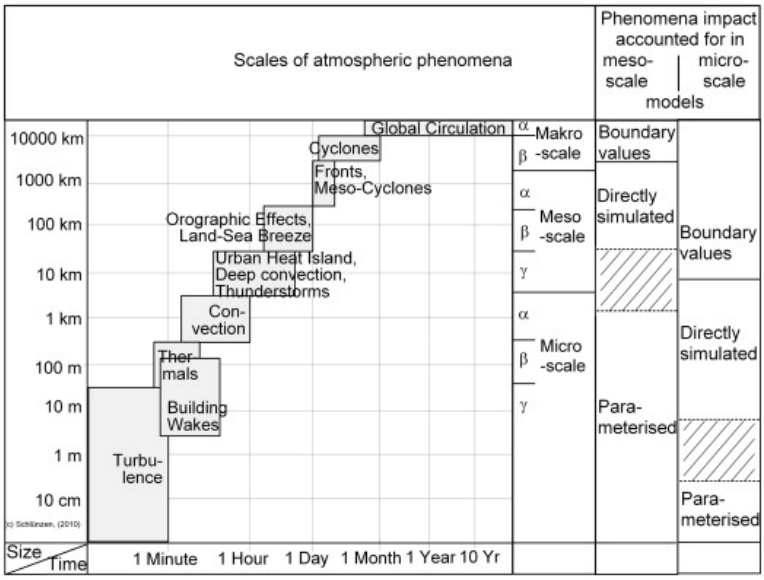

Figure 1.1: Spatial and temporal scales of atmospheric phenomena and how these phenomena are treated in Reynolds-averaged Navier–Stokes mesoscale or obstacle resolving microscale models (right columns). Source: Schlünzen et al. (2011).

Observational Data

Obervational datasets are often limited by a sparse density of rain gauges. Furthermore, station data can not be compared directly to grid box data from climate models (Osborn and Hulme, 1997). Hence, gridding methodologies are applied. Especially in only sparsely sampled regions, interpolation can lead to higher correlation lengths of rainfall events in the dataset than in reality. Furthermore, the methods of measurements as well as the number of rain gauges change in time leading to inhomogenous time series.

Climate Model Data

The atmosphere with its changing weather is a chaotic system, hence its predictability is limited (Latif, 2009, p. 111). To analyse the climate, the interest is not the exact prediction of detailed weather phenomena, but the analysis of the statistics of weather (Latif, 2009, p. 111). According to Lorenz (1970), climate projection is a typical boundary value problem, whereas weather prediction is an initial value problem.

It can be seen in Figure 1.2 that the resolution of general circulation models (GCMs)

became substantially higher since the first assessment report (FAR) of the Intergovernmental Panel on Climate Change (IPCC). However, they remain too coarse to resolve extreme precipitation events such as thunderstorms. The IPCC states that it is likely that the simulation of precipitation intensity will improve with sufficient resolution to explicitly resolve at least the large convective systems without using parameterisations for deep convection (Randall et al., 2007, p. 629). Iorio et al. (2004) as well as Duffy et al. (2003) found improved patterns of precipitation of seasonal means in the USA with enhanced spatial resolution of the Community Climate Model (CCM3) of the National Center for Atmospheric Research (NCAR). Wehner et al. (2010) found patterns of extreme precipitation (20 year return values) over the USA to improve with enhanced model resolution of the same model in comparison to observations.

Many studies found extreme precipitation events being underestimated in GCMs (for example Chen and Knutson (2008), Sun et al. (2006), Min et al. (2011), Allan and Soden (2008), Wehner et al. (2010)). Iorio et al. (2004) solved the problem with underestimated mean and extreme precipitation by embedding a cloud-resolving model at each grid cell and thereby replacing convective and stratiform parameterisations. In contrast to the highly resolved CCM3 this yielded too much precipitation in the form of extreme events even though little improvement of spatial patterns of seasonal-mean precipitation could be achieved (Iorio et al., 2004). The very large intermodel disagreements in the tropics suggest that some physical processes associated with extreme precipitation are not well represented in models (Kharin et al., 2007). This reduces confidence in the projected changes in extreme precipitation (Kharin et al., 2007). Chen and Knutson (2008) compared area-averages of different IPCC models to observations in the USA. They suggest this method rather than point estimates for the comparison of different models.

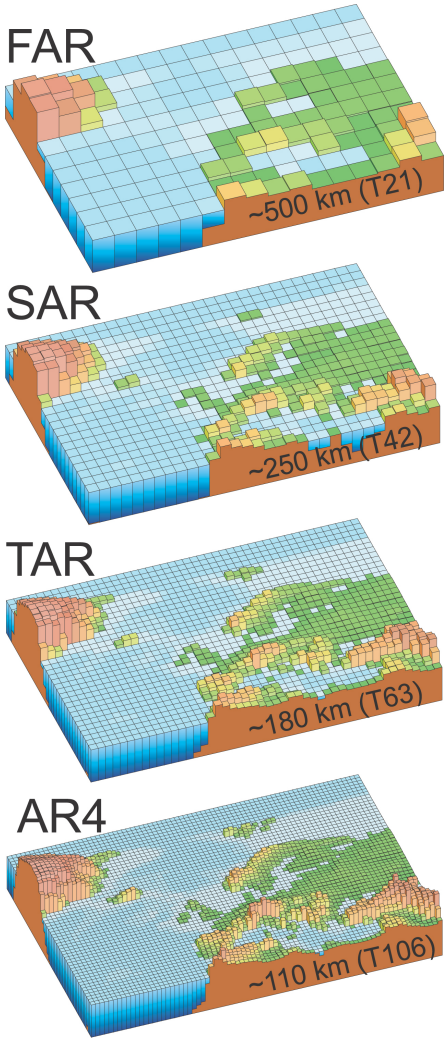

Figure 1.2: Geographic resolution characteristics of the generations of climate models used in the IPCC Assessment Reports: First assessment report (FAR) (1990), second assessment report (SAR) (1996), third assessment report (TAR) (2001), and fourth assessment report (AR4) (2007). The figures above show how successive generations of these global models increasingly resolved northern Europe. These illustrations are representative of the most detailed horizontal resolution used for short-term climate simulations. The century-long simulations cited in IPCC Assessment Reports after the FAR were typically run with the previous generations's resolution. Vertical resolution in both atmosphere and ocean models is not shown, but it has increased comparably with the horizontal resolution, beginning typically with a single-layer slab ocean and ten atmospheric layers in the FAR and progressing to about thirty levels in both atmosphere and ocean. Source: Le Treut et al. (2007, p. 113).

1.3 Objectives

Atmospheric general circulation models (AGCMs) still have coarse horizontal resolutions, much coarser than the scale of precipitation extremes. Hence, it is crucial to study the impact of horizontal model resolution on the representation of extreme precipitation events. Previous studies analysed the impact of horizontal model resolution on the representation of patterns of extreme precipitation. Area-averages were only used to compare results of different models with varying resolution. In this study, the scaling behaviour of area-averages of the same model varying in horizonzal resolution is analysed. Therefore, the AGCM ECHAM5 was run in different horizontal resolutions (T213, T159, T106, T63, T42, T31) with the same boundary forcing used in each simulation. The scaling behaviour of area-averages of return values, which are estimated quantiles of the generalised extreme value (GEV) distribution, is studied. Different regions and seasons are investigated to identify the impact of geographical region and season on the scaling behaviour of extreme precipitation. It is assessed whether a general scaling relationship can be identified which would yield a cheap and simple downscaling method. The highest resolution T213 averaged to coarser grid sizes is compared to the coarser resolutions of ECHAM5 in order to distinguish between the averaging effect and the physical representation effect. Thereby, the minimum AGCM resolution to represent extremes is identified.

In this study, present day simulations of ECHAM5 were carried out. Thus, the results can be validated by observational data. Amounts and scaling behaviours of mean precipitation totals, mean precipitation intensity and return levels of ECHAM5 are compared to observational datasets of the UK and the USA. The scaling behaviour of the observational dataset E-OBS in the UK is also validated with the UKMO dataset to assess the impact of the density of rain gauges included in observational datasets.

In chapter 2 the model as well as the observational datasets, which were used in this study, are described. Chapter 3 explains the statistical methods used to analyse the datasets. In chapter 4 the results of the ECHAM5 model resolution experiment are provided and discussed. In chapter 5 the results of the model ECHAM5 as well as the E-OBS observational dataset are validated with observational datasets. Finally, in chapter 6 a conclusion of the results as well as an outlook are given.

2 Data

For obvious reasons, no experiments can be carried out to examine the response of the Earth system to varying conditions, such as a higher amount of greenhouse gases in the atmosphere. To study the impact of changed conditions on the atmospheric circulation, mathematical models have been developed. These mathematical models present a very powerful tool to carry out an enormous range of different experiments. Any atmospheric general circulation model (AGCM) is based on the atmospheric *primitive equations* (Eq. 2.1 - 2.5) (Kiehl, 1992, p. 322).

$$\frac{\partial \mathbf{v}}{\partial t} = -\mathbf{v} \cdot \nabla \mathbf{v} - \omega \frac{\partial \mathbf{v}}{\partial p} + f\mathbf{k} \times \mathbf{v} - \nabla \Phi + \mathbf{D}_M \tag{2.1}$$

$$\frac{\partial T}{\partial t} = -\mathbf{v} \cdot \nabla T + \omega \left(\frac{\kappa T}{p} - \frac{\partial T}{\partial p} \right) + \frac{\tilde{Q}_{rad}}{c_p} + \frac{\tilde{Q}_{con}}{c_p} + D_H \tag{2.2}$$

$$\frac{\partial q}{\partial t} = -\mathbf{v} \cdot \nabla q - \omega \frac{\partial q}{\partial p} + E - C + D_q \tag{2.3}$$

$$\frac{\partial \omega}{\partial p} = -\nabla \cdot \mathbf{v} \tag{2.4}$$

$$\frac{\partial \Phi}{\partial p} = -\frac{RT}{p} \tag{2.5}$$

with:

$\mathbf{v}$:	three-dimensional velocity
ω:	vertical p-velocity
p:	pressure
$\mathbf{k}$:	unit vector in z-direction
$f = 2\Omega \sin \phi$:	Coriolis parameter
Ω:	earth angular velocity
ϕ:	latitude
Φ:	geopotential
$\mathbf{D}_M = (D_\lambda, D_\Phi)$:	dissipation terms for momentum
T:	temperature
κ:	thermal conductivity
$\tilde{Q}_{rad}$:	net radiative heating
$\tilde{Q}_{con}$:	heating due to condensational processes
c_p:	specific heat at constant pressure
D_H:	diffusion term for heating
q:	specific humidity
E:	rate of evaporation
C:	rate of condensation
D_q:	diffusion term for moisture
R:	gas constant

These highly nonlinear partial differential equations do not have closed-form solutions. Hence, a numerical approximative solution is required.

2.1 ECHAM5

2.1.1 Model Description

To assess the impact of model resolution on extreme precipitation, the fifth generation of the AGCM of ECHAM, developed at the Max Planck Institute for Meteorology (MPIM) is used. ECHAM has evolved originally from the spectral weather prediction model of the European Centre for Medium Range Weather Forecasts (ECMWF; Simmons et al. (1989)) (Roeckner et al., 2003), therefore its first letters EC. The parameterisation package was

developed in Hamburg, therefore the end letters HAM. A detailed description of ECHAM5 and its parameterisation can be found in Roeckner et al. (2003).

As the variation of a quantity around a latitude zone is necessarily periodic, the atmospheric fields can be held and manipulated in form of waves (Henderson-Sellers and McGuffie, 1987, p. 141). The advantage is, that fewer numbers are required to represent a global field and computation times are hence reduced (Henderson-Sellers and McGuffie, 1987, p. 141). The dynamical part of ECHAM is formulated in spherical harmonics (see Eq. 2.6) (Roeckner et al., 2003). Vorticity, divergence, temperature and the logarithm of surface pressure are computed by these (Roeckner et al., 2003).

Non-linear terms, including parameterisations, are evaluated in physical space on an associated rectangular finite-difference grid, the Gaussian grid (Roeckner et al., 2003). The basic idea behind spectral AGCMs is, that on each time step spectral fields are transformed into grid space and after the performance of grid point physics the selected variables are transformed back into spectral space (Henderson-Sellers and McGuffie, 1987, p. 140).

This is shown for an arbitrary variable in spectral space

$$X = \sum_{m=-M}^{M} \sum_{n=|m|}^{|m|+j} X_n^m Y_n^m$$

with X_n^m being the complex spectral coefficients. m denotes zonal wavenumber with the spectral truncation limits M and $|m| + j$. The spherical harmonics Y_n^m, being a function of longitude λ and latitude ϕ (Eq. 2.6) (Henderson-Sellers and McGuffie, 1987, p.142), is the eigensolution of the barotropic wave equation in spherical coordinates and, as such, constitute a complete and orthogonal expansion basis (Hack, 1992, p.302).

$$Y_n^m = P_n^m (\sin \phi) \exp (im\lambda) \tag{2.6}$$

with P_n^m being a Legendre polynomial of degree n and zonal wavenumber m (Henderson-Sellers and McGuffie, 1987, p. 142). To transform this variable X to the Gaussian grid first a Legendre transform is evaluated for each spectral variable at each of the Gaussian latitudes ϕ_j (Eq. 2.7). These latitudes are related to the resolution of the model such that they are the roots of the associated Legendre polynomial of order zero (Henderson-Sellers

and McGuffie, 1987, p. 143).

$$X_n^m \rightarrow X_{(m)}\left(\phi_j; t\right) = \sum_{n=|m|}^{|m|+j} X_n^m P_n^m \tag{2.7}$$

The Fourier harmonics $X_{(m)}$ at each of the Gaussian latitudes ϕ_j and at time t resulting from Eq. 2.7 are transformed via Fast Fourier transform (FFT) to longitudes $\lambda_l = 2\pi l/L$ with $1 < l < L$ (Eq. 2.8) (Henderson-Sellers and McGuffie, 1987, p. 143). The FFT is computationally very efficient (Hack, 1992, p.302).

$$X_{(m)} \rightarrow Z\left(\lambda_l, \phi_j; t\right) = \sum_{m=-M}^{M} X_{(m)} \exp\left(im\lambda_l\right) \tag{2.8}$$

Now, physical processes are computed in the Gaussian grid. Subsequently, variables are transformed back into spectral space by FFT followed by the performance of the inverse Legendre transformations for one latitude at a time using Gaussian quadrature (Eq. 2.9) (Henderson-Sellers and McGuffie, 1987, p. 143).

$$Z_n^m = \sum_{j=1}^{k} w_{j,k}\left(\phi_j\right) Z_{(m)}\left(\phi_j\right) P_n^m\left(\sin\phi_j\right) \tag{2.9}$$

The values for the variables, being back in spectral space, are now computed for the advanced time point etc..

The horizontal resolution of a spectral model is usually presented in terms of wavenumber truncation. ECHAM5 is truncated triangularly (Roeckner et al., 2003). The "T" in the resolution specification is for triangular truncation. The truncation number represents the number of waves resolved around a latitude zone. More precisely, the number is a description of the relationship between the largest Fourier wavenumber, the highest degree of the associated Legendre polynomial and the highest degree of the Legendre polynomial of order zero. These are termed M, K and N respectively. The triangular truncation type is defined as $M = N = K$ (Henderson-Sellers and McGuffie, 1987, p. 143). The advantage of triangular truncation compared to rhomboidal truncation is that the solution in a triangularly truncated system is invariant to an arbitrary coordinate rotation (Hack, 1992, p. 304).

To resolve the vertical atmospheric structure ECHAM5 uses a number of horizontal layers. The uppermost computational level is at 10 hPa with a total of either 19 or 31 layers (Roeckner et al., 2003).

2.1.2 Boundary and Initial Conditions of ECHAM5

For this study ECHAM5 has been run in resolutions of T213, T159, T106, T63, T42 and T31. This corresponds to horizontal resolutions in grid space of approximately $0.56°\times0.56°$, $0.75°\times0.75°$, $1.13°\times1.13°$, $1.88°\times1.88°$, $2.81°\times2.81°$ and $3.75°\times3.75°$ respectively. T213, T159, T106 and T63 have 31 vertical layers, whereas T31 and T42 have 19 vertical layers.

The model was forced with optimal interpolation $1/4$ degree daily sea surface temperature analysis (OISST) - version 2 of the National Oceancic and Atmospheric Administration (NOAA) (Reynolds et al., 2007) and high resolution (12.7 km) observed sea ice cover (SIC) from Grumbine et al. of the NOAA. NOAA produces two $0.25°$ daily SST products. One product uses the Advanced Very High Resolution Radiometer (AVHRR) infrared satellite SST data. The other uses AVHRR and Advanced Microwave Scanning Radiometer (AMSR) on the NASA Earth Observing System satellite SST data. Both products also use in situ data from ships and buoys and include a large-scale adjustment of satellite biases with respect to the in situ data (Reynolds et al., 2007). According to Reynolds et al. (2007), sea ice data were smoothed with a seven day median filter. This reduced the influence of occasional spurios day-to-day sea ice variation in summer resulting from satellite sensing errors of wet surfaces. SST and SIC data were interpolated to ECHAM grid by N. Keenlyside. All radiative forcing is kept constant at present day levels. Greenhouse gas forcing is observed concentrations. For the resolutions T106, T63, T42 and T31 three ensemble member runs with slightly different initial conditions have been carried out. The initial conditions are the conditions of a day in December 1981. For the ensemble members the conditions of different days in December 1981 were used. For the high resolution models T213 and T159, it was not possible to run ensemble members due to limited computation time. The model was run from 1982 - 2010, limited by the availability of the set of highly resolved boundary conditions. These model runs have been performed by V. Semenov and W. Tseng on the supercomputer of the North-German Supercomputing Alliance (HLRN).

2.1.3 Averaging of T213 to Coarser Resolutions

To evaluate the effect of increasing grid box size on the representation of precipitation, the daily precipitation of the T213 model run (corresponding to approximately 0.56°×0.56°) was spatially averaged to coarser resolutions. The average of the precipitation was taken over 2×2, 3×3, 4×4, 5×5, 6×6 and 7×7 grid boxes respectively, resulting in grid resolutions of approximately 1.125°×1.125°, 1.69°×1.69°, 2.25°×2.25°, 2.81°×2.81°, 3.38°×3.38° and 3.94°×3.94°. The original T213 model run will be refered to as $T213_{1\times1}$ in this study. The coarser resolutions averaged from the T213 run will accordingly be refered to as $T213_{2\times2}$, $T213_{3\times3}$, $T213_{4\times4}$, $T213_{5\times5}$, $T213_{6\times6}$ and $T213_{7\times7}$ in this study.

The statistics are applied after the working resolution is achieved.

2.2 Observational Datasets

For the validation of the ECHAM5 model results, the precipitation indices (see chapter 3) have been compared to precipitation indices derived from observational datasets.

2.2.1 UK

The gridded dataset of the UK Meteorological Office (UKMO) which is based on 2000 - 6000 rain gauges (Perry et al., 2009) has been used. The grid has a resolution of 5 km×5 km (Perry et al., 2009). To compare this dataset to the model output, its grid has to be transformed to a Gaussian grid. The difference between two latitudes corresponds to 111.325 km. Hence, 5 km on a longitude λ are equivalent to 0.045°. A distance on a latitude ϕ_{dist} can be calculated as in Eq. 2.10, dependent on the latitude ϕ.

$$\phi_{dist} = \cos(\phi) \times 111.325 \tag{2.10}$$

With the assumption that the UK is situated on average at 55°N, 5 km correspond to 0.078°. The period from 1958 to 2005 is covered by this dataset. Thus, it ends before the time period of the ECHAM5 model output. Consequently, a slightly different time period is analysed. According to chapter 2.1.3, this dataset was averaged to coarser resolutions which are provided in Table A.2.

Table 2.1: Averaged resolutions of the UKMO dataset.

Averaged grid boxes	Grid box size [km×km]	Gaussian grid box size [°×°]
1×1	5×5	0.045×0.078
2×2	10×10	0.090×0.156
3×3	15×15	0.135×0.234
4×4	20×20	0.180×0.312
5×5	25×25	0.225×0.390
7×7	35×35	0.315×0.546
10×10	50×50	0.450×0.780
15×15	75×75	0.675×1.17
20×20	100×100	0.900×1.56
25×25	125×125	1.13×1.95
30×30	150×150	1.35×2.34
35×35	175×175	1.58×2.73
40×40	200×200	1.80×3.12
45×45	225×225	2.03×3.51

2.2.2 E-OBS

The European daily high-resolution (0.25°×0.25°) gridded data set (E-OBS) of precipitation is used (Haylock et al., 2008). It has been developed in the framework of the ENSEMBLES project. The density of rain gauges is very irregular and in some regions very sparse, such as for the UK only 137 rain gauges are considered (Haylock et al., 2008). The same time period as for the ECHAM5 model runs is taken for analyses. According to chapter 2.1.3, this dataset was averaged to coarser resolutions. Therefore, the mean of 2×2 to 11×11 grid boxes respectively was taken, yielding resolutions of approximately 0.5°×0.5° to 2.75°×2.75°.

2.2.3 USA

The NOAA CPC (Climate Prediction Center) "US Unified Precipitation" dataset (Higgins et al., 2000) was used to validate the model results for the USA. It is based on approximately 35 000 rain gauges over the whole USA, sparsest in the western USA, and gridded to 0.25°×0.25° (Higgins et al., 2000). Data from before 1999 are not produced exactly the same way as data from 1999 onwards (Higgins et al., 2000). The same time period as for the ECHAM5 model runs is taken for analyses. According to chapter 2.1.3, this dataset was averaged to coarser resolutions. Therefore, the mean of 2×2 to 15×15 grid boxes was taken respectively, yielding resolutions of approximately 0.5°×0.5° to 3.75°×3.75°.

A summary of resolutions used in this study is given in appendix A.

3 Methods

The ECHAM5 model output of six hourly precipitation data was summed to daily data. Subsequently seasonal maxima for December, January and February (DJF) as well as for June, July and August (JJA) were taken. Furthermore, seasonal maxima were taken from daily observational precipitation and analysed by the methods described in this chapter.

3.1 Extreme Value Theory

In this section a statistical model for extreme value theory (EVT) is introduced. It focuses on the behaviour of

$$M_n = max\,\{X_1,...,X_n\}$$

where $X_1, \ldots, X_n$ is a sequence of independent and identically distributed random variables having a common distribution function F. M_n represents the maximum of a process over n time units. In the block maxima approach which is used in this study $X_1,...,X_n$ is broken up into blocks of size n. M_n is consequently the maximum of the block. n must be large enough to make sure, that the block maxima are independent events (Coles, 2004, p. 45). The limit distribution of M_n is the Generalised Extreme Value (GEV) family of distributions (Eq. 3.1) (Coles, 2004, p. 47).

$$G(z) = \exp\left\{-\left[1+\xi\left(\frac{z-\mu}{\sigma}\right)\right]^{-1/\xi}\right\} \tag{3.1}$$

with the location parameter μ, the scale parameter σ and the shape parameter ξ. μ describes the location of the distribution. Hence, an increasing μ yields a shift of the whole distribution towards higher values. σ specifies the width of the distribution. Thus, an enhanced σ results in a widening of the distribution, implicating higher variability. The

assymetry and hence, the tail of the distribution is determined by ξ as follows (Coles, 2004, p. 46):

- Extreme Value Type I: Gumbel $\xi \to 0$: infinite smooth tail
- Extreme Value Type II: Fréchet $\xi > 0$: infinite heavy tail
- Extreme Value Type III: Weibull $\xi < 0$: bounded tail

In Figure 3.1 a the probability density function and in Figure 3.1 b and c the corresponding random time series with added maxima for a block length of 20 for constant μ and σ but varying ξ are provided.

It can be clearly seen, that a larger value for ξ yields a heavier tail (see Figure 3.1 a) and accordingly higher maxima (see Figure 3.1 b). An enhanced positive ξ results in a lengthening of the high-end tail, indicating a tendency towards rare, but extreme events (see Figure 3.1 a and c). Hence, an increase in μ, σ and/or ξ leads to more extreme events.

Estimation of Return Values

In this study the block length is chosen to be 3 months, i.e. n is the number of observations of 3 months and the block maxima are seasonal maxima. Estimates of extreme quantiles can be obtained by inverting Eq. 3.1, yielding Eq. 3.2.

$$z_p = \begin{cases} \mu - \frac{\sigma}{\xi}\left[1 - \{-\log(1-p)\}^{-\xi}\right] & \text{for } \xi \neq 0 \\ \mu - \sigma \log\{-\log(1-p)\} & \text{for } \xi = 0 \end{cases}, \tag{3.2}$$

where $G(z_p) = 1 - p$ (Coles, 2004, p. 49). z_p is the return value associated with the return period $1/p$, since the value z_p is expected to be exceeded on average once in $1/p$ seasons, i.e. z_p is exceeded by the seasonal maximum in any particular season with probability p (Coles, 2004, p. 49).

Since the parameters of the GEV distribution are not estimated independently (see chapter 3.2), the following analyses compare quantiles of the GEV distribution, namely return values.

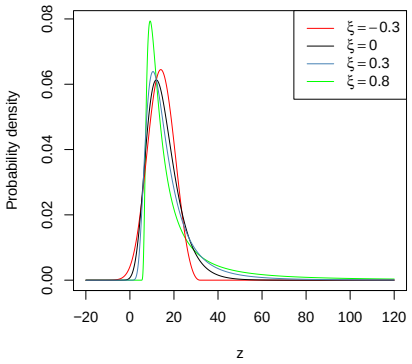

(a)

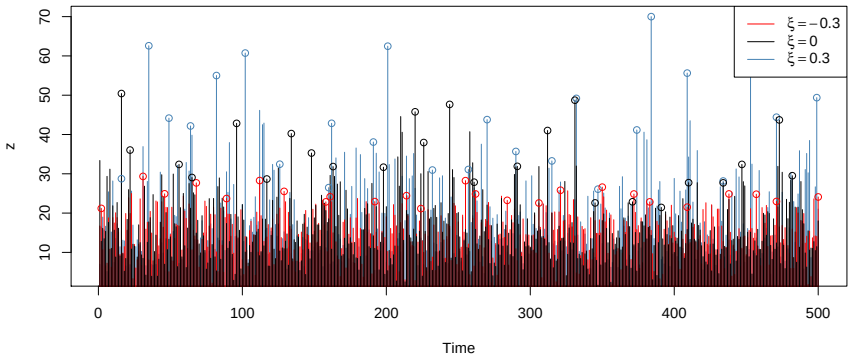

(b)

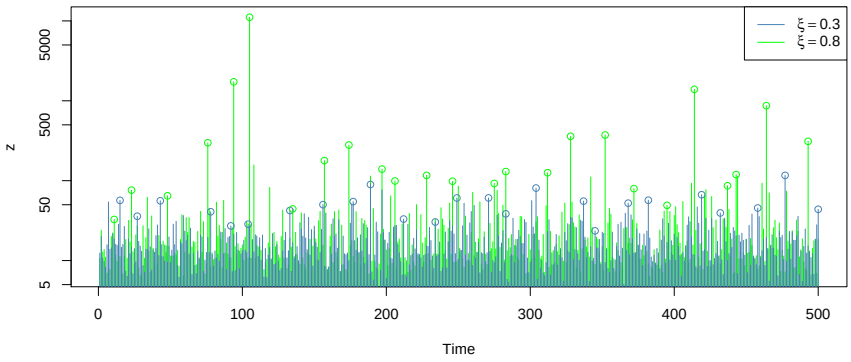

(c)

Figure 3.1: Probability density functions for varying ξ with constant $\mu = 12$ and $\sigma = 6$ (a) for an arbitrary variable z. Randomly generated time series with added maxima for a block length of 20 for the probability density functions shown in a (b and c). Note the logarithmic y-scale in c.

3.2 Probability Weighted Moments

The GEV model was fitted to the seasonal maxima by the method of probability weighted moments (PWM). The sample size is quite small as the model runs only cover 29 years, yielding 29 seasonal maxima per season. The power of PWM is its good performance for small sample sizes as well as its computational simplicity (Hosking et al., 1985). The biases of the estimators are small, except when estimating quantiles in the extreme tails of the GEV distribution (Hosking et al., 1985). Thus, this study compares 20 season return values (see Eq. 3.2 for the computation of return values).

The probability-weighted moments of a random variable X with distribution function $F(x) = P(X \leq x)$ are given by Eq. 3.3.

$$M_{p,r,s} = E\left[X^p \left\{F(X)\right\}^r \left\{1 - F(X)\right\}^s\right] \tag{3.3}$$

p, r, and s are real numbers (Greenwood et al., 1979). According to Hosking et al. (1985) the moments $\beta_r = M_{1,r,0} = E\left[X \left\{F(X)\right\}^r\right] (r = 0,1,2,\ldots)$ are considered.

Hence, the probability-weighted moments of the GEV distribution (Eq. 3.1) for $\xi \neq 0$ are shown in Eq. 3.4 (Hosking et al., 1985).

$$\beta_r = (r+1)^{-1}\left[\mu + \sigma\left\{1 - (r+1)^{-\xi}\,\Gamma(1+\xi)\right\}/\xi\right], \quad \xi > -1 \tag{3.4}$$

For $\xi \leq -1$, β_0 which is the mean of the distribution, and the rest of the β_r do not exist (Hosking et al., 1985).

Eq. 3.4 leads to Eq. 3.5, Eq. 3.6 and Eq. 3.7 (Hosking et al., 1985).

$$\beta_0 = \mu + \sigma\left\{1 - \Gamma(1+\xi)\right\}/\xi \tag{3.5}$$

$$2\beta_1 - \beta_0 = \sigma\Gamma(1+\xi)\left(1 - 2^{-\xi}\right)/\xi \tag{3.6}$$

$$\frac{3\beta_2 - \beta_0}{2\beta_1 - \beta_0} = \frac{1 - 3^{-\xi}}{1 - 2^{-\xi}} \tag{3.7}$$

The PWM estimators $\hat{\mu}$, $\hat{\sigma}$ and $\hat{\xi}$ are the solutions of Eq. 3.5 - Eq. 3.7 for μ, σ and ξ when β_r are replaced by their estimators.

The estimation of β_r for a random sample of size n from the distribution F is based on the ordered sample $x_1 \leq x_2 \leq \cdots \leq x_n$. b_r in Eq. 3.8 is an unbiased estimator of β_r (Landwehr et al., 1979).

$$b_r = n^{-1} \sum_{j=1}^{n} \frac{(j-1)(j-2)\cdots(j-r)}{(n-1)(n-2)\cdots(n-r)} x_j \tag{3.8}$$

Eq. 3.7 is almost linear over the range of values $-\frac{1}{2} < \xi < \frac{1}{2}$. Hence, low-order polynomial approximations for $\hat{\xi}$ are very accurate. Thus, Hosking et al. (1985) suggest the estimator Eq. 3.9 rather than Eq. 3.7.

$$\hat{\xi} = 7.8590c + 2.9554c^2, \qquad c = \frac{2b_1 - b_0}{3b_2 - b_0} - \frac{\log 2}{\log 3} \tag{3.9}$$

With $\hat{\xi}$, the scale and location parameters can be estimated according to Eq. 3.10 and Eq. 3.11 respectively.

$$\hat{\sigma} = \frac{(2b_1 - b_0)\,\hat{\xi}}{\Gamma\left(1 + \hat{\xi}\right)\left(1 - 2^{-\hat{\xi}}\right)} \tag{3.10}$$

$$\hat{\mu} = b_0 + \hat{\sigma}\left\{\Gamma\left(1 + \hat{\xi}\right) - 1\right\}/\hat{\xi} \tag{3.11}$$

The PWM estimation in this study has been performed with the "fExtremes" package (Wuertz et al., 2009) of the R-Project (R Development Core Team, 2011).

3.3 Analysis of the Scaling Behaviour of Return Values

Only terrestrial extreme precipitation is studied. Therefore, the matrices of calculated return values were multiplied with a landmask. On the one hand, extreme precipitation is mainly studied with the aim to better understand the impact of extreme precipitation events on human society and ecosystems. On the other hand, ECHAM5 overestimates precipitation over the oceans, particularly in high-resolution simulations (Hagemann et al., 2006). This is a genereal problem in current GCMs, which could be due to insufficient atmospheric absorption of solar radiation by aerosols, water vapor or clouds (Hagemann et al., 2006).

The estimated return values are spatially averaged over certain regions (see section 3.4) within each resolution. For the resolutions T106, T63, T41 and T31 ensemblemeans of the calculated return values were taken, i.e. for each region the return values of the three ensemble runs were averaged. Additionally the 95 % confidence interval for each region was calculated and added as error bars.

Subsequently, the averaged return values are plotted against their associated spatial length scale. The spatial length scale is the length of one side of the rectangular grid boxes, such as the spatial length scale of a 2°×2° grid box is 2°. $T213_{1\times1}$ - $T213_{7\times7}$ as well as the coarser resolutions T159, T106, T63, T42 and T31 are plotted in the same plot to compare their scaling behaviours. In the comparisons to observational datasets, these are added to the plots.

The UK dataset is on a 0.045° × 0.078° grid. As this is not a rectangular grid, $\sqrt{0.045 \times 0.078} = 0.059°$ was supposed to be the spatial length scale of $UK_{1\times1}$. Accordingly the spatial length scales for $UK_{2\times2}$ - $UK_{45\times45}$ are 0.118°, 0.177°, 0.236°, 0.295°, 0.413°, 0.590°, 0.885°, 1.180°, 1.475°, 1.770°, 2.065°, 2.360° and 2.655° respectively.

3.4 Definition of Regions

For the comparison of area averages, regions have to be defined. In order to avoid averaging over areas with substantially different values, the studied regions were defined according to the slopes of the GEV location parameter μ of $T213_{1\times1}$ - $T213_{7\times7}$ in the plots, described in section 3.3, which can be seen for return values in section 4.2. The coarsest resolution of the averaged T213 resolutions is the $T213_{7\times7}$ grid (corresponding to a spatial length scale of approximately 3.94°). Therefore, μ of every T213 resolution ($T213_{1\times1}$ - $T213_{6\times6}$) was averaged to the $T213_{7\times7}$ grid. As the $T213_{7\times7}$ grid was originally averaged from

the $T213_{1\times1}$ grid (see section 2.1.3), μ in the $T213_{1\times1}$ resolution can easily be averaged over 7×7 grid boxes to be on a $T213_{7\times7}$ grid. However, this is not possible for $T213_{2\times2}$ - $T213_{6\times6}$.Therefore, the nearest neighbour of the $T213_{7\times7}$ grid boxes for each grid box of $T213_{2\times2}$ - $T213_{6\times6}$ respectively was identified by Euclidean distance measure using the "fields" package (Furrer et al., 2010) of the R-project (R Development Core Team, 2011). Hence, per $T213_{7\times7}$ grid box a certain number of $T213_{1\times1}$ - $T213_{6\times6}$ grid boxes are averaged respectively. Finally $T213_{1\times1}$ - $T213_{7\times7}$ are on the same horizontal grid, namely the $T213_{7\times7}$ grid.

Thereupon, a moving average of μ over 3x3 grid boxes of $T213_{1\times1}$ - $T213_{7\times7}$ on the $T213_{7\times7}$ grid respectively was carried out. Subsequently, within each grid box a linear regression of the μ values of $T213_{1\times1}$ - $T213_{7\times7}$ against the associated spatial length scale was performed.

Finally, a map containing the slopes of these linear regressions was plotted. According to this map the regions have been defined by identifying patterns of equal or similar slopes. The moving average was used to smooth the patterns. These maps of the seasons being analysed in this study, DJF and JJA, are provided in Figure 3.2 and Figure 3.3 respectively. In Figure 3.3 a the whole range of slopes is shown to identify the patterns of heavy slopes whereas in Figure 3.3 b the range of slopes has been limited at the bottom to $-10\ \mathrm{mm}(\mathrm{d}^\circ)^{-1}$ to better identify the patterns of less heavy slopes in JJA. The defined regions are provided in Table 3.1.

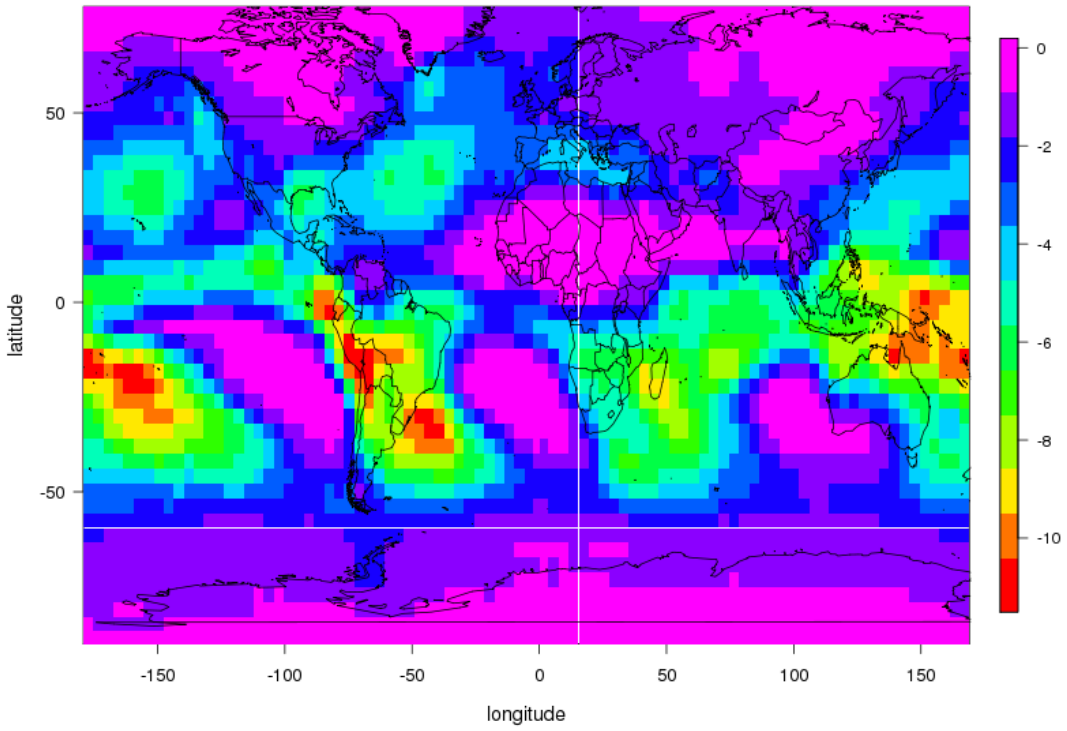

Figure 3.2: Slopes $\left[\mathrm{mm(d^{\circ})^{-1}}\right]$ of linear regressions of the GEV - location parameter μ $\left[\mathrm{mm(d)^{-1}}\right]$ in DJF of the resolutions $T213_{1\times1}$ - $T213_{7\times7}$ of ECHAM5, being all on a $T213_{7\times7}$ grid (approximately 3.94°×3.94°), against their associated spatial length scale [°]. A moving average over 3×3 grid boxes was applied before the regression. From this map patterns of equal or similar slopes were identified for December, January, February (DJF).

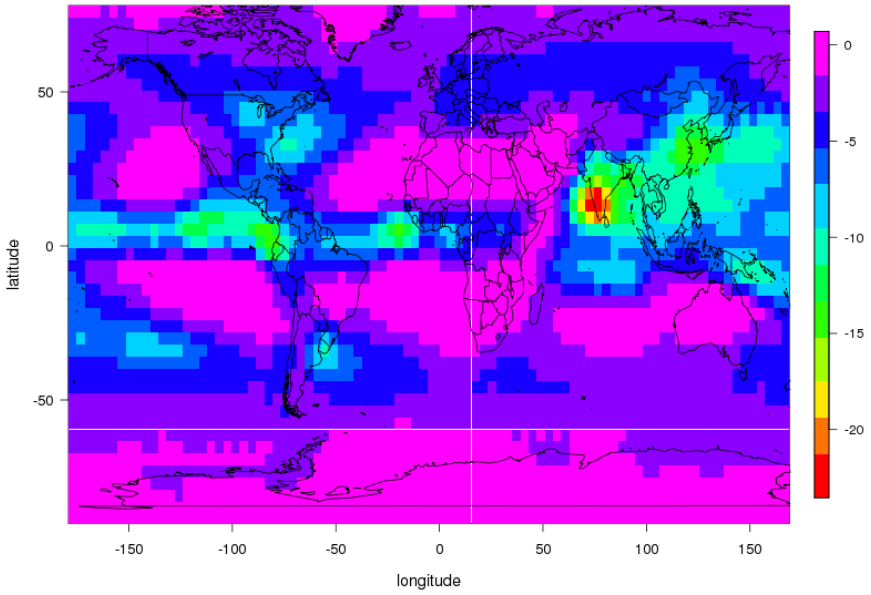

(a)

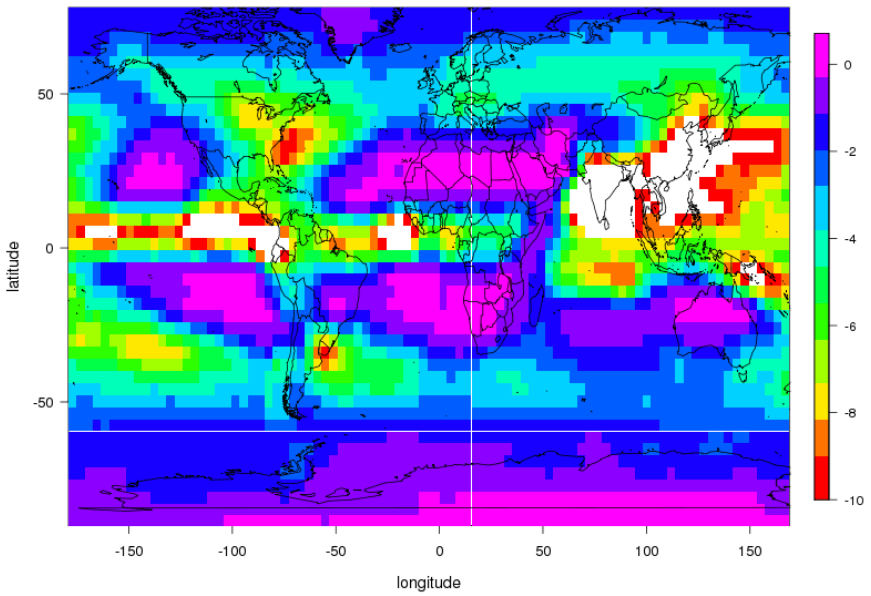

(b)

Figure 3.3: Slopes $\left[\mathrm{mm(d^{\circ})^{-1}}\right]$ of linear regressions of the GEV - location parameter μ $\left[\mathrm{mm(d)^{-1}}\right]$ in JJA of the resolutions $T213_{1\times1}$ - $T213_{7\times7}$ of ECHAM5, being all on a $T213_{7\times7}$ grid (approximately 3.94°×3.94°), against their associated spatial length scale [°]. A moving average over 3×3 grid boxes was applied before the regression. From these maps patterns of equal or similar slopes were identified for June, July, August (JJA). In (a) the plot range is unlimited, allowing mainly to identify patterns of heavy slopes, in (b) the plot range is limited at the bottom to -10 $\left[\mathrm{mm(d^{\circ})^{-1}}\right]$ to indentify patterns of less heavy slopes.

Table 3.1: The regions for the analysis of the region specific scaling behaviour for DJF and JJA, as identified from Figure 3.2 and Figure 3.3. Note that several regions are different in DJF and JJA.

Region	Latitudes [°]	Longitudes [°]
DJF and JJA		
Northern Europe	47 N - 75 N	10 W – 40 E
Southern Europe	35 N – 47 N	10 W – 40 E
Eastern Asia	20 N – 50 N	110 E – 150 E
Eastern Australia-New Zealand	52 S – 20 S	145 E – 180 E
Western Siberia	50 N – 75 N	60 E – 90 E
Central USA	30 N – 50 N	110 W – 100 W
Northeastern USA	40 N – 50 N	100 W – 60 W
Southeastern USA	25 N – 40 N	100 W – 60 W
Canada-Alaska-Greenland	50 N – 85 N	180 W – 20 W
Southwestern South America	60 S – 20 S	80 W – 60 W
Southeastern South America	40 S – 20 S	60 W – 40 W
DJF (December, January, February)		
Central Africa	10 S - 0	5 E - 40 E
Southern Africa	35 S – 10 S	10 E – 50 E
Indonesia-northern Australia	15 S – 20 N	90 E – 160 E
Western USA	30 N – 50 N	130 W – 110 W
Amazon region	20 S – 10 S	60 W – 35 W
	10 S – 0	70 W – 35 W
Peru-Bolivia-Ecuador	20 S – 10 S	85 W – 60 W
	10 S – 0	85 W – 70 W
Northern South America-southern Central America	0 – 12 N	90 W – 50 W
Central America	12 N – 25 N	115 W – 82 W
	25 N – 30 N	120 W – 100 W
JJA (June, July, August)		
India	5 N – 25 N	65 E – 93 E
Indonesia	10 S – 20 N	90 E – 160 E
Russia	50 N – 70 N	40 E – 180 E
Central Africa	10 S – 12 N	20 W – 40 E
Southern Peru-Bolivia-central Amazon	20 S – 10 S	85 W – 60 W
	10 S – 5 S	85 W – 35 W
Northern Peru-Ecuador-Colombia	5 S – 8 N	82 W – 70 W
Northeastern South America	0 – 12 N	70 W – 50 W
Central America	5 N – 22 N	110 W – 80 W
Western USA-northern Mexico	30 N – 50 N	130 W – 110 W

3.5 Validation of Model Data by Comparison to Observational Data

The return values, which have been calculated from the model output of ECHAM5 have been compared to return values, that were calculated from observational datasets. Furthermore, the scaling behaviour of mean precipitation totals as well as of mean precipitation intensities are examined and compared to the scaling behaviour of extremes. The seasonal mean precipitation totals are the total precipitation over each whole season respectively summed over the whole period, divided by the number of years. The mean precipitation intensity is the mean precipitation total divided by the mean number of wet days. A wet day is defined as a day with at least 1 mm of precipitation. These indices are averaged over the regions defined in section 3.4 and plotted as described in section 3.3.

4 Results of the ECHAM5 Resolution Experiment

In this chapter the results of the modeled datasets, yielding from the ECHAM5 model, are presented. The influence of spatial scale on the representation of patterns of 20 season return values over Europe is assessed in section 4.1. Subsequently in section 4.2 the scaling behaviour of area averaged 20 season return values for different regions is shown.

4.1 The Impact of Model Resolution on Precipitation Return Value Patterns over Europe

To check the representation of patterns of the 20 season DJF return values in the model ECHAM5, maps of different spatial resolutions are examined. Since the spatial scale of heavy precipitation events is often less than all considered resolutions, the return values are expected to decrease with bigger grid size due to the effect of describing a small scaled event in a bigger area, i.e. point processes are represented in grid boxes. To account for the averaging effect, the patterns in the coarser model resolutions T159 - T31 are compared to those in the respective equal or most similar resolution of $T213_{2\times2}$ - $T213_{7\times7}$. Consequently, the averaging effect is included in both graphics. Hence, the visible difference is due to a different model performance in coarser resolutions such as unresolved physical processes. In Figure 4.1 a the 20 season return values of Europe in DJF of the T213 model run in its original resolution $T213_{1\times1}$ as well as of those of the coarser model resolutions Figure 4.1 b - f T159, T106, T63, T42 and T31 are shown. In Figure 4.2 a - f the 20 season return values of Europe in DJF of the T213 model run, spatially averaged to coarser resolutions $T213_{2\times2}$, $T213_{3\times3}$, $T213_{4\times4}$, $T213_{5\times5}$, $T213_{6\times6}$ and $T213_{7\times7}$, respectively are provided.

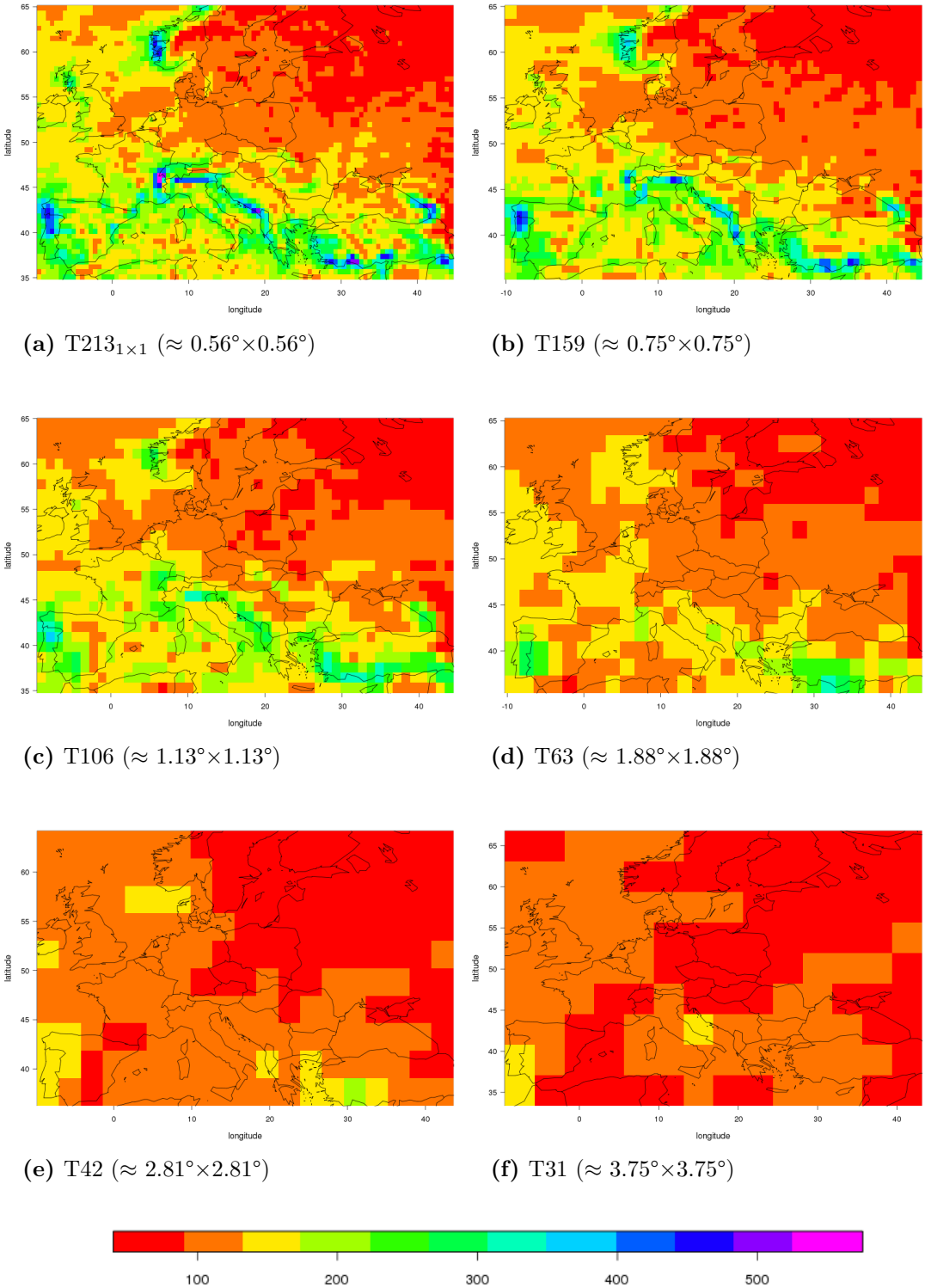

(a) $T213_{1\times1}$ ($\approx 0.56°\times0.56°$)

(b) T159 ($\approx 0.75°\times0.75°$)

(c) T106 ($\approx 1.13°\times1.13°$)

(d) T63 ($\approx 1.88°\times1.88°$)

(e) T42 ($\approx 2.81°\times2.81°$)

(f) T31 ($\approx 3.75°\times3.75°$)

Figure 4.1: Maps of Europe showing the 20 season DJF return value in mm/d of $T213_{1\times1}$ (a) and the coarser model resolutions T159 - T31 (b - f).

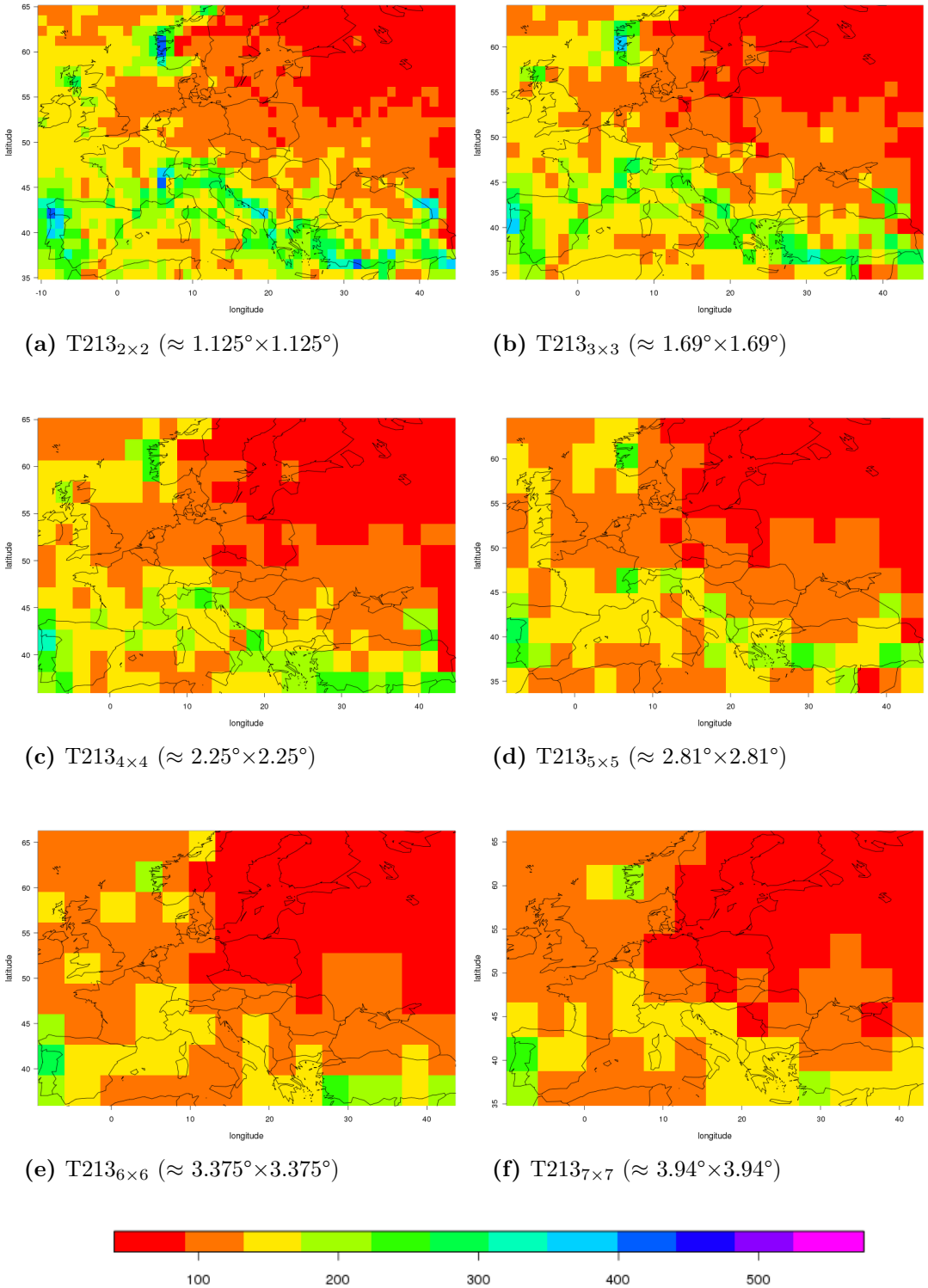

(a) $T213_{2\times2}$ ($\approx 1.125°\times1.125°$) **(b)** $T213_{3\times3}$ ($\approx 1.69°\times1.69°$)

(c) $T213_{4\times4}$ ($\approx 2.25°\times2.25°$) **(d)** $T213_{5\times5}$ ($\approx 2.81°\times2.81°$)

(e) $T213_{6\times6}$ ($\approx 3.375°\times3.375°$) **(f)** $T213_{7\times7}$ ($\approx 3.94°\times3.94°$)

Figure 4.2: Maps of Europe showing the 20 season DJF return value in mm/d of the original T213 model resolution (a) and the T213 model run spatially averaged over a different number of grid boxes (b - f). The indices of T213 show the number of grid boxes averaged before the statistics are applied.

It can be seen that the highest 20 season return values in the maps decrease, as expected, with increasing grid box size in the averaged T213 resolutions $T213_{1\times1}$ - $T213_{7\times7}$ (see Figure 4.1 a and 4.2) as well as in the decreasing model resolutions $T213_{1\times1}$ - T31 (see Figure 4.1). However, in the averaged T213 model resolutions $T213_{1\times1}$ - $T213_{7\times7}$ the return values show a higher variability than in the coarser model resolutions T159 - T31. This is due to fewer physical processes resolved in the coarser model resolutions. T159 yields a similar pattern as $T213_{1\times1}$, although some maximum return values such as at the west coasts of Scandinavia and in the Alps are lower in T159.

T106 is in general able to reproduce a similar pattern as $T213_{2\times2}$ (see Figure 4.1 c and 4.2 a respectively). However, slight differences are detected in the spatial extent of several patterns between T106 and $T213_{2\times2}$. Additionally, the maximum 20 season return values are higher in $T213_{2\times2}$ than in T106, for example at the west coast of Scandinavia.

T63 is still able to capture the general pattern of the 20 season return values compared to $T213_{3\times3}$ (see Figure 4.1 d and 4.2 b respectively). However, the extent of the pattern is generally slightly less in T63 than in $T213_{3\times3}$. The highest return values of $T213_{3\times3}$ such as at the west coast of Scandinavia are not reproduced by T63.

T42 compared to $T213_{5\times5}$ does not reproduce the general pattern anymore, such as the Alps having the same 20 season return values in T42 as the surrounding regions (see Figure 4.1 e and 4.2 d respectively). The only elementary pattern which can be seen in T42 is the enhanced return values at the west coasts of Scandinavia, Denmark, the Iberian peninsula, Albania, Turkey as well as at the west coast of Ireland. T31 does not reproduce any pattern that can be seen in $T213_{7\times7}$. For example,the higher 20 season return values at the Scandinavian west coast are not visible at all (see Figure 4.1 f versus 4.2 f).

Summarised, a decline in the ability to simulate the variety of precipitation over Europe with decreasing model resolution is obvious. T63 appears to be the minimal required model resolution to capture the pattern of precipitation return values. Certainly, higher model resolutions always yield a better representation of this pattern, e.g. T106 shows an improved pattern compared to T63. T213 as well as T159 resolve very detailed variabilities. T42 can only detect some very basic schemes such as west coasts, whereas T31 is not even able to capture those very simple properties. Maps of further regions are not provided as this study focuses on area averages. Since for the validation of extreme precipitation in Europe no appropriate observational dataset is available, the patterns are not validated.

4.2 Scaling Behaviour of Area Averaged Return Values

To assess the scaling behaviour, the 20 season return values were averaged over the geographic regions described in section 3.4 (note that some geographic regions are defined differently in DJF and JJA) and plotted against their corresponding spatial length scale. The scaling behaviour of the return values of the model run with the highest resolution T213 averaged to coarser resolutions is compared to the scaling behaviour of the return values of the coarser model resolutions T159 - T31 for the seasons DJF as well as JJA.

In the averaged T213 resolutions $T213_{1\times1}$ - $T213_{7\times7}$ the effect of increasing grid box size on the representation of the return values is covered whereas the decreasing model resolutions T213 - T31 show the effect of increasing grid box size as well as the effect of physical representation in the coarser model resolution. Hence, the difference between the two curves should be mainly due to physical processes which are not resolved by the coarser model resolutions.

Main Scaling Behaviours

According to the position of the curve of the area averaged return values of $T213_{1\times1}$ - $T213_{7\times7}$ in relation to the position of the curve of the area averaged return values of $T213_{1\times1}$ - T31, in DJF and JJA roughly three different main qualitative scaling behaviours and three further qualitative scaling behaviours, which are in between of these main scaling behaviours, could be identified. In this section examples of each qualitative scaling behaviour are provided.

Figure 4.3 shows the scaling behaviour of northern Europe (a) as well as the scaling behaviour of the northeastern USA (b) in DJF. As can be seen in Figure 4.3, in northern Europe as well as in the northeastern USA the 20 season DJF return value of the averaged T213 model resolutions $T213_{1\times1}$ - $T213_{7\times7}$ decreases more steeply with increasing spatial length scale than the return values of the lower model resolutions $T213_{1\times1}$ - T31. Surprisingly, the coarser model resolutions yield higher return values than expected due to the averaging effect. The responsible mechanism is unclear. A possible explanation is that physical model parameterisations in the coarser resolutions of ECHAM5 lead to more intense return values and hence, overestimate the latter compared to the expected intensity from the averaging effect. Another potential reason is that parameterisations in the highest resolution T213 lead to the simulation of comparably low extreme precipitation in these

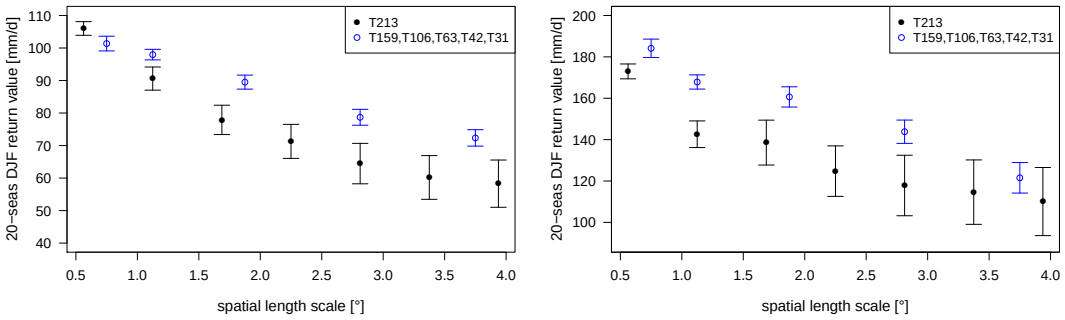

(a) Northern Europe DJF **(b)** Northeastern USA DJF

Figure 4.3: Area-averaged total precipitation 20 season return values over northern Europe (a) and the northeastern USA (b) in DJF estimated from ECHAM5 model output in the resolutions $T213_{1\times1}$ - $T213_{7\times7}$, T159, T106, T63, T42 and T31 against spatial length scale. The error bars are the 95 % confidence interval of the area average. Note the different scales of the y-axes.

regions.

A similar scaling behaviour was found for the regions Canada-Alaska-Greenland, Western Siberia and Eastern Asia in DJF, as well as for eastern Australia-New Zealand in JJA (see Figure B.1 a - d respectively). Apparently this scaling behaviour is only found in several regions in winter.

Figure 4.4 shows the scaling behaviours of eastern Australia-New Zealand (a) as well as of the southeastern USA (b) in DJF, which is summer in eastern Australia-New Zealand and winter in the southeastern USA. In eastern Australia-New Zealand as well as in the southeastern USA in DJF the 20 season return values of $T213_{1\times1}$ - $T213_{7\times7}$ show the same decreasing behaviour as those of the lower model resolutions T213 - T31 (Figure 4.4), i.e. the return values are in the 95 % confidence interval. Thus, the decreasing return values can be explained by grid box effects only.

Indonesia-northern Australia shows in DJF the same scaling behaviour as eastern Australia-New Zealand (see Figure B.2 a). Similarly does Central America in DJF, except for the T106 return value, being slightly higher (see Figure B.2 b). In JJA in Indonesia, southwestern South America as well as southern Europe the scaling behaviours of $T213_{1\times1}$ - $T213_{7\times7}$ and T213 - T31 are in their reciprocal 95 % confidence interval (see Figure B.3 a - c repectively). Furthermore, the western as well as the central USA in DJF show similar

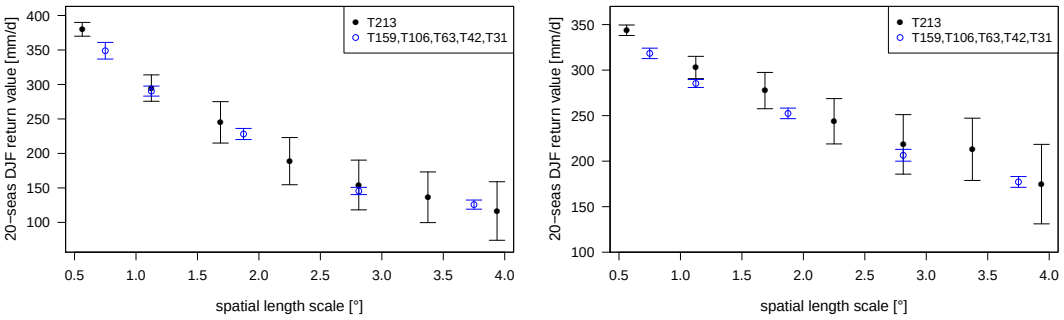

(a) Eastern Australia-New Zealand DJF **(b)** Southeastern USA DJF

Figure 4.4: Area-averaged total precipitation 20 season return values over eastern Australia-New Zealand (a) and the southeastern USA (b) in DJF estimated from ECHAM5 model output in the resolutions $T213_{1\times1}$ - $T213_{7\times7}$, T159, T106, T63, T42 and T31 against spatial length scale. The error bars are the 95 % confidence interval of the area average. Note the different scales of the y-axes.

scaling behaviours (see Figure B.4). However, the return values of $T213_{1\times1}$ - $T213_{7\times7}$ have much larger error bars than in the other regions. In contrast, T159 - T31 do not have larger error bars than those in the other regions with this scaling behaviour. Hence, the return values of $T213_{1\times1}$ - $T213_{7\times7}$ in the western and the central USA in DJF seem to be more variable than those of T159 - T31 and those in other regions.

In Figure 4.5 the scaling behaviours of the Amazon region (a) as well as of southwestern South America (b) are shown. In the Amazon region as well as in southwestern South America a scaling behaviour of faster decreasing 20 season return values in the coarser model resolutions T213 - T31 than in the averaged T213 resolutions $T213_{1\times1}$ - $T213_{7\times7}$ was found (see Figure 4.5). However, in the Amazon region the $T213_{1\times1}$ - T31 return values decrease much steeper than in southwestern South America. In southwestern South America T31 is on the same level as T42. The return values of $T213_{1\times1}$ - T42 decrease almost linearly.

The difference between the $T213_{1\times1}$ - $T213_{7\times7}$ and the $T213_{1\times1}$ - T31 return values can be explained by physical processes which are not resolved in the models with coarser resolutions. A scaling behaviour like this has been expected for every grid box, only being variable in the slopes, the space between the two curves and their curvature, such as the difference between the Amazon region and southwestern South America.

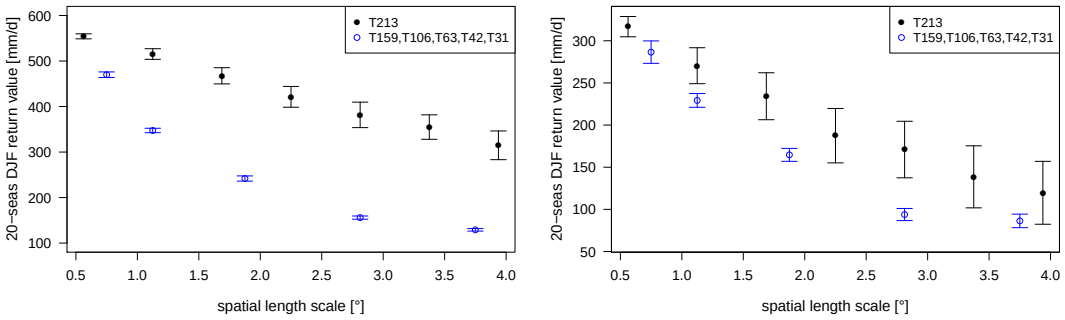

(a) Amazon region DJF **(b)** Southwestern South America DJF

Figure 4.5: Area-averaged total precipitation 20 season return values over the Amazon region (a) and southwestern South America (b) in DJF estimated from ECHAM5 model output in the resolutions $T213_{1\times1}$ - $T213_{7\times7}$, T159, T106, T63, T42 and T31 against spatial length scale. The error bars are the 95 % confidence interval of the area average. Note the different scales of the y-axes.

In DJF, central Africa, southern Africa, Peru-Bolivia-Ecuador, northern South America-southern Central America as well as southeastern South America (see Figure B.5 a - e respectively) and in JJA central Africa, Northern Peru-Ecuador-Colombia, northeastern South America and southeastern South America (see Figure B.6 a - d respectively) show similar scaling behaviours, only varying in their slopes, their curvature and the interspace between the $T213_{1\times1}$ - $T213_{7\times7}$ and the $T213_{1\times1}$ - T31 return values. T31 is not following the scaling behaviour of $T213_{1\times1}$ - T42. This supports the hypotheses stated above. Furthermore, India in JJA shows a similar scaling behaviour (see Figure B.6 e). It is again noticeable that T31 is not further decreasing, suggesting again T31 being too coarse to represent extreme precipitation. Additionally, western Siberia as well as Russia show a similar scaling behaviour in JJA (see Figure B.7). However, both show a scaling behaviour which is almost linear for $T213_{1\times1}$ - $T213_{7\times7}$ as well as for $T213_{1\times1}$ - T31 with a steeper slope for the return values $T213_{1\times1}$ - T31. Furthermore, the central as well as the southeastern USA in JJA show similar scaling behaviours (see Figure B.8). However, it is noticeable that $T213_{1\times1}$ - $T213_{7\times7}$ and T159 - T31 have very different slopes, namely the slope of T159 - T31 being much steeper. Further, it is remarkable that in the central as well as in the southeastern USA the return value of T159 is higher than the one of $T213_{1\times1}$.

Intermediate Scaling Behaviours

In Figure 4.6 the scaling behaviours of Southern Europe in DJF (a) and Canada-Alaska-Greenland in JJA (b) are provided. The scaling behaviours of southern Europe in DJF

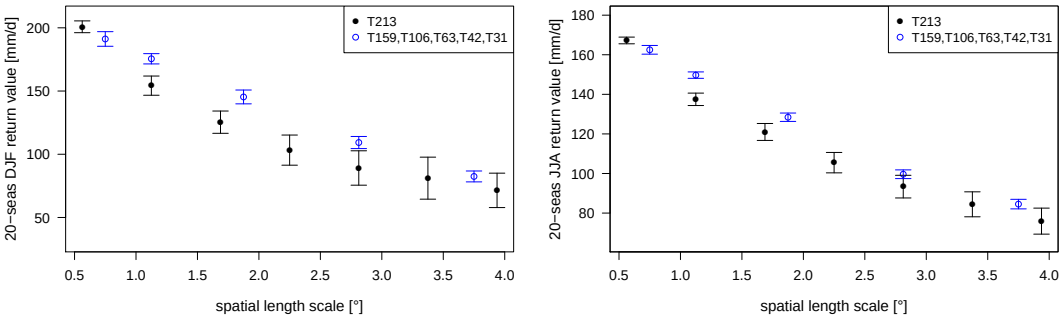

(a) Southern Europe DJF **(b)** Canada-Alaska-Greenland JJA

Figure 4.6: Area-averaged total precipitation 20 season return values over southern Europe (a) in DJF and Canada-Alaska-Greenland (b) in JJA estimated from ECHAM5 model output in the resolutions $T213_{1\times1}$ - $T213_{7\times7}$, T159, T106, T63, T42 and T31 against spatial length scale. The error bars are the 95 % confidence interval of the area average. Note the different scales of the y-axes.

(Figure 4.6 a) and Canada-Alaska-Greenland in JJA (Figure 4.6 b) are in between of those of northern Europe/the northeastern USA in DJF (Figure 4.3) and eastern Australia-New Zealand/the southeastern USA DJF (Figure 4.4). According to northern Europe and the northeastern USA in DJF the 20 season return values of $T213_{1\times1}$ - $T213_{7\times7}$ decrease steeper than those of $T213_{1\times1}$ - T31 although the interspace between them is much less. In contrast to Australia-New Zealand and the southeastern USA in DJF, the difference between $T213_{1\times1}$ - $T213_{7\times7}$ and $T213_{1\times1}$ - T31 exceeds the 95 % confidence interval.

In Figure 4.7 the scaling behaviours of northern Europe as well as the northeastern USA in JJA are provided. The scaling behaviours of northern Europe (Figure 4.7 a) and the northeastern USA in JJA (Figure 4.7 b) are inverse to southern Europe in DJF and Canada-Alaska-Greenland in JJA, namely $T213_{1\times1}$ - T31 decreases slightly faster than $T213_{1\times1}$ - $T213_{7\times7}$. Hence, the scaling behaviours of northern Europe and the northeastern USA in JJA are in between of those of the Amazon region/southwestern South America in DJF (see Figure 4.5) and eastern Australia-New Zealand/the southeastern USA in DJF (see Figure 4.4).

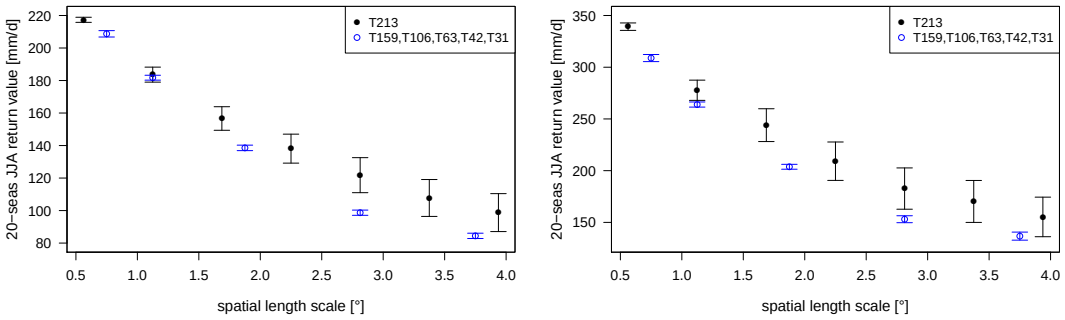

(a) Northern Europe JJA **(b)** Northeastern USA JJA

Figure 4.7: Area-averaged total precipitation 20 season return values over northern Europe (a) and the northeastern USA (b) in JJA estimated from ECHAM5 model output in the resolutions $T213_{1\times1}$ - $T213_{7\times7}$, T159, T106, T63, T42 and T31 against spatial length scale. The error bars are the 95 % confidence interval of the area average. Note the different scales of the y-axes.

A similar scaling behaviour was found for eastern Asia and Central America in JJA (see Figure B.9 a and b respectively).

In Figure 4.8 the scaling behaviours of Southern Peru-Bolivia-central Amazon as well as of the western USA-northern Mexico in JJA are provided. The scaling behaviours of the 20 season return value of Southern Peru-Bolivia-central Amazon as well as of the western USA-northern Mexico in JJA are a special case as the return values of T159 - T63 are in the 95 % confidence interval of those of $T213_{1\times1}$ - $T213_{4\times4}$ even though those of T42 as well as of T31 are below those of $T213_{5\times5}$ - $T213_{7\times7}$. This suggests the resolutions T42 and T31 being too coarse to represent extremes.

ECHAM5 distinguishes in the model output between large scale and convective precipitation. So far, the return values estimated from their sum were compared. The results of the separate analyses of large scale and convective precipitation are provided in appendix B.2. The separate analysis yields that the extreme precipitation events in all studied regions are due to large scale precipitation. The area-averaged return values estimated from large scale precipitation are higher in all regions than those estimated from convective precipitation. This is due to the parameterisations of ECHAM5. In ECHAM5, cumulus convection contributes to large scale air moisture, resulting in large scale precipitation (Roeckner et al.,

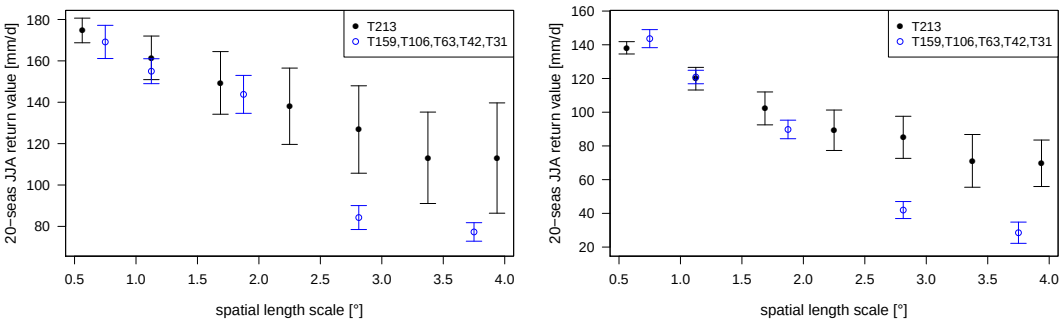

(a) Southern Peru-Bolivia-central Amazon JJA

(b) Western USA JJA

Figure 4.8: Area-averaged total precipitation 20 season return values over Southern Peru-Bolivia-central Amazon (a) and the western USA (b) in JJA estimated from ECHAM5 model output in the resolutions $T213_{1\times1}$ - $T213_{7\times7}$, T159, T106, T63, T42 and T31 against spatial length scale. The error bars are the 95 % confidence interval of the area average. Note the different scales of the y-axes.

2003). Convective rainfall is only the excess moisture falling to the surface where the convectional updraft happens (Roeckner et al., 2003). Hence, the amount of convective precipitation in the model output does not represent the amount of precipitation due to cumulus convective processes (Roeckner et al., 2003). However, it indicates convectional processes happening in that grid box (Roeckner et al., 2003). Therefore, it is not useful to analyse the scaling behaviour of large scale and convective precipitation separately with the aim to better understand the responsible processes leading to extreme precipitation events. Thus, the separate analyses of convective and large scale precipitation are not discussed in detail. It is remarkable that the 20 season return value of convective precipitation in most regions does not change significantly with increasing spatial scale in $T213_{1\times1}$ - T63. However, in several regions the return values of T42 and T31 are significantly below (such as Figure B.13 d) or above (such as Figure B.26 b) those of T213 - T63.

Discussion

A limitation of this study is that due to long computation time, the highest resolutions T213 and T159 do not have several ensemble members. However, all area-averages of the ensemble members of the lower resolutions do not show significant differences (see Figure B.29). This study shows that it is not reliable to compare results of one model with results of another model having a different resolution. Extreme precipitation of different resolutions has to be compared dependent on the respective spatial scale. This is consistent with Chen and Knutson (2008). It is shown in Figure 1.1 in section 1.2 that atmospheric phenomena of small spatial scales, have small time scales. In this experimental setup only daily precipitation is investigated. For events on a very low scale this time scale might be too long. The model run ECHAM5 only covers 29 years. This yields only 29 data points per season to fit the distribution parameters. However, in much longer times series a trend might be present and hence, the time series would have to be broken into several periods to have stationary time series that would be analysed separately. Using a shorter block length to get more values has the disadvantage that some regions could not be analysed anymore as there are not enough heavy rain events for a reliable fit, for example the Mediterranean region in JJA. Another limit of the block maxima approach is that much data is wasted by only taking seasonal maxima. For example, in one season the second highest event might be the second highest event in the whole time series, which is neglected.

5 Comparison of Model Results to Observations

To validate the results of the model study the results derived from the model output are compared to observational datasets, namely the UKMO dataset for the UK, the E-OBS dataset for Europe and the NOAA CPC dataset for the USA. Thereby, the E-OBS dataset is validated. Due to the number of included rain gauges, the UKMO dataset is more reliable than the E-OBS dataset. Thus, the UKMO dataset is used to validate the E-OBS dataset. Initially the scaling behaviours of mean precipitation totals, the mean precipitaiton intensity and precipitation extremes, namely 20 season return values over the UK are validated in section 5.1, followed by the same indices over the central, the northeastern and the total continental USA (excluding Alaska and Hawaii) in 5.2 and finally in section 5.3 over the southeastern USA. The western USA have not been examined separately as the density of rain gauges is sparsest in this part of the USA (Higgins et al., 2000). Furthermore, the mountaineous region is very inhomogenous. Therefore, a very high density of rain gauges is required to estimate reliable precipitation indices.

5.1 UK

Mean Precipitation Totals

Figure 5.1 shows the scaling behaviours of area-averages of mean precipitation totals over the UK of the averaged T213 resolutions $T213_{1\times1}$ - $T213_{7\times7}$, the coarser model resolutions T159 - T31 as well as of the observational datasets UKMO and E-OBS in DJF (a - b) and JJA (c - d). The precipitation totals of the averaged T213 resolutions $T213_{1\times1}$ - $T213_{7\times7}$ show a decreasing scaling behaviour in DJF as well as in JJA, whereas those of the coarser model resolutions $T213_{1\times1}$ - T31 stay almost constant. In JJA the mean return values of T31 and especially of T42 are on a lower level than the other return values. This indicates T42 and T31 being too coarse to represent precipitation totals correctly in the UK in JJA. However, the UK is rather small, hence, T42 and T31 only have very few grid boxes over the

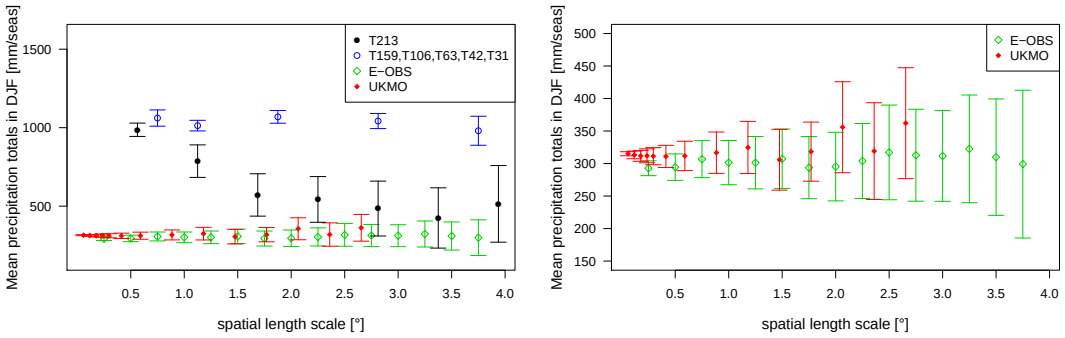

(a) DJF **(b)** DJF

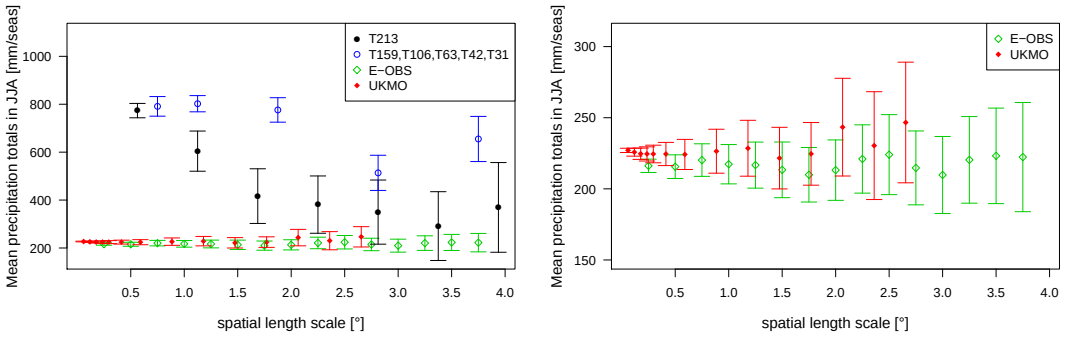

(c) JJA **(d)** JJA

Figure 5.1: Area-averaged mean precipitation totals of total precipitation over the UK in DJF (a) - (b) and JJA (c) - (d) of ECHAM5 model output in the resolutions $T213_{1\times1}$ - $T213_{7\times7}$, T159, T106, T63, T42 and T31 and of the observational datasets UKMO and E-OBS against spatial length scale (a) and (c) and zoomed to the scaling behaviour of UKMO and E-OBS precipitation totals only (b) and (d). The error bars are the 95 % confidence interval of the area average. Note the different scales of the y-axes.

UK. The precipitation totals of the observations do not show a scaling behaviour. The only scaling effect in the observational datasets is an increasing 95 % confidence interval with enhanced spatial scale. The precipitation totals of the models overestimate the observed precipitation totals approximately by a factor of three. In T213 precipitation totals are less spatial coherent than in the observations. Hence, the qualitative scaling behaviour is not well represented in T213. The spatial correlation length of precipitation totals is too short

in T213.

The precipitation totals of the E-OBS dataset are in the 95 % confidence interval of those of the UKMO dataset in DJF as well as in JJA. This indicates that the E-OBS dataset is appropriate to validate precipitation totals of climate models, at least in the UK.

Mean Precipitation Intensity

In Figure 5.2 the scaling behaviours of area-averages of the mean precipitation intensity in the UK of $T213_{1\times1}$ - $T213_{7\times7}$, T159 - T31 as well as of the observational datasets UKMO and E-OBS in DJF (a - b) and JJA (c - d) are provided. In DJF as well as in JJA the mean precipitation intensity of the averaged T213 resolutions $T213_{1\times1}$ - $T213_{7\times7}$ decreases. However, in DJF the mean precipitation intensity of the coarser model resolutions T159 - T31 stays almost constant on the same level as $T213_{1\times1}$, whereas in JJA the mean precipitation intensity of T213 - T106 shows only a slightly varying behaviour, followed by T42 on a much lower level, and T31 below T213 - T106 as well but slightly higher than T42. This indicates, as stated in chapter 4, T42 and T31 being too coarse. The mean precipitation intensity is overestimated by the model with approximately a factor between two and three.

In DJF the difference between the mean precipitation intensity of the E-OBS and the UKMO dataset is low. Primarily, the mean precipitation intensity of the UKMO dataset starts higher and decreases more steeply. Subsequently, the mean precipitation intensity of the E-OBS dataset is in the 95 % confidence interval of the mean precipitation intensity of the UKMO dataset. However, in JJA the mean precipitation intensity of the E-OBS dataset is below the UKMO dataset. Additionally, their scaling behaviours look qualitatively different. This indicates that the E-OBS dataset is not appropriate for the validation of climate models in JJA.

Return Values

In Figure 5.3 the scaling behaviour of the 20 season return values of the UK, estimated from the datasets obtained by the ECHAM5 model, is compared to the scaling behaviours of the 20 season return values estimated from the UKMO as well as from the E-OBS oberservational datasets for DJF (a - b) and JJA (c - d). It is obvious that the ECHAM5 model runs overestimate the 20 season return value, approximately by a factor between four and five. Hence, in the UK the bias in the return values is higher than in the precipitation

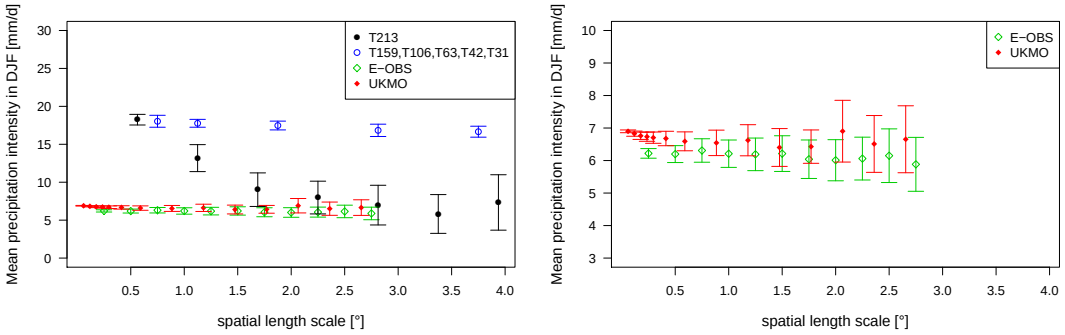

(a) DJF (b) DJF

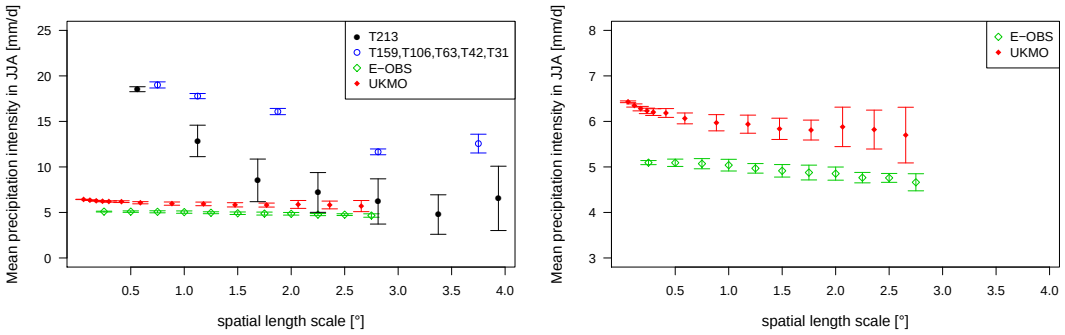

(c) JJA (d) JJA

Figure 5.2: Area-averaged mean precipitation intensity of total precipitation over the UK in DJF (a) and JJA (b) of ECHAM5 model output in the resolutions $T213_{1\times1}$ - $T213_{7\times7}$, T159, T106, T63, T42 and T31 and of the observational datasets UKMO and E-OBS against spatial length scale. The error bars are the 95 % confidence interval of the area average. Note the different scales of the y-axes.

totals. However, without regard to the order of magnitude, the decreasing UKMO values (Figure 5.3 b and d) show a similar qualitative behaviour to those of $T213_{1\times1}$ - $T213_{7\times7}$. For the comparison of the scaling behaviours of $T213_{1\times1}$ - $T213_{7\times7}$ and T159 - T31, see section 4.2.

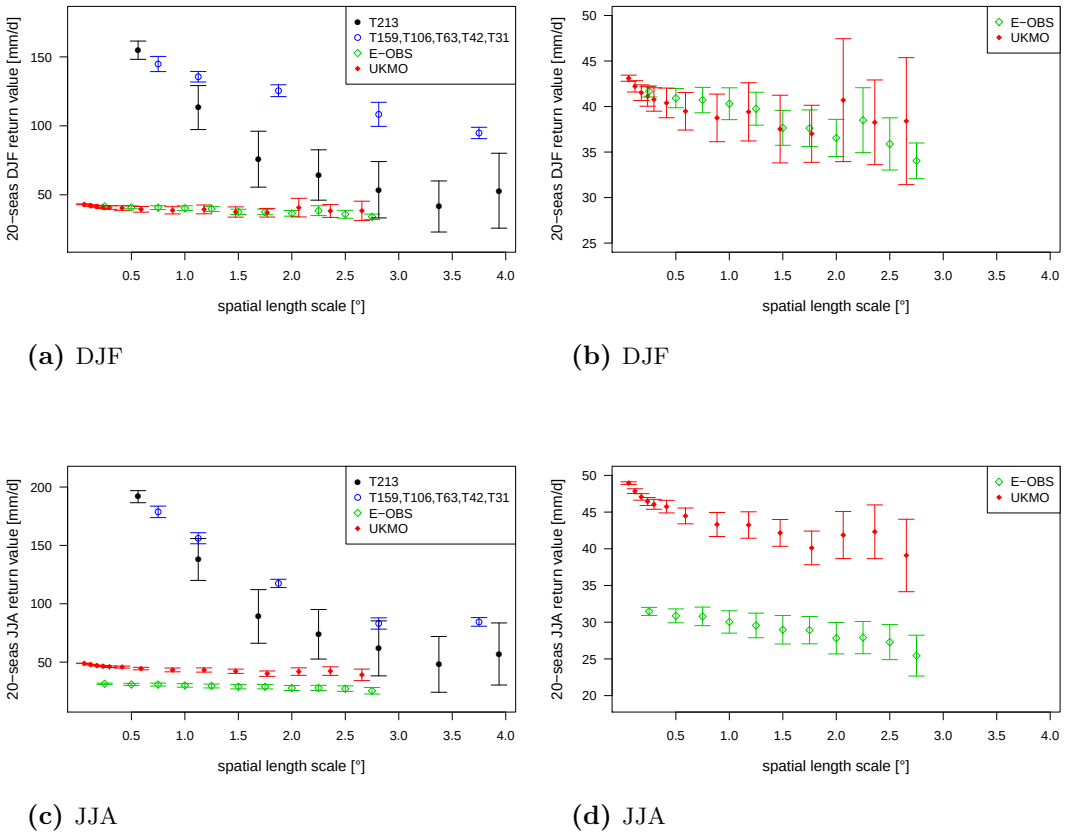

(a) DJF (b) DJF

(c) JJA (d) JJA

Figure 5.3: Area-averaged total precipitation 20 season return values over the UK in DJF (a) - (b) and JJA (c) - (d) estimated from ECHAM5 model output in the resolutions $T213_{1\times1}$ - $T213_{7\times7}$, T159, T106, T63, T42 and T31 and estimated from the observational datasets UKMO and E-OBS against spatial length scale (a) and (c) and zoomed to the scaling behaviour of UKMO and E-OBS return values only (b) and (d). The error bars are the 95 % confidence interval of the area average. Note the different scales of the y-axes.

Limitations of the E-OBS Dataset

The return values of the E-OBS dataset in DJF are in the corresponding 95 % confidence interval of the UKMO return values. However, in JJA the return values of the E-OBS dataset are considerably lower than those of the UKMO dataset. Furthermore, the scaling behaviour of the E-OBS dataset in JJA is almost linear whereas the return values derived from the UKMO dataset decrease primarily very fast and later slower, hence, the scaling

behaviours of the UKMO and the E-OBS datasets are quantitatively as well as qualitatively significantly different. In the UK, precipitation is frequent but not heavy (Manley, 1970, p. 115). December is the month with the highest number of rain days (Manley, 1970, p. 117), which are mainly due to large scale warm and cold fronts (Manley, 1970, p. 119). Hence, the spatial correlation length of precipitation events in DJF is relatively high. However, in JJA, due to thunderstorms, heavy precipitation events of short time scales occur (Manley, 1970, p. 99), and thus, have a lower spatial correlation length. It can be clearly seen in Figure 5.3 d that the spatial correlation lengths of heavy precipitation in JJA is much smaller than the distance between rain gauges, included in the E-OBS dataset. Hence, the E-OBS dataset is not appropriate for the validation of precipitation return values in climate models whenever precipitation on small spatial scales is present. It should only be used very carefully for the validation of climate models. Consequently, in this study it is not further used to validate other European regions. In other European regions, the density of rain gauges in the E-OBS dataset can be considerably different than in the UK. Hence, the usability of the E-OBS dataset can not be extrapolated to other regions. The result that the applicability of the E-OBS dataset to validate or to study extreme precipitation is questionable, is consistent with Hofstra et al. (2009). Furthermore, Maraun et al. (2011) found the location and the scale parameter of the GEV distribution as well as the amplitude of the airflow relationships to be considerably underestimated. Additionally, the spatial variability of the considered validation indices in the E-OBS dataset is often too low, indicating the rather poor representation of local features (Maraun et al., 2011).

5.2 USA

Mean Precipitation Totals

Mean precipitation totals of the central USA (a), the northeastern USA (b) and the total USA (c) of the resolutions $T213_{1\times1}$ - $T213_{7\times7}$ and T159 - T31 of the model ECHAM5 in comparison to the observations as well as only the observational precipitation totals (d) are provided for DJF in Fig 5.4 and for JJA in Figure 5.5. In Figure 5.4 as well as in

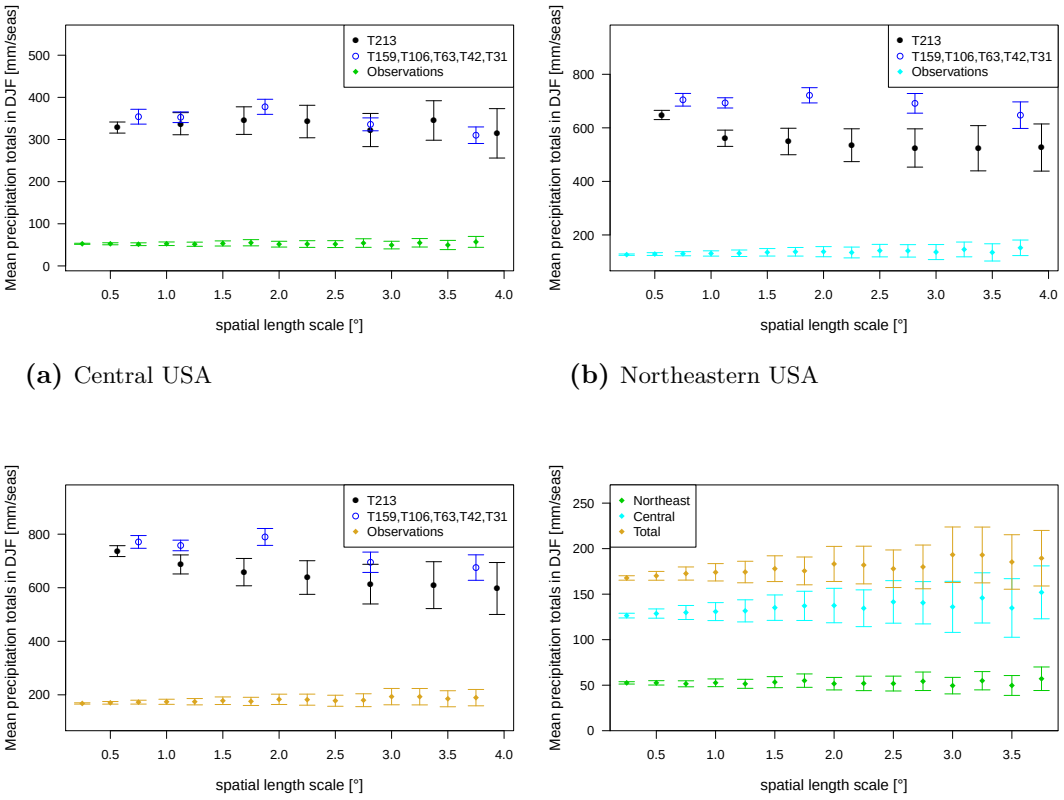

(a) Central USA

(b) Northeastern USA

(c) Total USA

(d) Observations

Figure 5.4: Area-averaged mean precipitation totals of total DJF precipitation over the central USA (a), the northeastern USA (b) and the total USA (c) of ECHAM5 model output in the resolutions $T213_{1\times1}$ - $T213_{7\times7}$, T159, T106, T63, T42 and T31 and of the observational dataset NOAA CPC against spatial length scale and zoomed to the scaling behaviour of the observational return values only (d). The error bars are the 95 % confidence interval of the area average. Note the different scales of the y-axes.

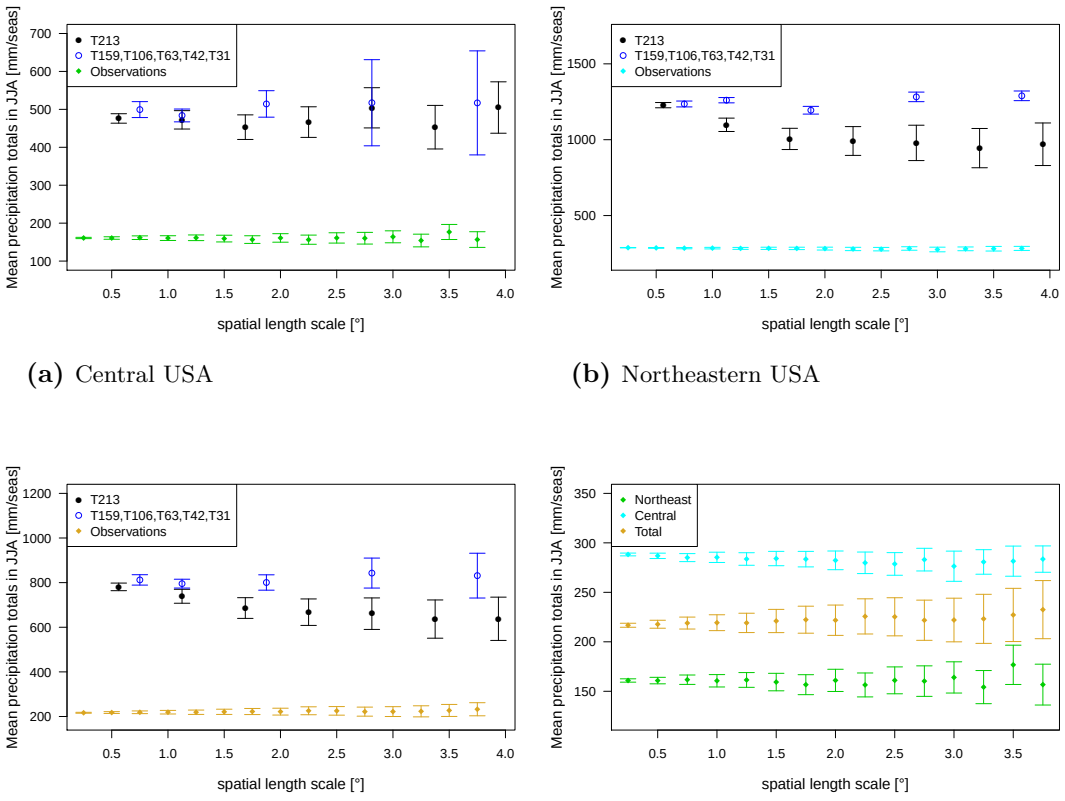

(a) Central USA **(b)** Northeastern USA

(c) Total USA **(d)** Observations

Figure 5.5: Area-averaged mean precipitation totals of total JJA precipitation over the central USA (a), the northeastern USA (b) and the total USA (c) of ECHAM5 model output in the resolutions $T213_{1\times1}$ - $T213_{7\times7}$, T159, T106, T63, T42 and T31 and of the observational dataset NOAA CPC against spatial length scale and zoomed to the scaling behaviour of the observational return values only (d). The error bars are the 95 % confidence interval of the area average. Note the different scales of the y-axes.

Figure 5.5 no scaling behaviour can be identified for the mean precipitation totals in the model resolutions $T213_{1\times1}$ - T31. In the northeastern USA as well as in the total USA the mean precipitation totals of $T213_{1\times1}$ - $T213_{7\times7}$ show a shallow decreasing behaviour, however, in the central USA no scaling behaviour can be detected in $T213_{1\times1}$ - $T213_{7\times7}$ and additionally, the values of T159 - T31 are in the 95 % confidence interval of $T213_{1\times1}$ - $T213_{7\times7}$ in the central USA. In the northeastern USA as well as in the total USA the interspace between $T213_{1\times1}$ - $T213_{7\times7}$ and T159 - T31 is only small. The observational

precipitation totals show no important scaling behaviour. The only difference is the enhanced 95 % confidence interval with increasing spatial length scale. This confirms the results that precipitation totals are not sensitive to spatial scale from section 5.1. Furthermore, the shallow decreasing behaviour of precipitation totals of $T213_{1\times1}$ - $T213_{7\times7}$ in DJF as well as in JJA indicates again precipitation totals in T213 being less spatial coherent than in the observations. In the central USA in JJA (see Figure 5.5 a) the 95 % confidence intervals of T42 and T31 are considerably higher than those of the other precipitation totals. In the USA, mean precipitation totals in DJF are overestimated by the models approximately by a factor between five and six, in JJA approximately by a factor between three and five. Thus, the bias in precipitation totals of ECHAM5 is higher over the USA than over the UK.

Mean Precipitation Intensity

The mean precipitation intensity of the central USA (a), the northeastern USA (b) and the total USA (c) of the resolutions $T213_{1\times1}$ - $T213_{7\times7}$ and T159 - T31 of the model ECHAM5 in comparison to the observations as well as only the observational mean precipitation intensity (d) are given for DJF in Fig 5.6 and for JJA in Figure 5.7. The mean precipitation intensity in DJF (see Figure 5.6) as well as in JJA (see Figure 5.7) is slightly decreasing with spatial scale in the central USA, the northeastern USA and the total USA in the averaged T213 resolutions $T213_{1\times1}$ - $T213_{7\times7}$ as well as in the coarser model resolutions $T213_{1\times1}$ - T31. However, the mean precipitation intensity of T159 - T31 stays slightly above the mean precipitation intensity of $T213_{1\times1}$ - $T213_{7\times7}$ in the northeastern USA as well as in the total USA. In the central USA in DJF the mean precipitation intensity of T159 - T31 is in the 95 % confidence interval of the mean precipitation intensity of $T213_{1\times1}$ - $T213_{7\times7}$. The mean precipitation intensity in the observations shows no scaling behaviour in DJF. Hence, in the model ECHAM5 the mean precipitation intensity is dependent on spatial scale, whereas it is not in the observations. However, in JJA the observations show a qualitatively similar scaling behaviour as the model, namely decreasing. The mean precipitation intensity in the model is biased approximately by a factor between three and four, thus, a higher bias than the mean precipitation intensity in the UK and lower than the bias in their respective precipitation totals.

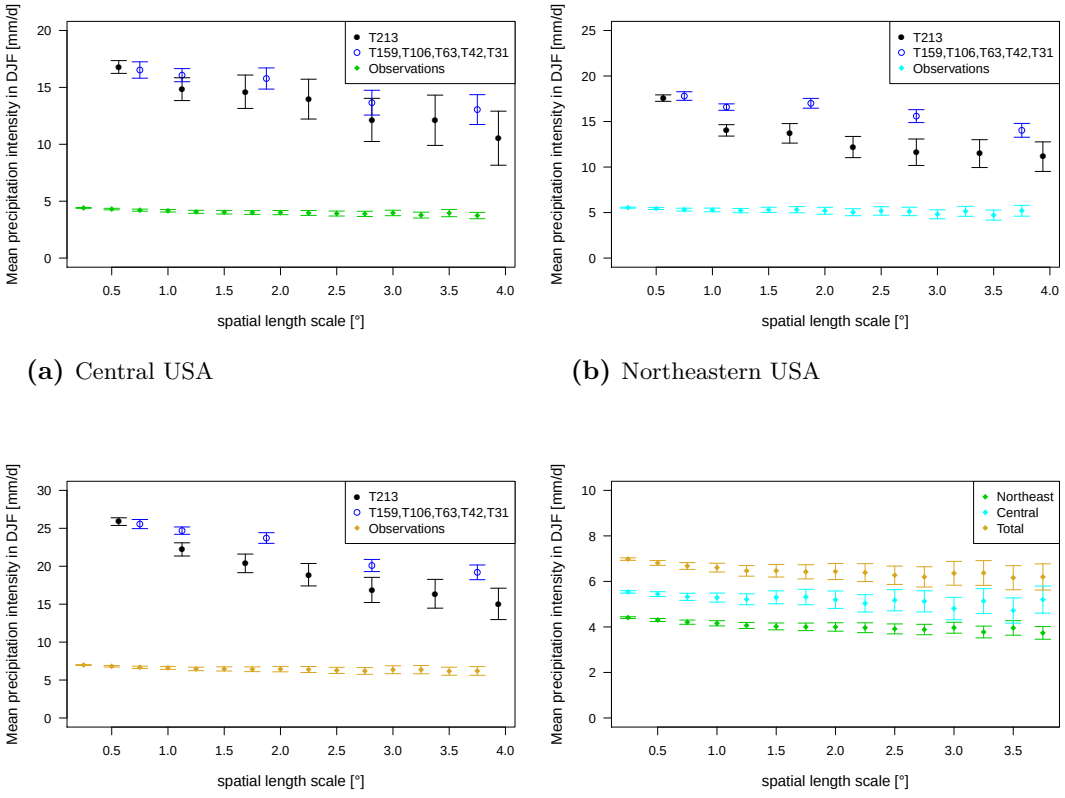

(a) Central USA

(b) Northeastern USA

(c) Total USA

(d) Observations

Figure 5.6: Area-averaged mean precipitation intensity of total DJF precipitation over the central USA (a), the northeastern USA (b) and the total USA (c) of ECHAM5 model output in the resolutions $T213_{1\times1}$ - $T213_{7\times7}$, T159, T106, T63, T42 and T31 and of the observational dataset NOAA CPC against spatial length scale. The error bars are the 95 % confidence interval of the area average. Note the different scales of the y-axes.

Return Values

The 20 season return values of the central USA (a), the northeastern USA (b) as well as the total USA (c) of the model resolutions $T213_{1\times1}$ - $T213_{7\times7}$ and T159 - T31 in comparison to 20 season return values of observational data as well as only the observational 20 season return values (d) are given for DJF in Fig 5.8 and for JJA in Figure 5.9. The model bias of 20 season return values over the USA is similar to the UK, namely approximately a factor

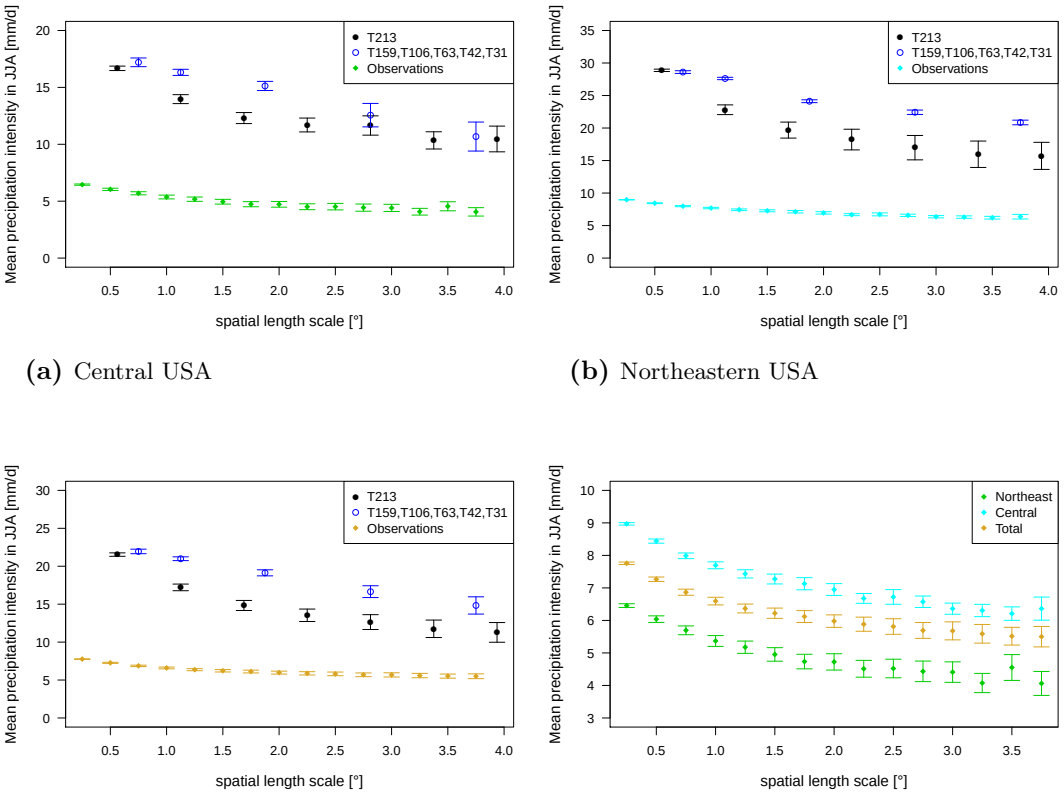

(a) Central USA **(b)** Northeastern USA

(c) Total USA **(d)** Observations

Figure 5.7: Area-averaged mean precipitation intensity of total JJA precipitation over the central USA (a), the northeastern USA (b) and the total USA (c) of ECHAM5 model output in the resolutions $T213_{1\times1}$ - $T213_{7\times7}$, T159, T106, T63, T42 and T31 and of the observational dataset NOAA CPC against spatial length scale. The error bars are the 95 % confidence interval of the area average. Note the different scales of the y-axes.

between four and five (see Figure 5.8 a - c and 5.9 a - c respectively). As observed in the UK, the decreasing scaling behaviour of the observational data (Figure 5.8 d and 5.9 d respectively) is qualitatively similar to $T213_{1\times1}$ - $T213_{7\times7}$. In JJA, the return values derived from model output as well as those derived from observational data decrease steeper for all shown regions than in DJF, indicating a lower spatial correlation length of precipitation events in JJA. This is generally expected over the USA as thunderstorms supply summer rainfall over almost the whole USA (Court, 1974, p. 226). In the central USA in winter

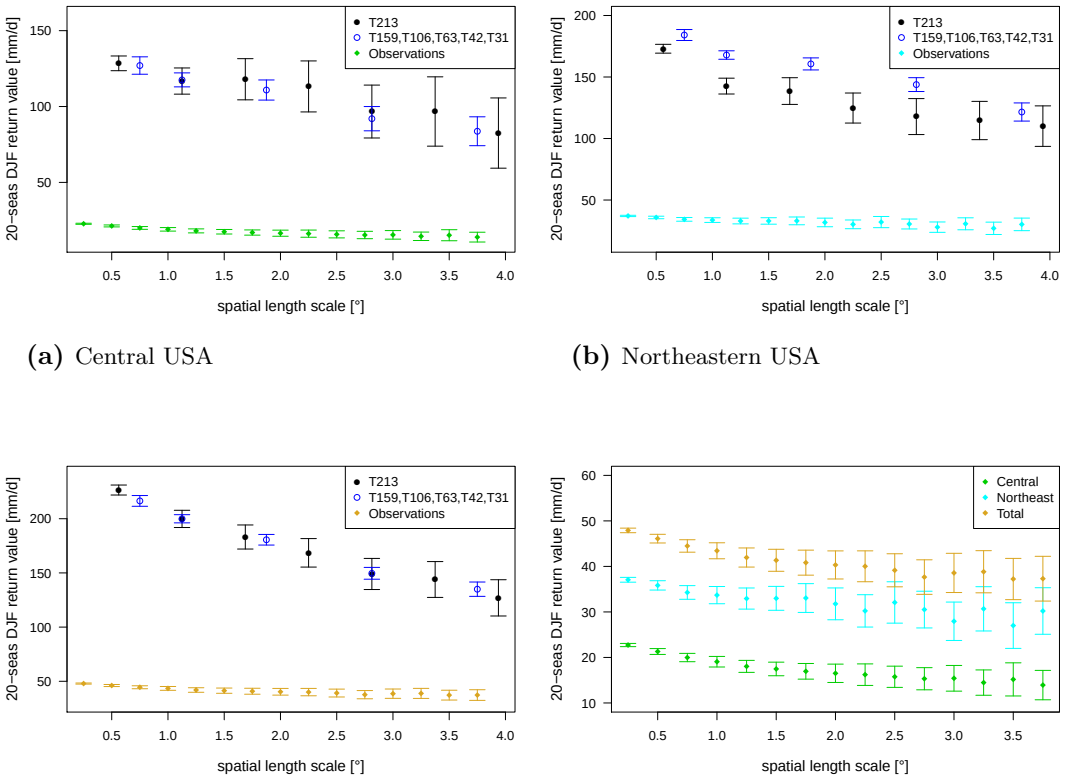

(a) Central USA

(b) Northeastern USA

(c) Total USA

(d) Observations

Figure 5.8: Area-averaged total precipitation 20 season DJF return values over the central USA (a), the northeastern USA (b) and the total USA (c) estimated from ECHAM5 model output in the resolutions $T213_{1\times1}$ - $T213_{7\times7}$, T159, T106, T63, T42 and T31, and estimated from the observational dataset NOAA CPC against spatial length scale and zoomed to the scaling behaviour of the observational return values only (d). The error bars are the 95 % confidence interval of the area average. Note the different scales of the y-axes.

precipitation is mainly due to warm and cold fronts (Court, 1974, p. 213), however, in summer the largest and most intense thunderstorms appear, tending to form in the lee of the Rocky Mountains and propagate eastward (Court, 1974, p. 227).

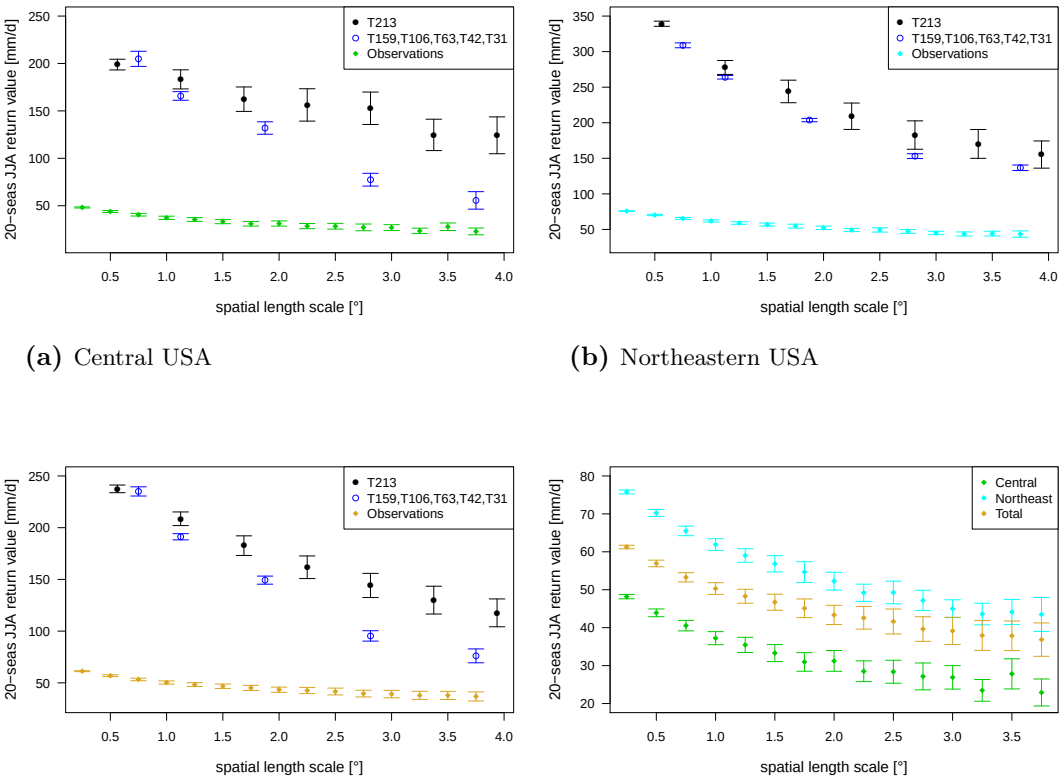

(a) Central USA

(b) Northeastern USA

(c) Total USA

(d) Observations

Figure 5.9: Area-averaged total precipitation 20 season JJA return values over the central USA (a), the northeastern USA (b) and the total USA (c) estimated from ECHAM5 model output in the resolutions $T213_{1\times1}$ - $T213_{7\times7}$, T159, T106, T63, T42 and T31, and estimated from the observational dataset NOAA CPC against spatial length scale and zoomed to the scaling behaviour of the observational return values only (d). The error bars are the 95 % confidence interval of the area average. Note the different scales of the y-axes.

5.3 Southeastern USA

Mean Precipitation Totals

Figure 5.10 shows the scaling behaviour of area-averages of mean precipitation totals over the southeastern USA of the averaged T213 resolutions $T213_{1\times1}$ - $T213_{7\times7}$, the coarser model resolutions T159 - T31 as well as of the observational data in DJF (a - b) and JJA (c - d). In the southeastern USA in DJF as well as in JJA the precipitation totals of

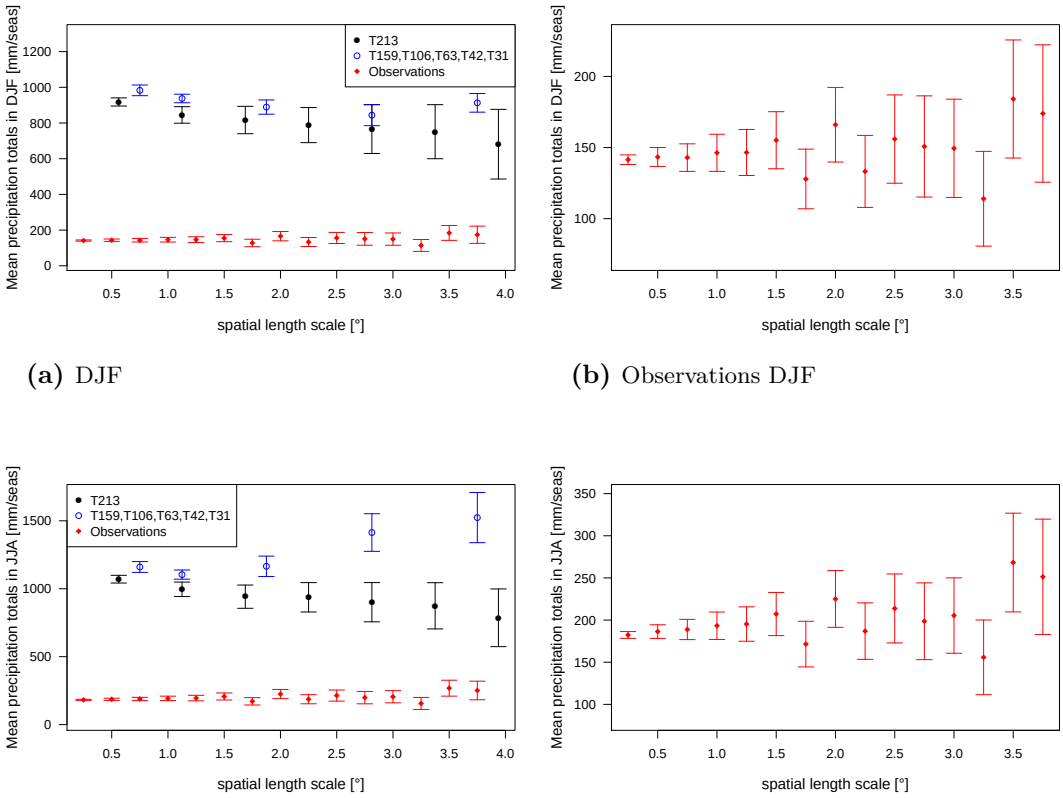

(a) DJF **(b)** Observations DJF

(c) JJA **(d)** Observations JJA

Figure 5.10: Area-averaged mean precipitation totals of total precipitation over the southeastern USA in DJF (a) and JJA (c) of ECHAM5 model output in the resolutions $T213_{1\times1}$ - $T213_{7\times7}$, T159, T106, T63, T42 and T31 and of the observational dataset NOAA CPC against spatial length scale and zoomed to the scaling behaviour of the observational mean precipitation totals in DJF (b) and JJA (d) only. The error bars are the 95 % confidence interval of the area average. Note the different scales of the y-axes.

$T213_{1\times1}$ - $T213_{7\times7}$ show a very shallow decreasing behaviour, however, the precipitation totals of the observations only show an enhanced variability with increasing grid box size. In DJF the precipitation totals of $T213_{1\times1}$ - T31 are only slightly varying, whereas in JJA the precipitation totals of T42 and T31 are considerably higher than the others (see Figure 5.10 c), indicating T42 and T31 being too coarse to represent precipitation totals in JJA in the southeastern USA. The precipitation totals in the southeastern USA are overestimated by ECHAM5 approximately by a factor of six, thus, the bias in precipitation totals in the southeastern USA is in the same range as in the other US regions.

Mean Precipitation Intensity

In Figure 5.11 the scaling behaviours of area-averages of the mean precipitation intensity over the southeastern USA of the averaged T213 resolutions $T213_{1\times1}$ - $T213_{7\times7}$, the coarser model resolutions T159 - T31 as well as of the observational data in DJF (a - b) and JJA (c - d) are provided. The mean precipitation intensity in DJF (see Figure 5.11 a) as well as in JJA (see Figure 5.11 c) is slightly decreasing with spatial scale in the southeastern USA in the averaged T213 resolutions $T213_{1\times1}$ - $T213_{7\times7}$ as well as in the coarser model resolutions $T213_{1\times1}$ - T31 of ECHAM5. The mean precipitation intensity of T159 - T31 stays slightly above the mean precipitation intensity of $T213_{1\times1}$ - $T213_{7\times7}$ in DJF. However, in JJA $T213_{1\times1}$ - T31 stay constantly on the same level whereas $T213_{1\times1}$ - $T213_{7\times7}$ show a decreasing scaling behaviour (see Figure 5.11 c). In DJF the mean precipitation intensity in the observations stays constant (see Figure 5.11 b) whereas in JJA the latter decreases shallow. Hence, the mean precipitation intensity in the southeastern USA is only slightly dependent on spatial scale. The bias in the mean precipitation intensity in the southeastern USA is higher than in other US regions, i.e. approximately a factor between five and eight. The amount of mean precipitation intensity in the observations is similar in DJF and JJA whereas the latter in ECHAM5 is considerably higher than in JJA, indicating that ECHAM5 is not able to simulate the seasonal cycle correctly in the southeastern USA.

Return Values

In Figure 5.12 the scaling behaviour of the 20 season return value of the decreasing T213 model resolutions $T213_{1\times1}$ - $T213_{7\times7}$ as well as of the model runs with coarser resolutions T159 - T31, compared to 20 season return values of observational data of the southeastern USA in DJF (a) as well as in JJA (c) are provided. In Figure 5.12 b and d only the

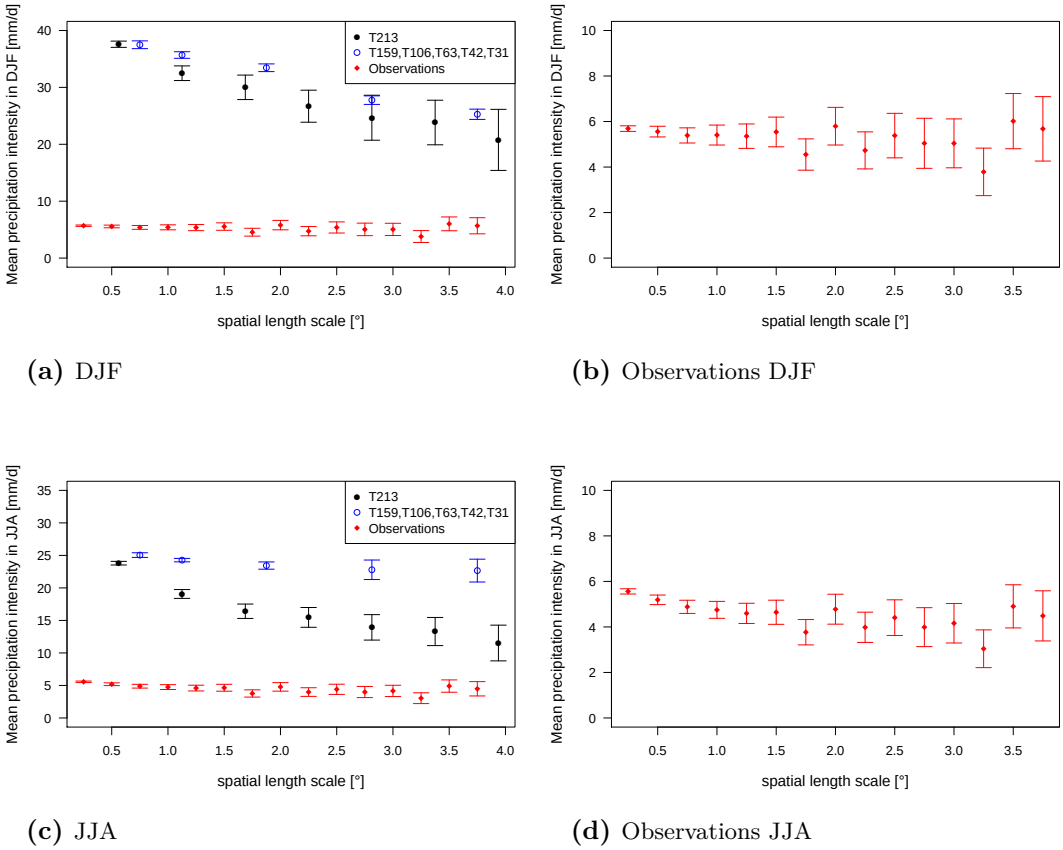

(a) DJF **(b)** Observations DJF

(c) JJA **(d)** Observations JJA

Figure 5.11: Area-averaged mean precipitation intensity of total precipitation over the southeastern USA in DJF (a) and JJA (c) of ECHAM5 model output in the resolutions $T213_{1\times1}$ - $T213_{7\times7}$, T159, T106, T63, T42 and T31 and of the observational dataset NOAA CPC against spatial length scale and zoomed to the scaling behaviour of the observational mean precpitation intensity in DJF (b) and JJA (d) only. The error bars are the 95 % confidence interval of the area average. Note the different scales of the y-axes.

observational return values of DJF and JJA respectively are shown. In the return values of the southeastern USA the bias is higher than in the other regions, namely the return values estimated from ECHAM5 model output are approximately between six and seven times higher than those derived from the observational dataset. Again, the averaged return values of the model output $T213_{1\times1}$ - $T213_{7\times7}$ look qualitatively similar to those of the observations in DJF as well as in JJA. For the comparison of the scaling behaviours of

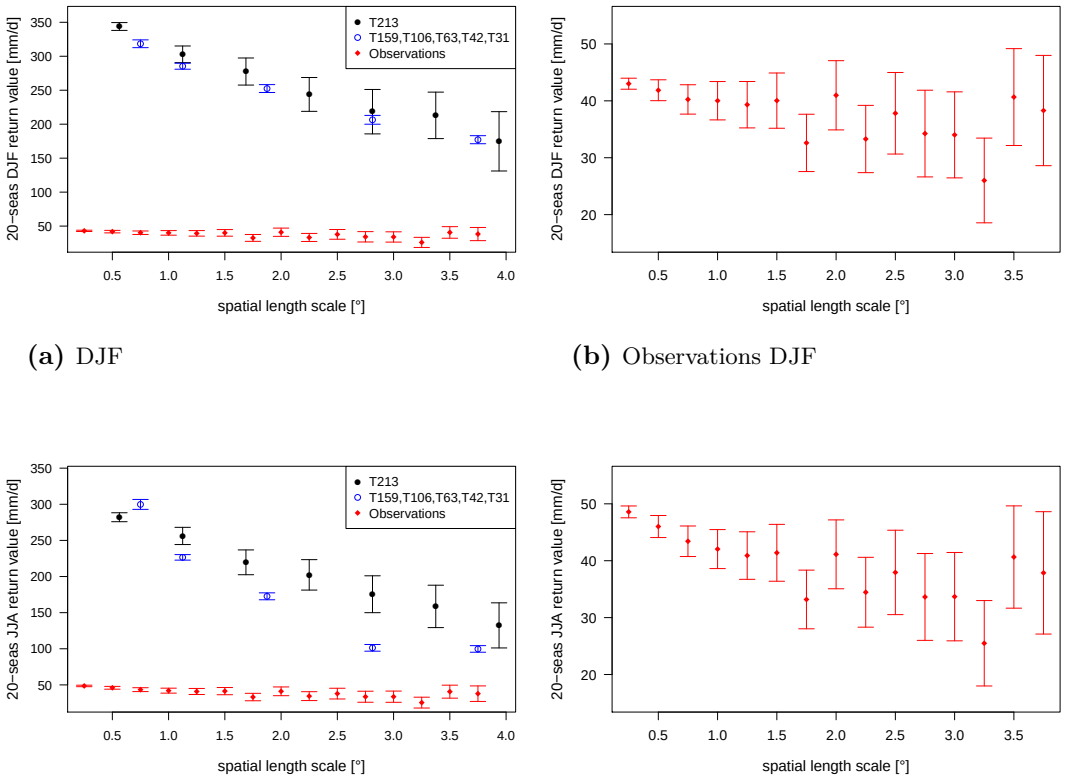

(a) DJF **(b)** Observations DJF

(c) JJA **(d)** Observations JJA

Figure 5.12: Area-averaged total precipitation 20 season return values over the southeastern USA in DJF (a) and JJA (c) estimated from ECHAM5 model output in the resolutions $T213_{1\times1}$ - $T213_{7\times7}$, T159, T106, T63, T42 and T31, and estimated from the observational dataset NOAA CPC against spatial length scale and zoomed to the scaling behaviour of the observational return values of DJF (b) and JJA (d) only. The error bars are the 95 % confidence interval of the area average. Note the different scales of the y-axes.

$T213_{1\times1}$ - $T213_{7\times7}$ and T159 - T31, see section 4.2. In contrast to the UK as well as to the other regions of the USA, the scaling behaviours of DJF and JJA are very similar for return values estimated from the model output as well as for those estimated from the observations. In JJA the scaling behaviour is only slightly steeper. However, in the model output the return values are higher in DJF than in JJA, although in T106 the return value in JJA is higher than in DJF. This is inconsistent with the observations. Thus, the model

was found to have a bias in this region in the seasonal cycle, at least in the high resolutions.

Most of the eastern third of the USA has no dominant month or season of precipitation (Court, 1974, p. 213). However, along the east coast, especially in the south, in the hurricane season from June-November 10-15 % of total rainfall are due to tropical cyclones, yielding very heavy precipitation events (Court, 1974, p. 225). Even though tropical cyclones are large scale phenomena over the ocean, they cover small spatial scales over land as they die quickly when they are cut off from their oceanic energy source (Emanuel, 2005, p. 57). These cyclones as well as summer thunderstorms explain the slightly steeper decreasing return values in JJA. Furthermore, the tropical cyclones are a possible explanation for the bias in the seasonal cycle. ECHAM5 might not be able to simulate the frequency and intensity of tropical cyclones correctly.

5.4 Discussion

The observation that precipitation totals do not show a scaling behaviour whereas return values do can be explained by the fact that return values are rare events of extremely high precipitation that are mainly due to low scale heavy precipitation. These rare events are only a very small part of total precipitation. Most precipitation is due to large scale fronts. In the UK only about 3 % of total precipitation over the whole year can be ascribed to thunderstorm rains (Manley, 1970, p. 119), however the amount of thunderstorms in summer is notably higher than in the rest of the year (Manley, 1970, p. 99). In the central USA 83 % of precipitation is due to frontal precipitation, however, these frontal effects are less in summer (Court, 1974, p. 213). At the east coast of the USA 10-15 % of total rainfall are due to tropical cyclones (Court, 1974, p. 225). If only the extremes are analysed, mainly these heavy events influence the results. In this study, the return values are estimated from seasonal maxima. It is likely that the highest seasonal event was on a small spatial scale. In contrast, its contribution to the respective precipitation total is low. Thus, for analyses of extremes higher resolutions are required than for the investigation of precipitation totals. Additionally, extremes can not be projected from precipitation totals as their scales are due to different physical processes. For example in the southeastern USA the bias in precipitation totals is similar to the bias in the other regions, even though the bias in the 20 season return values is notably higher than the bias in the other regions. The mean precipitation intensity seems to be independent on spatial scale in DJF and slightly dependent on spatial scale in JJA. This confirms the argumentation that in DJF the main

part of precipitation is due to large scale fronts, whereas in summer a considerable part of precipitation is due to small scale mechanisms, also influencing the mean precipitation intensity.

Various studies show that extreme precipitation is underestimated in AGCMs (see section 1.2) even when mean precipitation is realistically captured. In contrast, the model setup of ECHAM5, used in this study, overestimates extreme precipitation. However, in the central, the northeastern and the total USA precipitation totals are overestimated by a higher factor than precipitation extremes. In the southeastern USA the bias in precipitation totals and return values is similar. In the UK the bias of return values is slightly higher than in precipitation totals. Certainly, as only the UK and the USA were compared to observational datasets, the bias found in this regions cannot be extrapolated to other regions.

Hagemann et al. (2006) found the sensitivity to horizontal resolution of annual mean precipitation over land in ECHAM5 to be relatively low. This is consistent with the results of this study. In this study only in JJA even precipitation totals seem to be badly captured by T42 and T31 however. Hagemann et al. (2006) found precipitation in DJF to be overestimated along steep mountain slopes (Andes, Himalaya, Rocky Mountains), over Europe and in a region stretching from the southwestern USA to the west coast of South America. In JJA precipitation is too high at high northern latitudes (Canada and Siberia). Hence, Hagemann et al. (2006) found as well a tendency of ECHAM5 to overestimate precipitation in certain regions. However, the results of their study can not be directly compared to this study as their experiment covers a different time period (Hagemann et al., 2006). The model in their experiment is forced with observed sea surface temperature and sea ice concentrations like in this study. However, due to the different time period, the boundary forcing is slightly different. Hagemann et al. (2006) found precipitation being underestimated in some regions such as Australia and the rainforest climate in central Africa during the dry season. In this study only extremely heavy precipitation was analysed. Therefore, particularly dry regions were not studied.

Wehner et al. (2010) found the resolution $0.5°\times0.675°$ (similar to T213) of the finite volume dynamics version of the Community Atmospheric Model (fvCAM2) being a breakthrough resolution for the representation of extreme precipitation. On coarser resolutions the resolution itself limits extreme events rather than any model parameterisation effect (Wehner et al., 2010). $0.5°\times0.675°$ is found to still limit precipitation intensity, particularly for tropical cyclones (Wehner et al., 2010). However, their study only compares spatial patterns of the USA but no area averages or other regions (Wehner et al., 2010). In the

present study, it appears that tropical cyclones are not simulated correctly, especially in the high resolutions T213 and T159. For tropical cyclones T106 was identified to be the qualitatively most realistic resolution. However, in the other regions of the USA as well as the UK T63 was identified to be the minimal required model resolution. All resolutions analysed here are limited by resolution itself, namely the averaging effect. In the UK the spatial coherence of precipitation in T213 appears to be too low.

Roeckner et al. (2004) found higher resolutions of ECHAM5 not automatically reducing the systematic errors. However, there are indications that some individual processes are better captured at higher horizontal resolutions (Roeckner et al., 2004). This is consistent with this study. Bengtsson et al. (1995) found high resolution in ECHAM3 to be particularly important in the tropics. For example tropical cyclones are hardly resolved at T42 resolution but well captured in a T106 model simulation with respect to structure and frequency of occurence (Bengtsson et al., 1995). In this study, T106 appears to be the most appropriate resolution to represent tropical cyclones, however, enhanced resolutions than T106 yield worse results in the model setup of ECHAM5 analysed in this study.

6 Conclusion and Outlook

In this diploma thesis the impact of spatial resolution on the representation of present day extreme precipitation in terms of area-averages of return values in the AGCM ECHAM5 was investigated. The highest resolution T213 averaged to coarser grid sizes ($T213_{1\times1}$ - $T213_{7\times7}$) was compared to the coarser resolutions (T159 - T31) to analyse the scaling behaviour of return values as well as to distinguish between the averaging effect and the physical representation effect. Furthermore, the minimal required model resolution of ECHAM5 to represent extremes was sought after. The representation of extreme precipitation in terms of return values was found to be strongly dependent on model resolution. This result is consistent with Wehner et al. (2010) and Chen and Knutson (2008). No simple general relationship between area averages of the 20 season return value and the spatial length scale could be detected. Different qualitative scaling behaviours were found, varying dependent on region and season. Wehner (2004) already found the representation of return values being strongly dependent on the seasonal cycle. However, the regional differences were not studied before. The only obvious common feature of all regions and seasons is that the 20 season return value decreases as expected with increasing grid box size. The scaling behaviour of the area-averages shows that on lower resolutions than T63 the scaling behaviour of 20 season return values changes qualitatively. Thus, T63 is is the model resolution that is minimally required to represent extremes, although higher model resolutions than T63 certainly improve the result. This is confirmed by the patterns of return values over Europe. The varying scaling behaviours indicate that results from different resolutions are not directly comparable. If extreme precipitation of different resolutions is compared, it should only be done with respect to spatial scale as suggested by Chen and Knutson (2008). Additionally, the respective region and season should be taken into account. When comparing annual return values, differences in the return values could also be due to the extreme event being located in a different season and therefore due to a different process. The performance of ECHAM5 in simulating extreme precipitation is dependent on season and region. A possible explanation is that model performance could

depend on the responsible physical process and its associated spatial scale, and different processes are important depending on region.

Furthermore, area-averages of mean precipitation totals, the mean precipitation intensity as well as of return values, derived from the ECHAM5 model output of the resolutions $T213_{1\times1}$ - $T213_{7\times7}$ as well as T159 - T31 were compared to area-averages of mean precipitation totals, the mean precipitation intensity and of return values estimated from observational datasets of the UK and the USA in order to examine the performance of ECHAM5 and to identify whether a general relationship exists that would allow to rescale heavy precipitation to higher resolutions. The observational indices were compared to the indices of ECHAM5 with respect to spatial scale. Precipitation return values, precipitation totals as well as the mean precipitation intensity of the model ECHAM5 were found to have a bias over the UK as well as over the USA. This result is in accordance with Hagemann et al. (2006), who found ECHAM5 to overestimate mean precipitation. Many GCMs were found in previous studies (for example Chen and Knutson (2008), Sun et al. (2006), Min et al. (2011), Allan and Soden (2008), Wehner et al. (2010)) to underestimate extreme precipitation. In contrast, extreme precipitation was found to be overestimated by ECHAM5 in this study. The ratio between the bias in precipitation totals and the bias in return values is regionally varying. In the UK the bias in the area-averaged return values exceeds the bias in the area-averaged total precipitation whereas in the southeastern USA the bias in return values is similar to the bias in precipitation totals. In the remaining USA regions the bias in precipitation totals exceeds the bias in return values. This shows that the performance of ECHAM5 in simulating precipitation characteristics is regionally varying. Regional differences in the performance of ECHAM5 to simulate the hydrological cycle were also found by Hagemann et al. (2006). Wehner et al. (2010) found $0.5°\times0.675°$ (similar to T213) of the fvCAM2 to be a breakthrough resolution for the representation of patterns of return values over the USA by validating the latter with observational patterns of return values. In this experiment T63 was found to be the minimally required resolution by comparing qualitative scaling behaviours of area-averages. The model ECHAM5 was found to be generally able to reproduce the qualitative scaling behaviour of return values. However, the highest resolutions T213 and T159 were found to simulate the seasonal cycle in the southeastern USA incorrectly. This might be due to a lack in the ability of ECHAM5 to simulate the tropical storms correctly in high resolutions. The fact that higher resolutions not automatically reduce systematic errors in ECHAM5 was also found by Roeckner et al. (2004). Kharin et al. (2007) stated that the very large intermodel disagreements in the

tropics suggest that some physical processes associated with extreme precipitation are not well represented in models, which is confirmed by this study. Precipitation totals were found to be independent on spatial scale. This is consistent with Hagemann et al. (2006). A simple general law to rescale heavy precipitation events to higher resolutions could not be identified. This is very likely due to regionally and seasonally different underlying processes.

Finally, the E-OBS dataset of Haylock et al. (2008), which was designed to evaluate regional climate models, was also validated with the UKMO dataset. The E-OBS dataset was found to be inappropriate for the validation of extreme precipitation in climate models over the UK in JJA. However, in DJF the E-OBS dataset shows realistic return values compared to the UKMO dataset. Mean precipitation totals in the E-OBS and the UKMO dataset are not significantly different. The applicability of the E-OBS precipitation dataset was already qestioned previously by Hofstra et al. (2009) and Maraun et al. (2011). In the E-OBS dataset the representation of return values is dependent on the spatial correlation length of the responsible events. This is due to not enough rain gauges being included in the E-OBS dataset to capture small scaled heavy precipitation extremes.

Outlook

In order to gain more information on the performance of ECHAM5 in simulating precipitation extremes, more regions, especially the tropics should be validated with observational datasets. For this purpose, gridded datasets with a high density of rain gauges are required. The availability of such datasets will limit furhter studies. To increase available possibilities for the validation of model results, an analysis would be useful, which tackles the question whether area-averaged precipitation indices derived from station data could be used to validate model data in regions, where no gridded dataset is provided. For this purpose, the minimum rain gauge density in this area-average has to be identified. Furthermore, the minimal required density of rain gauges in gridded datasets should be investigated.

Since no simple relationship could be identified to describe the scaling behaviour of extreme precipitation, it can be examined whether more sophisticated functions are able to describe the scaling behaviour of extreme precipitation. Such a function would yield a cheap and straightforward downscaling method that could be applied in cases where a better downscaling approach is not available. However, the complicated relationships influencing extreme precipitation will render it difficult, if not impossible to find such a function. This function must be dependent on at least region, season and spatial scale. Further

understanding has to be gained on factors and processes influencing the representation of extreme precipitation such as different time scales. In this study, only the dependence of extreme precipitation on spatial scales is analysed. Extreme precipitation is also dependent on time scales. On the one hand, very extreme events often happen on small time scales, on the other hand severe flooding can be due to rainfall that is not extreme in one event whereas it is extreme by covering a longer time period. To improve the understanding of the dependence of extreme weather events on spatial scale, more weather parameters should be studied such as extreme wind speeds.

To gain a better understanding of regional and seasonal dependence of the spatial scaling behaviour, the spatial pattern of the scaling behaviour of extreme precipitation will be analysed seasonwise. A seasonal shift in the patterns is expected to yield further understanding of responsible processes. In preparation for this analysis a scan of the performance of this method is given in Figure 6.1.

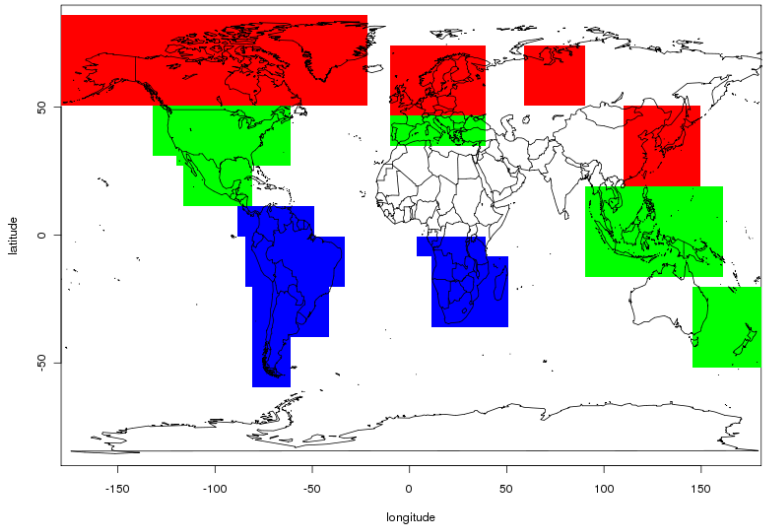

(a) DJF

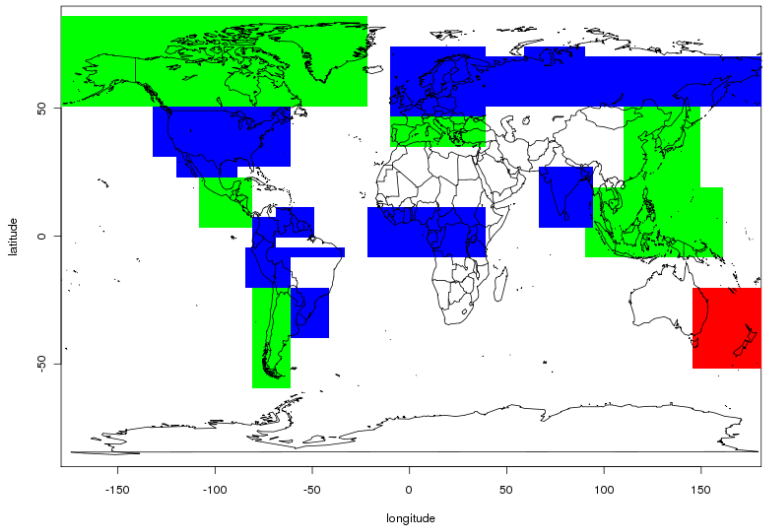

(b) JJA

Figure 6.1: Scan of the performance of the method to study seasonal shifts in spatial patterns of the spatial scaling behaviour of area-averages of return values for DJF (a) and JJA (b). For this purpose, a linear regression of the $T213_{1\times1}$ - $T213_{7\times7}$ as well as of the T213 - T31 curve in each studied region was carried out. The slopes of both regressions were compared. If the slope of T213 - T31 is equal to the slope of $T213_{1\times1}$ - $T213_{7\times7}$ $\pm$ 20 % they are assumed to be equal (green). If the slope of T213 - T31 exceeds the slope of $T213_{1\times1}$ - $T213_{7\times7}$ in more than 20 %, it was considered to be higher, i.e. flatter (red). If the slope of T213 - T31 is more than 20 % lower than the slope of $T213_{1\times1}$ - $T213_{7\times7}$, it is considered to be lower, i.e. steeper (blue). This method will be further developed such that more increments and smaller regions will be used.

Acknowledgements

Place of work for this diploma thesis was the Helmholtz Centre for Ocean Research (GEOMAR) in Kiel. I would like to thank Prof. Dr. Mojib Latif, Head of Department of Marine Meteorology, for giving me the opportunity to work on this very intersting topic and for institutional support as well as fruitful discussions. I thank Prof. Dr. Douglas Maraun, Dr. Vladimir Semenov and Prof. Dr. Otto Richter for supervising my thesis and for valuable feedback and helpful suggestions and discussions. I wish to thank Dr. Vladimir Semenov, Wan-Ling Tseng and Prof. Dr. Noel Keenlyside for running ECHAM5 in different resolutions and support in post processing of model output.

Dr. Peter Stott from the UK Met Office is acknowledged for providing the high resolution UKMO precipitation dataset of the UK. CPC US Unified Precipitation data are provided by the NOAA/OAR/ESRL PSD, Boulder, Colorado, USA, from their Web site at http://www.esrl.noaa.gov/psd/. I acknowledge the E-OBS dataset from the EU-FP6 project ENSEMBLES (http://ensembles-eu.metoffice.com) and the data providers in the ECA&D project (http://eca.knmi.nl). Warm regards and thanks to colleagues of the Dept. of Marine Meteorology for fruitful discussions and the very nice working climate. A special thanks here to Ana and Yann for the nice office atmosphere. Thanks to Leo, the online dictionary. I thank my parents for supporting and funding me during my whole studies.

Bibliography

Alexander, L. V.; Zhang, X.; Peterson, T. C.; Caesar, J.; Gleason, B.; Klein Tank, a. M. G.; Haylock, M.; Collins, D.; Trewin, B.; Rahimzadeh, F.; Tagipour, A.; Rupa Kumar, K.; Revadekar, J.; Griffiths, G.; Vincent, L.; Stephenson, D. B.; Burn, J.; Aguilar, E.; Brunet, M.; Taylor, M.; New, M.; Zhai, P.; Rusticucci, M. and Vazquez-Aguirre, J. L. 2006. Global observed changes in daily climate extremes of temperature and precipitation. Journal of Geophysical Research, **111**(D05109).

Allan, Richard P and Soden, Brian J. 2008. Atmospheric warming and the amplification of precipitation extremes. Science (New York, N.Y.), **321**(5895), 1481–4.

Allen, Myles R and Ingram, William J. 2002. Constraints on future changes in climate and the hydrologic cycle. Nature, **419**(6903), 224–32.

Bengtsson, L; Botzet, M and Esch, M. 1995. Hurricane-type vortices in a general circulation model. Tellus, **47 A.**(2), 175–196.

Chen, Cheng-Ta and Knutson, Thomas. 2008. On the verification and comparison of extreme rainfall indices from climate models. Journal of Climate, **21**(7), 1605–1621.

Coles, Stuart. 2004. An introduction to statistical modeling of extreme values. London: Springer-Verlag.

Court, A. 1974. The Climate of the Conterminous United States. Chap. 3, pages 193–343 In: Landsberg, H.E:; Bryson, R.A. and Hare, F.K. (Editor), World Survey of Climatology Volume 11. Amsterdam, London, New York: Elsevier.

Duffy, P. B.; Govindasamy, B.; Iorio, J. P.; Milovich, J.; Sperber, K. R.; Taylor, K. E.; Wehner, M. F. and Thompson, S. L. 2003. High-resolution simulations of global climate, part 1: present climate. Climate Dynamics, **21**(5-6), 371–390.

Emanuel, K. 2005. Divine Wind: the history and science of hurricanes. Oxford University Press.

Emori, S. and Brown, Simon J. 2005. Dynamic and thermodynamic changes in mean and extreme precipitation under changed climate. Geophysical Research Letters, **32**(L17706).

Furrer, Reinhard; Nychka, Douglas and Sain, Stephen. 2010. fields: Tools for spatial data. R package version 6.3.

Greenwood, J Arthur; Landwehr, J M; Matalas, N C and Wallis, J R. 1979. Probability Weighted Moments: Definition and Relation to Parameters of Several Distributions Expressable in Inverse Form. Water Resources Research, **15**(5), 1049–1054.

Groisman, P.Y.; Knight, R.W.; Easterling, D.R.; Karl, T.R.; Hegerl, G.C. and Razuvaev, V.N. 2005. Trends in intense precipitation in the climate record. Journal of Climate, **18**(9), 1326–1350.

Grumbine, et al. Sea ice cover data. NOAA. http://polar.ncep.noaa.gov/seaice/.

Hack, J J. 1992. Climate system simulation: basic numerical & computational concepts. Chap. 9, pages 283–317 In: Trenberth, K (Editor), Climate system modeling. Cambridge University Press.

Hagemann, S; Arpe, K and Roeckner, E. 2006. Evaluation of the hydrological cycle in the ECHAM5 model. Journal of climate, **19**(16), 3810–3827.

Haylock, M. R.; Hofstra, N.; Klein Tank, a. M. G.; Klok, E. J.; Jones, P. D. and New, M. 2008. A European daily high-resolution gridded data set of surface temperature and precipitation for 1950–2006. Journal of Geophysical Research, **113**(D20119), 1–12.

Henderson-Sellers, A and McGuffie, K. 1987. A climate modelling primer. John Wiley & Sons Ltd.

Higgins, RW; Shi, W; Yarosh, E and Joyce, R. 2000. Improved US Precipitation Quality Control System and Analysis. NCEP/Climate Prediction Center ATLAS No. 7, National Centers for Environmental Prediction, Climate Prediction Center, Camp Springs, Maryland. Available at http://www.cpc.ncep.noaa.gov/research.

Hofstra, Nynke; Haylock, Malcolm; New, Mark and Jones, Phil D. 2009. Testing E-OBS European high-resolution gridded data set of daily precipitation and surface temperature. Journal of Geophysical Research, **114**(D21101).

Hosking, JRM; Wallis, J.R. and Wood, EF. 1985. Estimation of the generalized extreme-value distribution by the method of probability-weighted moments. Technometrics, **27**(3), 251–261.

Iorio, J.P.; Duffy, P.B.; Govindasamy, B.; Thompson, S.L.; Khairoutdinov, M. and Randall, D. 2004. Effects of model resolution and subgrid-scale physics on the simulation of precipitation in the continental United States. Climate Dynamics, **23**(3-4), 243–258.

Kharin, Viatcheslav V.; Zwiers, Francis W.; Zhang, Xuebin and Hegerl, Gabriele C. 2007. Changes in temperature and precipitation extremes in the IPCC ensemble of global coupled model simulations. Journal of Climate, **20**(8), 1419–1444.

Kharin, VV and Zwiers, FW. 2005. Intercomparison of near-surface temperature and precipitation extremes in AMIP-2 simulations, reanalyses, and observations. Journal of Climate, **18**(24), 5201–5223.

Kiehl, J T. 1992. Atmospheric general circulation modeling. Chap. 10, pages 319–368 In: Trenberth, K E (Editor), Climate system modeling. Cambridge University Press.

Landwehr, J.M.; Matalas, NC and Wallis, JR. 1979. Probability weighted moments compared with some traditional techniques in estimating Gumbel parameters and quantiles. Water Resources Research, **15**(5), 1055–1064.

Latif, M. 2009. Klimawandel und Klimadynamik. Stuttgart: Eugen Ulmer.

Le Treut, H.; Cubasch, U and Allen, M. 2007. Historical Overview of Climate Change Science. Chap. 1, pages 93–128 In: Solomon, S.; Qin, D; Manning, M; Marquis, M; Averyt, K B; Tignor, M; Miller, H L and Chen, Z (Editor), Climate Change 2007: The Physical Science Basis. Contribution of Working Group I to the Fourth Assessment Report of the Intergovernmental Panel on Climate Change. Cambridge, United Kingdom and New York, NY, USA: Cambridge University Press.

Lorenz, E.N. 1970. Climatic change as a mathematical problem. Journal of Applied Meteorology, **9**(3), 325–329.

Manley, G. 1970. The Climate of the British Isles. pages 81–133 In: Landsberg, H.E.; Bryson, R.A.; Flohn, H.; Gentilli, J.; Arakawa, H; Griffiths, J.F.; Lydolph, P.E.; Orvig, S.; Rex, D.F.; Schwerdtfeger, W.; Thomsen, H. and Wallen, C. C. (Editor), World Survey of Climatology Volume 5. Amsterdam, London, New York: Elsevier.

Maraun, Douglas; Osborn, Timothy J. and Rust, Henning W. 2011. The influence of synoptic airflow on UK daily precipitation extremes. Part II: regional climate model and E-OBS data validation. Climate Dynamics, **36**(1-2), 261–275.

Meehl, Gerald A; Arblaster, J M and Tebaldi, C. 2005. Understanding future patterns of increased precipitation intensity in climate model simulations. Geophysical Research Letters, **32**(18).

Min, Seung-Ki; Zhang, Xuebin; Zwiers, Francis W and Hegerl, Gabriele C. 2011. Human contribution to more-intense precipitation extremes. Nature, **470**(7334), 378–81.

Osborn, TJ and Hulme, M. 1997. Development of a relationship between station and grid-box rainday frequencies for climate model evaluation. Journal of Climate, **10**(8), 1885–1908.

Perry, Matthew; Hollis, Dan and Elms, Margaret. 2009. The generation of daily gridded datasets of temperature and rainfall for the UK. Climate Memorandum, **No 24**.

R Development Core Team. 2011. R: A Language and Environment for Statistical Computing. R Foundation for Statistical Computing, Vienna, Austria. ISBN 3-900051-07-0.

Randall, D.A.; Wood, R.A.; Bony, S.; Colman, R.; Fichefet, T.; Fyfe, J.; Kattsov, V.; Pitman, A.; Shukla, J.; Srinivasan, J. and Others. 2007. Climate models and their evaluation. Chap. 8, pages 589–662 In: Solomon, S.; Qin, D.; Manning, M.; Chen, Z.; Marquis, M.; Averyt, K.B.; Tignor, M. and Miller, H.L. (Editor), Climate Change 2007: The Physical Science Basis. Contribution of Working Group I to the Fourth Assessment Report of the Intergovernmental Panel on Climate Change, vol. 323. Cambridge, United Kingdom and New York, NY, USA: Cambridge University Press Cambridge, UK and New York.

Reynolds, Richard W.; Smith, Thomas M.; Liu, Chunying; Chelton, Dudley B.; Casey, Kenneth S. and Schlax, Michael G. 2007. Daily High-Resolution-Blended Analyses for Sea Surface Temperature. Journal of Climate, **20**(22), 5473–5496.

Roeckner, E; Bäuml, G; Bonaventura, L; Brokopf, R; Esch, M; Giorgetta, M; Hagemann, S; Kirchner, I; Kornblueh, L; Manzini, E; Rhodin, A; Schlese, U; Schulzweida, U and Tompkins, A. 2003. The atmospheric general circulation model ECHAM5. Part I: Model description. In: Rep. 349, vol. No. 349. Hamburg, Germany: Max-Planck-Institute for Meteorology.

Roeckner, E; Brokopf, R; Esch, M; Giorgetta, M; Hagemann, S; Kornblueh, L; Manzini, E; Schlese, U and Schulzweida, U. 2004. The atmospheric general circulation model ECHAM5 - Part II : Sensitivity of simulated climate to horizontal and vertical resolution. In: Rep. 354, vol. No. 354. Hamburg, Germany: Max-Planck-Institute for Meteorology.

Russo, Simone and Sterl, Andreas. 2012. Global changes in seasonal means and extremes of precipitation from daily climate model data. Journal of Geophysical Research, **117**(November 2011).

Schlünzen, K. Heinke; Grawe, David; Bohnenstengel, Sylvia I.; Schlüter, Ingo and Koppmann, Ralf. 2011. Joint modelling of obstacle induced and mesoscale changes—Current limits and challenges. Journal of Wind Engineering and Industrial Aerodynamics, **99**(4), 217–225.

Semenov, V and Bengtsson, L. 2002. Secular trends in daily precipitation characteristics: greenhouse gas simulation with a coupled AOGCM. Climate Dynamics, **19**(2), 123–140.

Simmons, AJ; Burridge, DM; Jarraud, M; Girard, C and Wergen, W. 1989. The ECMWF medium-range prediction models development of the numerical formulations and the impact of increased resolution. Meteorology and Atmospheric Physics, **40**(1), 28–60.

Sun, Y.; Solomon, S.; Dai, A. and Portmann, R.W. 2006. How often does it rain? Journal of Climate, **19**(6), 916–934.

Trenberth, K.E. 1999. Conceptual framework for changes of extremes of the hydrological cycle with climate change. Climatic Change, **42**(1), 327–339.

Wehner, M.F. 2004. Predicted twenty-first-century changes in seasonal extreme precipitation events in the parallel climate model. Journal of climate, **17**(21), 4281–4290.

Wehner, Michael F.; Smith, Richard L.; Bala, G. and Duffy, Phillip. 2010. The effect of horizontal resolution on simulation of very extreme US precipitation events in a global atmosphere model. Climate Dynamics, **34**(2-3), 241–247.

Wuertz, Diethelm; many others and see the SOURCE file. 2009. fExtremes: Rmetrics - Extreme Financial Market Data. R package version 2100.77.

A Tables of Resolutions

Table A.1: Resolutions used in this study of the model ECHAM5.

Denotation	Gaussian grid box size [°×°]
ECHAM5	
$T213_{1\times1}$	0.56×0.56
$T213_{2\times2}$	1.125×1.125
$T213_{3\times3}$	1.69×1.69
$T213_{4\times4}$	2.25×2.25
$T213_{5\times5}$	2.81×2.81
$T213_{6\times6}$	3.38×3.38
$T213_{7\times7}$	3.94×3.94
T159	0.75×0.75
T106	1.13×1.13
T63	1.88×1.88
T42	2.81×2.81
T31	3.75×3.75

Table A.2: Resolutions used in this study of the UKMO observational dataset.

Denotation	Gaussian grid box size [°×°]
UKMO	
$\text{UKMO}_{1\times1}$	0.045×0.078
$\text{UKMO}_{2\times2}$	0.090×0.156
$\text{UKMO}_{3\times3}$	0.135×0.234
$\text{UKMO}_{4\times4}$	0.180×0.312
$\text{UKMO}_{5\times5}$	0.225×0.390
$\text{UKMO}_{7\times7}$	0.315×0.546
$\text{UKMO}_{10\times10}$	0.450×0.780
$\text{UKMO}_{15\times15}$	0.675×1.17
$\text{UKMO}_{20\times20}$	0.900×1.56
$\text{UKMO}_{25\times25}$	1.13×1.95
$\text{UKMO}_{30\times30}$	1.35×2.34
$\text{UKMO}_{35\times35}$	1.58×2.73
$\text{UKMO}_{40\times40}$	1.80×3.12
$\text{UKMO}_{45\times45}$	2.03×3.51

Table A.3: Resolutions used in this study of the E-OBS observational dataset.

Denotation	Gaussian grid box size [°×°]
E-OBS	
$\text{E-OBS}_{1\times1}$	0.25×0.25
$\text{E-OBS}_{2\times2}$	0.5×0.5
$\text{E-OBS}_{3\times3}$	0.75×0.75
$\text{E-OBS}_{4\times4}$	1×1
$\text{E-OBS}_{5\times5}$	1.25×1.25
$\text{E-OBS}_{6\times6}$	1.5×1.5
$\text{E-OBS}_{7\times7}$	1.75×1.75
$\text{E-OBS}_{8\times8}$	2.×2
$\text{E-OBS}_{9\times9}$	2.25×2.25
$\text{E-OBS}_{10\times10}$	2.5×2.5
$\text{E-OBS}_{11\times11}$	2.75×2.75

Table A.4: Resolutions used in this study of the CPC US Unified Precipitation observational dataset.

Denotation	Gaussian grid box size [°×°]
USA	
$USA_{1\times1}$	0.25×0.25
$USA_{2\times2}$	0.5×0.5
$USA_{3\times3}$	0.75×0.75
$USA_{4\times4}$	1×1
$USA_{5\times5}$	1.25×1.25
$USA_{6\times6}$	1.5×1.5
$USA_{7\times7}$	1.75×1.75
$USA_{8\times8}$	2.×2
$USA_{9\times9}$	2.25×2.25
$USA_{10\times10}$	2.5×2.5
$USA_{11\times11}$	2.75×2.75
$USA_{12\times12}$	3×3
$USA_{13\times13}$	3.25×3.25
$USA_{14\times14}$	3.5×3.5
$USA_{15\times15}$	3.75×3.75

B Area Averaged Return Values

In appendix B the Figures referred to in section 4.2 are given.

B.1 Total Precipitation

Main Scaling Behaviours

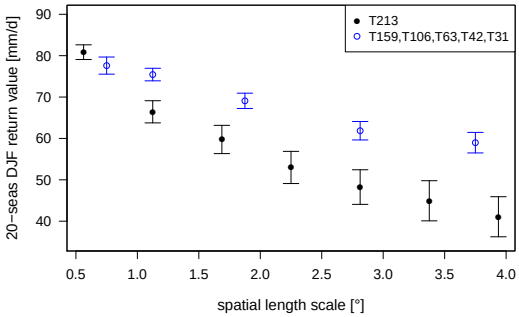

(a) Canada-Alaska-Greenland DJF

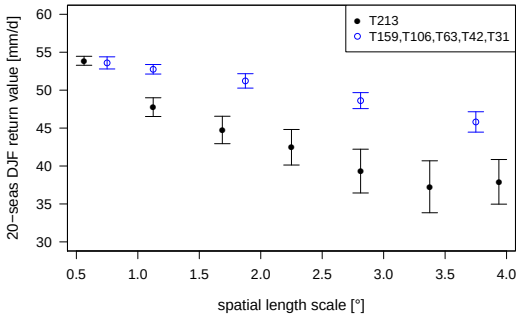

(b) Western Siberia DJF

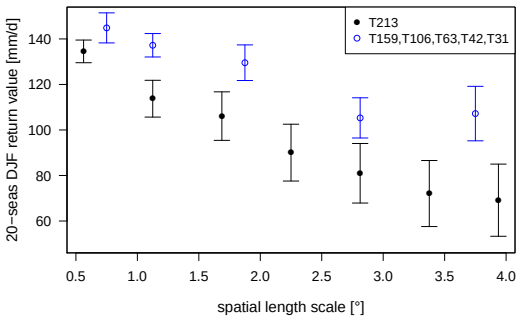

(c) Eastern Asia DJF

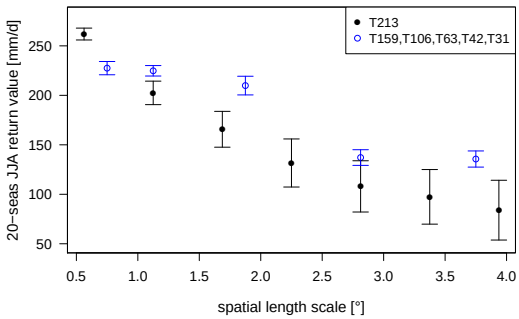

(d) Eastern Australia-New Zealand JJA

Figure B.1: Area-averaged total precipitation 20 season return values over Canada-Alaska-Greenland in DJF (a), Western Siberia in DJF (b), Eastern Asia in DJF (c) and Eastern Australia-New Zealand in JJA (d) in JJA estimated from ECHAM5 model output in the resolutions $T213_{1\times1}$ - $T213_{7\times7}$, T159, T106, T63, T42 and T31 against spatial length scale. The error bars are the 95 % confidence interval of the area average. Note the different scales of the y-axes. The scaling behaviours are similar to northern Europe and the northeastern USA in DJF shown in section 4.2.

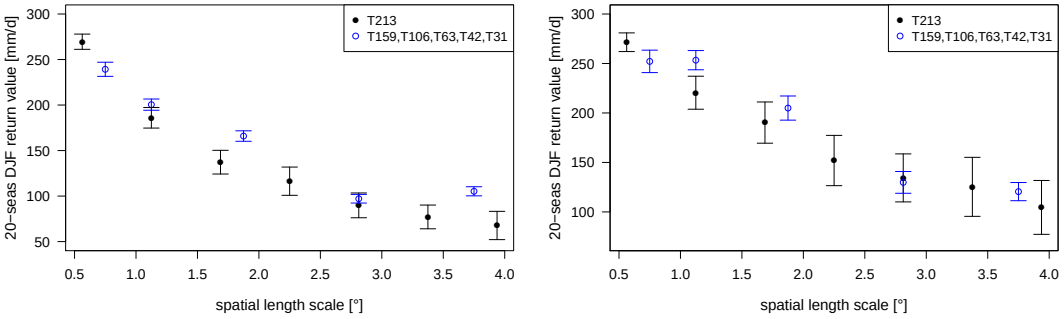

(a) Indonesia DJF **(b)** Central America DJF

Figure B.2: Area-averaged total precipitation 20 season return values over Indonesia in DJF (a) and Central America in DJF (b) estimated from ECHAM5 model output in the resolutions $T213_{1\times1}$ - $T213_{7\times7}$, T159, T106, T63, T42 and T31 against spatial length scale. The error bars are the 95 % confidence interval of the area average. Note the different scales of the y-axes. The scaling behaviours are similar to eastern Australia-New Zealand in DJF and the southeastern USA in DJF shown in section 4.2.

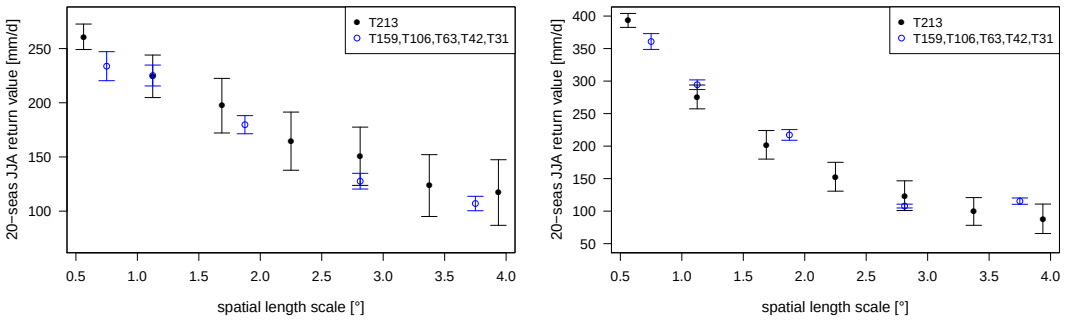

(a) Southwestern South America JJA **(b)** Southern Europe JJA

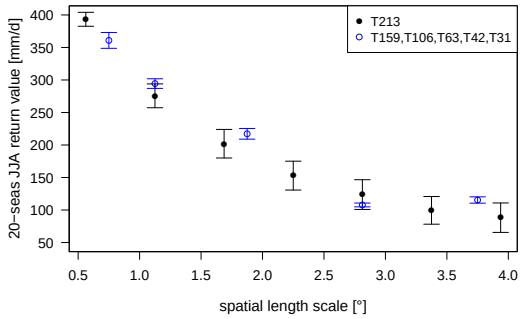

(c) Indonesia JJA

Figure B.3: Area-averaged total precipitation 20 season return values over southwestern South America in JJA (a), southern Europe in JJA (b) and Indonesia in JJA estimated from ECHAM5 model output in the resolutions $T213_{1\times1}$ - $T213_{7\times7}$, T159, T106, T63, T42 and T31 against spatial length scale. The error bars are the 95 % confidence interval of the area average. Note the different scales of the y-axes. The scaling behaviour is similar to eastern Australia-New Zealand in DJF and the southeastern USA in DJF shown in section 4.2.

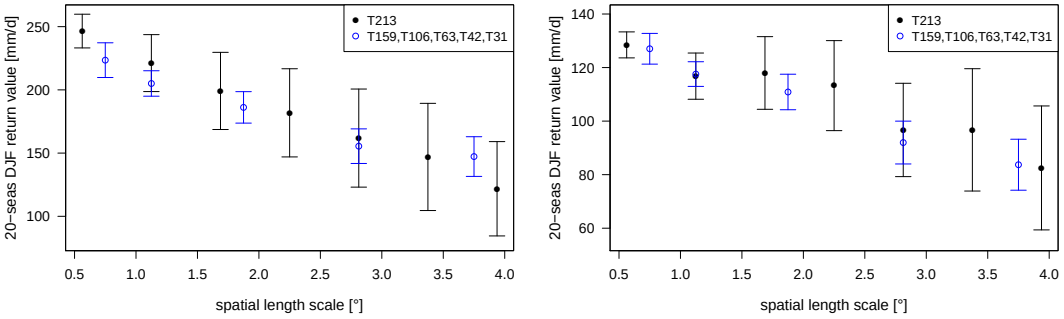

(a) Western USA DJF **(b)** Central USA DJF

Figure B.4: Area-averaged total precipitation 20 season return values over the western USA in DJF (a) and the central USA in DJF (b) estimated from ECHAM5 model output in the resolutions $T213_{1\times1}$ - $T213_{7\times7}$, T159, T106, T63, T42 and T31 against spatial length scale. The error bars are the 95 % confidence interval of the area average. Note the different scales of the y-axes. The scaling behaviours are similar to eastern Australia-New Zealand in DJF and the southeastern USA in DJF shown in section 4.2.

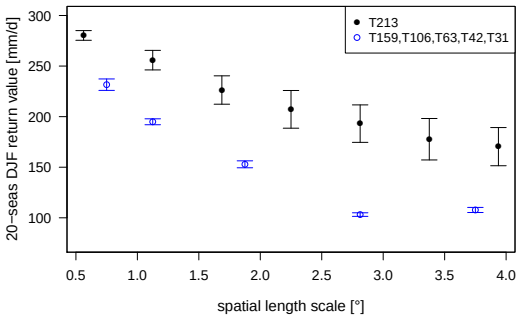

(a) Central Africa DJF

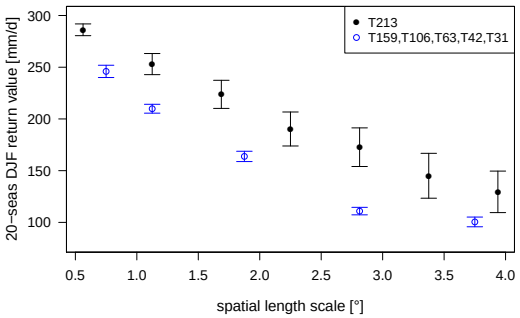

(b) Southern Africa DJF

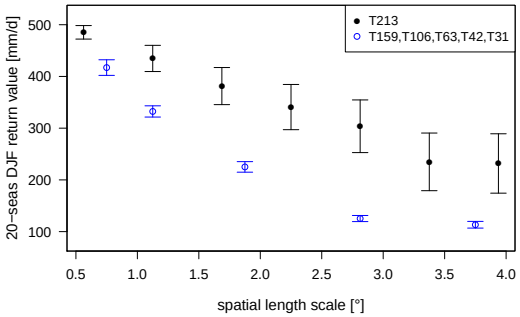

(c) Peru-Bolivia-Ecuador DJF

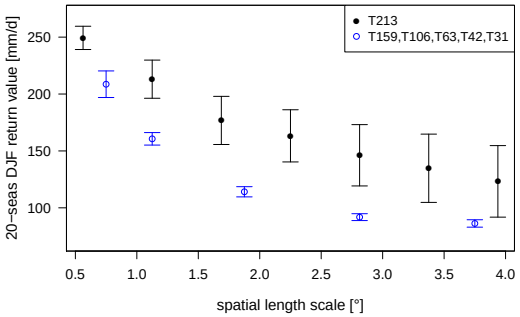

(d) Northern South America-southern Central America DJF

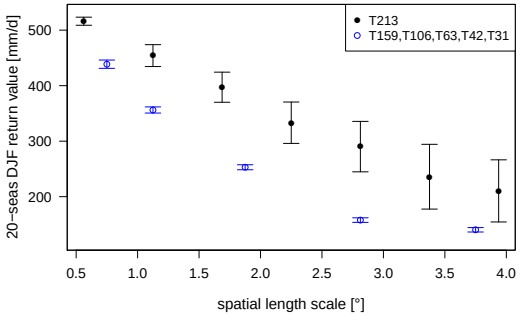

(e) Southeastern South America DJF

Figure B.5: Area-averaged total precipitation 20 season return values over central Africa in DJF (a), southern Africa in DJF (b), Peru-Bolivia-Ecuador in DJF (c), northern South America-southern Central America in DJF (d) and southeastern South America in DJF (e) estimated from ECHAM5 model output in the resolutions $T213_{1\times1}$ - $T213_{7\times7}$, T159, T106, T63, T42 and T31 against spatial length scale. The error bars are the 95 % confidence interval of the area average. Note the different scales of the y-axes. The scaling behaviours are similar to the Amazon region in DJF and southwestern South America in DJF shown in section 4.2.

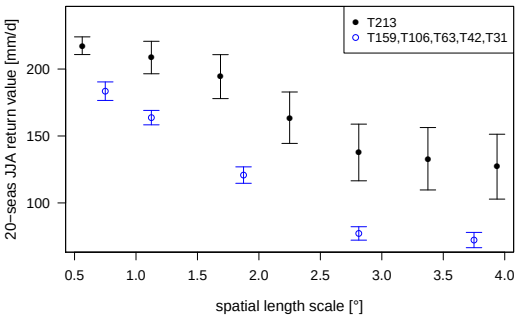

(a) Central Africa JJA

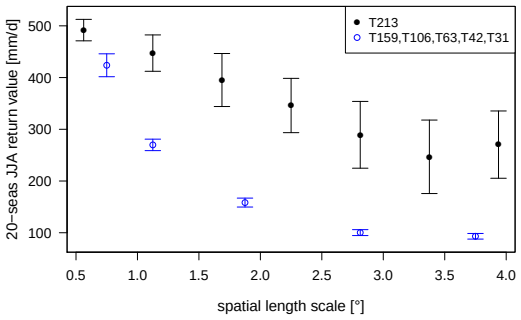

(b) Northern Peru-Ecuador-Colombia JJA

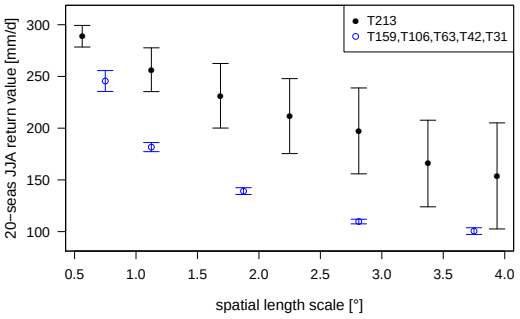

(c) Northeastern South America JJA

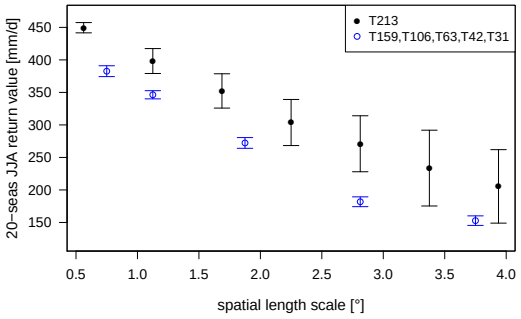

(d) Southeastern South America JJA

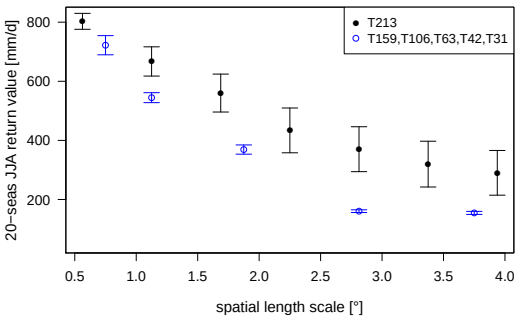

(e) India JJA

Figure B.6: Area-averaged total precipitation 20 season return values over central Africa in JJA (a), northern Peru-Ecuador-Colombia in JJA (b), northeastern South America in JJA (c), southeastern South America in JJA (d) and India in JJA (e) estimated from ECHAM5 model output in the resolutions $T213_{1\times1}$ - $T213_{7\times7}$, T159, T106, T63, T42 and T31 against spatial length scale. The error bars are the 95 % confidence interval of the area average. Note the different scales of the y-axes. The scaling behaviours are similar to the Amazon region in DJF and southwestern South America in DJF shown in section 4.2.

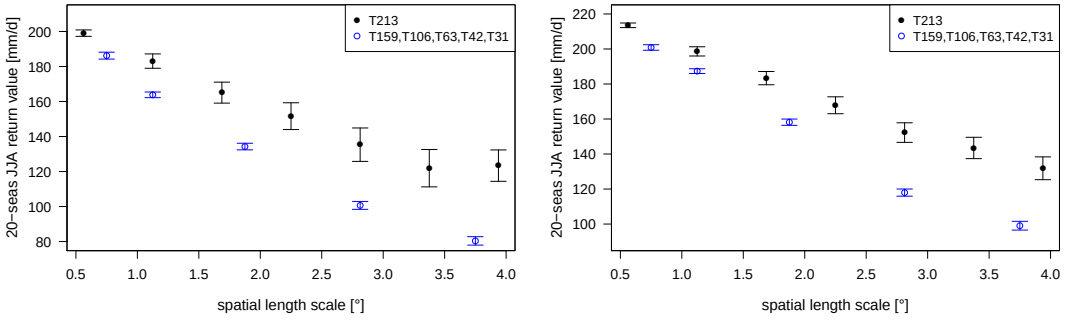

(a) Western Siberia JJA **(b)** Russia JJA

Figure B.7: Area-averaged total precipitation 20 season return values over Western Siberia in JJA (a) and Russia in JJA (b) estimated from ECHAM5 model output in the resolutions $T213_{1\times1}$ - $T213_{7\times7}$, T159, T106, T63, T42 and T31 against spatial length scale. The error bars are the 95 % confidence interval of the area average. Note the different scales of the y-axes. The scaling behaviour is similar to the Amazon region in DJF and southwestern South America in DJF shown in section 4.2.

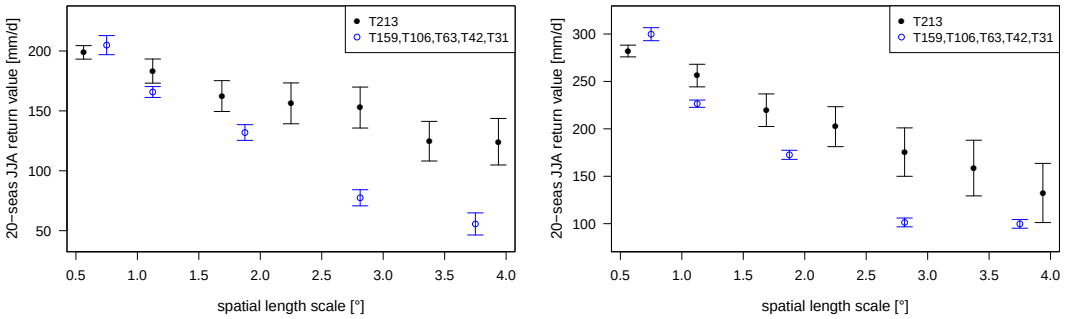

(a) Central USA JJA **(b)** Southeastern USA JJA

Figure B.8: Area-averaged total precipitation 20 season return values over the central USA in JJA (a) and the southeastern USA in JJA (b) estimated from ECHAM5 model output in the resolutions $T213_{1\times1}$ - $T213_{7\times7}$, T159, T106, T63, T42 and T31 against spatial length scale. The error bars are the 95 % confidence interval of the area average. Note the different scales of the y-axes. The scaling behaviour is similar to the Amazon region in DJF and southwestern South America in DJF shown in section 4.2.

Intermediate Scaling Behaviours

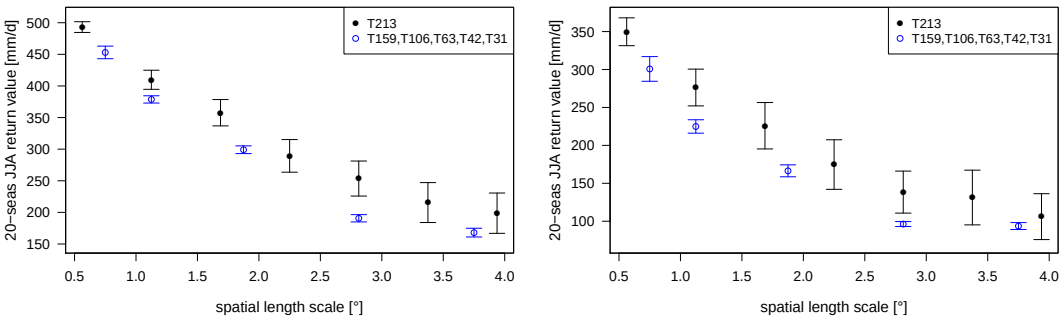

(a) Eastern Asia JJA **(b)** Central America JJA

Figure B.9: Area-averaged total precipitation 20 season return values over eastern Asia in JJA (a) and Central America in JJA (b) estimated from ECHAM5 model output in the resolutions $T213_{1\times1}$ - $T213_{7\times7}$, T159, T106, T63, T42 and T31 against spatial length scale. The error bars are the 95 % confidence interval of the area average. Note the different scales of the y-axes. The scaling behaviour is similar to northern Europe in JJA and the northeastern USA in JJA shown in section 4.2.

B.2 Large Scale and Convective Precipitation

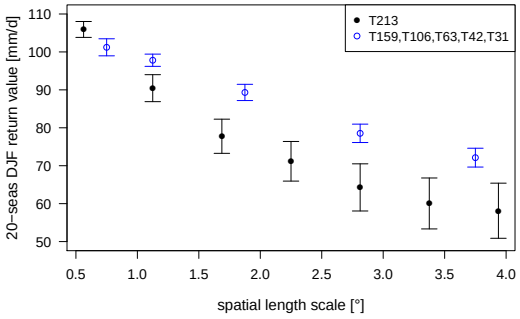

(a) Northern Europe DJF large scale

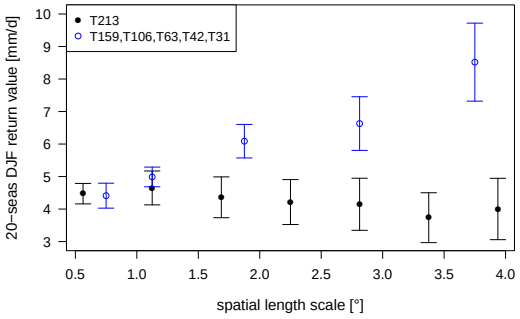

(b) Northern Europe DJF convective

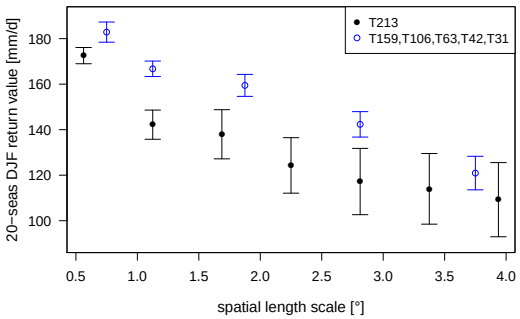

(c) Northeastern USA DJF large scale

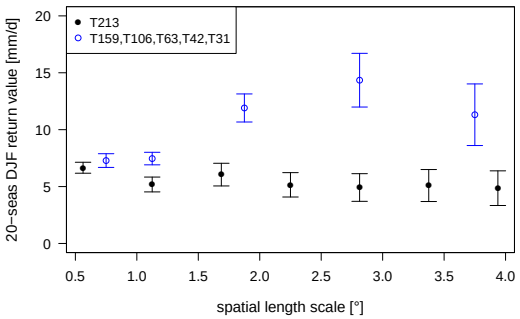

(d) Northeastern USA DJF convective

Figure B.10: Area-averaged large scale (a, c) and convective precipitation (b, d) 20 season return values over northern Europe (a, b) and the northeastern USA (c, d) in DJF estimated from ECHAM5 model output in the resolutions $T213_{1\times1}$ - $T213_{7\times7}$, T159, T106, T63, T42 and T31 against spatial length scale of ECHAM5 in the resolutions $T213_{1\times1}$ - $T213_{7\times7}$, T159, T106, T63, T42 and T31. The error bars are the 95 % confidence interval of the area average. Note the different scales of the y-axes.

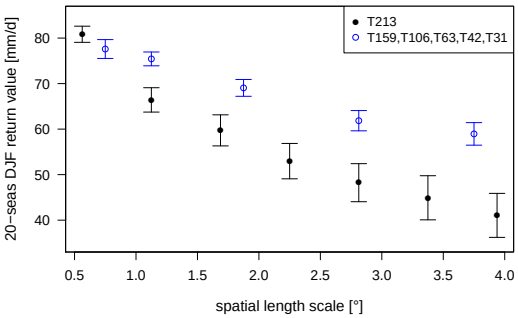

(a) Canada-Alaska-Greenland DJF large scale

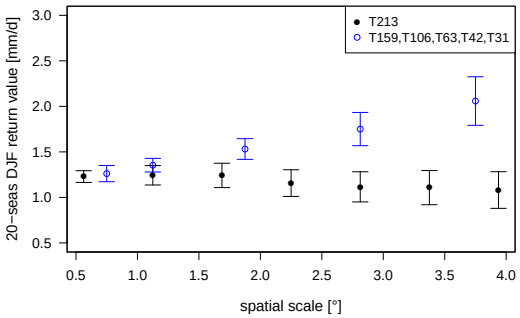

(b) Canada-Alaska-Greenland DJF convective

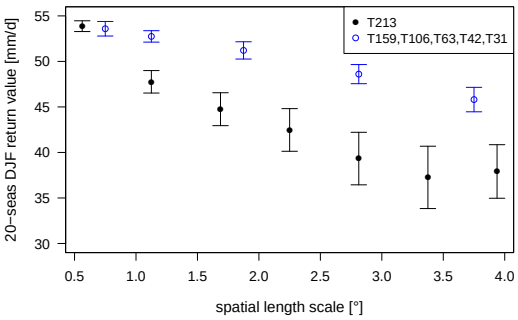

(c) Western Siberia DJF large scale

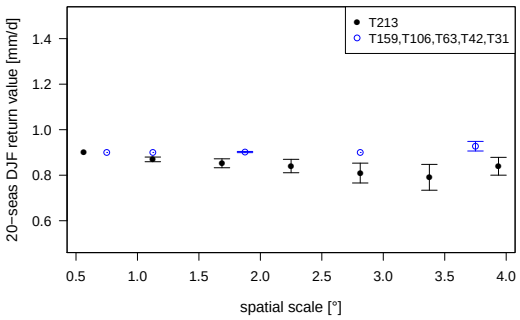

(d) Western Siberia DJF convective

Figure B.11: Area-averaged large scale (a, c) and convective precipitation (b, d) 20 season return values over Canada-Alaska-Greenland (a, b) and the Western Siberia (c, d) in DJF estimated from ECHAM5 model output in the resolutions $T213_{1\times1}$ - $T213_{7\times7}$, T159, T106, T63, T42 and T31 against spatial length scale of ECHAM5 in the resolutions $T213_{1\times1}$ - $T213_{7\times7}$, T159, T106, T63, T42 and T31. The error bars are the 95 % confidence interval of the area average. Note the different scales of the y-axes.

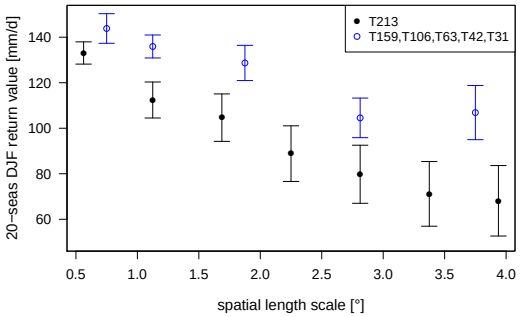

(a) Eastern Asia DJF large scale

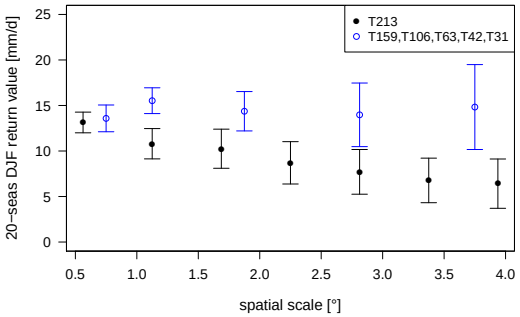

(b) Eastern Asia DJF convective

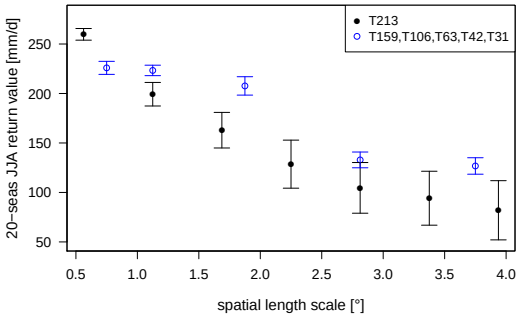

(c) Eastern Australia-New Zealand JJA large scale

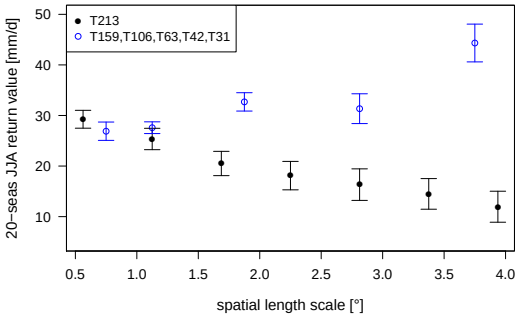

(d) Eastern Australia-New Zealand JJA convective

Figure B.12: Area-averaged large scale (a, c) and convective precipitation (b, d) 20 season return values over eastern Asia in DJF (a, b) and the eastern Australia-New Zealand in JJA (c, d) estimated from ECHAM5 model output in the resolutions T213$_{1\times1}$ - T213$_{7\times7}$, T159, T106, T63, T42 and T31 against spatial length scale of ECHAM5 in the resolutions $\mathrm{T213}_{1\times1}$ - $\mathrm{T213}_{7\times7}$, T159, T106, T63, T42 and T31. The error bars are the 95 % confidence interval of the area average. Note the different scales of the y-axes.

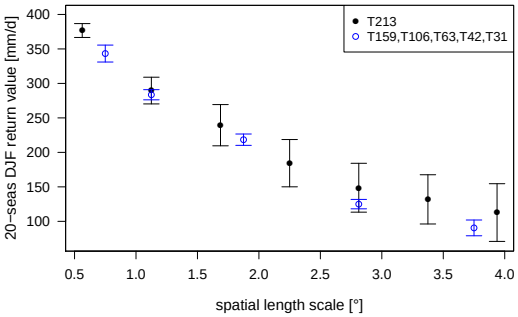

(a) Eastern Australia-New Zealand DJF large scale

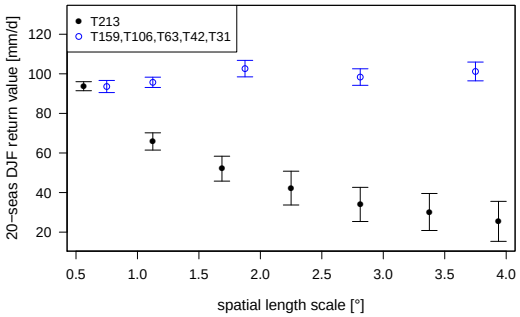

(b) Eastern Australia-New Zealand DJF convective

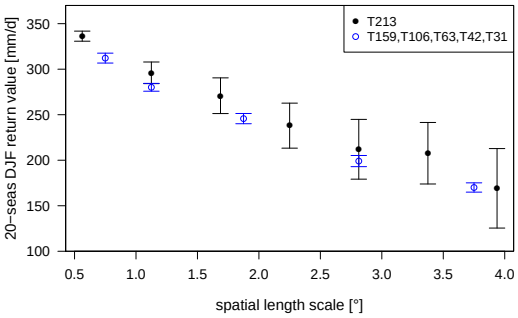

(c) Southeastern USA DJF large scale

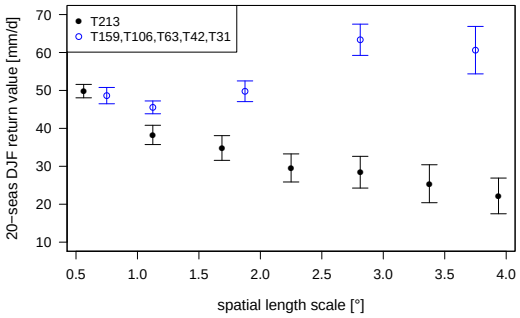

(d) Southeastern USA DJF convective

Figure B.13: Area-averaged large scale (a, c) and convective precipitation (b, d) 20 season return values over eastern Australia-New Zealand (a, b) and the southeastern USA (c, d) in DJF estimated from ECHAM5 model output in the resolutions T213$_{1\times1}$ - T213$_{7\times7}$, T159, T106, T63, T42 and T31 against spatial length scale of ECHAM5 in the resolutions $\mathrm{T213}_{1\times1}$ - $\mathrm{T213}_{7\times7}$, T159, T106, T63, T42 and T31. The error bars are the 95 % confidence interval of the area average. Note the different scales of the y-axes.

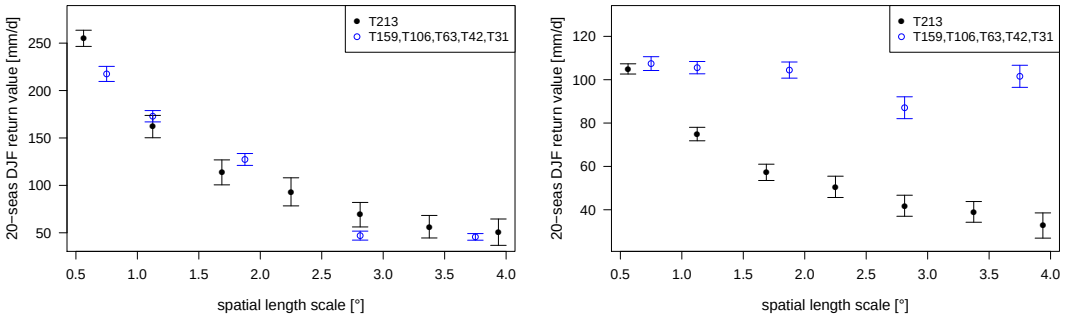

(a) Indonesia DJF large scale

(b) Indonesia DJF convective

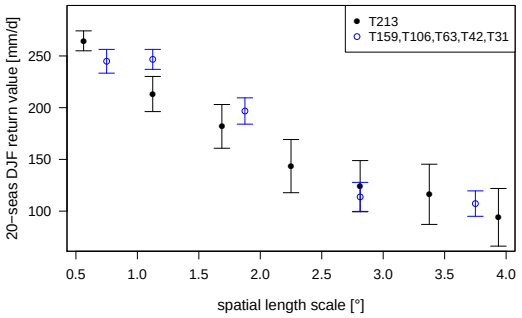

(c) Central America DJF large scale

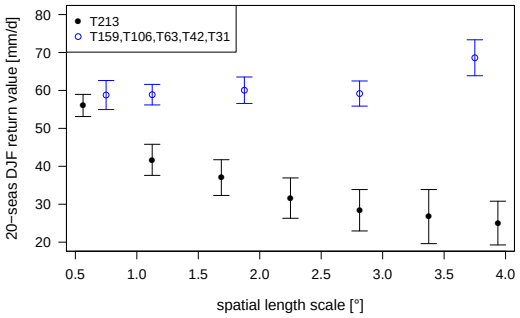

(d) Central America DJF convective

Figure B.14: Area-averaged large scale (a, c) and convective precipitation (b, d) 20 season return values over Indonesia (a, b) and Central America (c, d) in DJF estimated from ECHAM5 model output in the resolutions $T213_{1\times1}$ - $T213_{7\times7}$, T159, T106, T63, T42 and T31 against spatial length scale of ECHAM5 in the resolutions $T213_{1\times1}$ - $T213_{7\times7}$, T159, T106, T63, T42 and T31. The error bars are the 95 % confidence interval of the area average. Note the different scales of the y-axes.

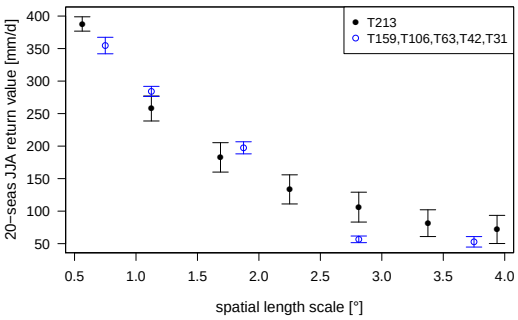

(a) Indonesia JJA large scale

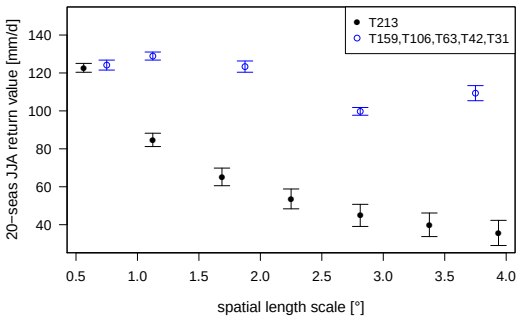

(b) Indonesia JJA convective

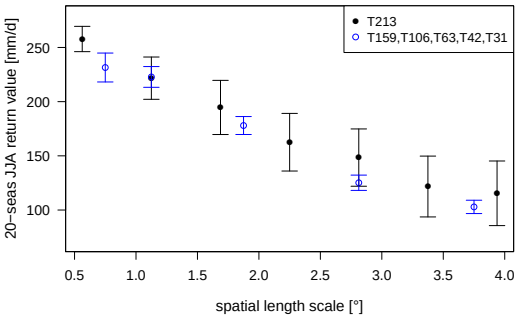

(c) Southwestern South America JJA large scale

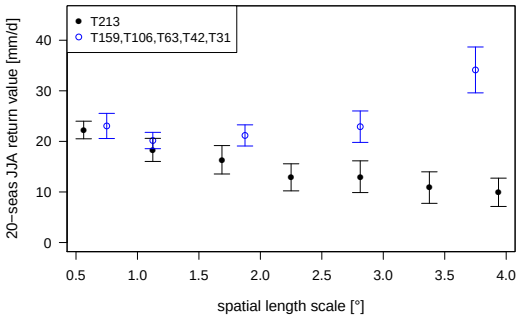

(d) Southwestern South America JJA convective

Figure B.15: Area-averaged large scale (a, c) and convective precipitation (b, d) 20 season return values over Indonesia (a, b) and the southwestern South America (c, d) in JJA estimated from ECHAM5 model output in the resolutions $T213_{1\times1}$ - $T213_{7\times7}$, T159, T106, T63, T42 and T31 against spatial length scale of ECHAM5 in the resolutions $T213_{1\times1}$ - $T213_{7\times7}$, T159, T106, T63, T42 and T31. The error bars are the 95 % confidence interval of the area average. Note the different scales of the y-axes.

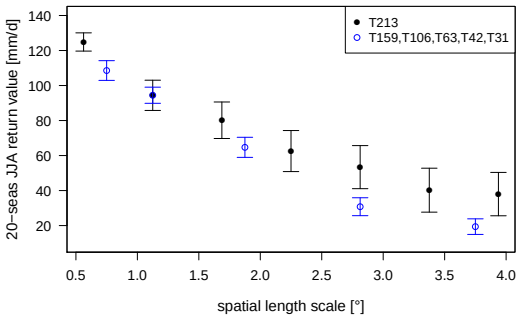

(a) Southern Europe JJA large scale

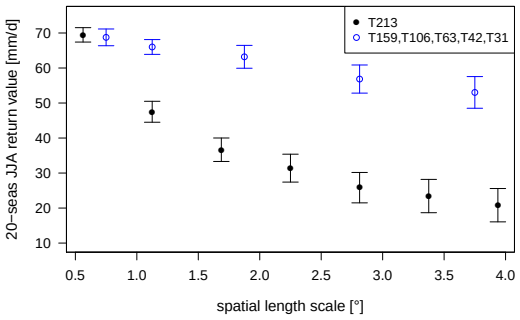

(b) Southern Europe JJA convective

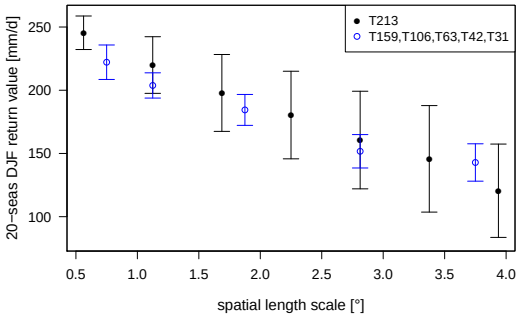

(c) Western USA DJF large scale

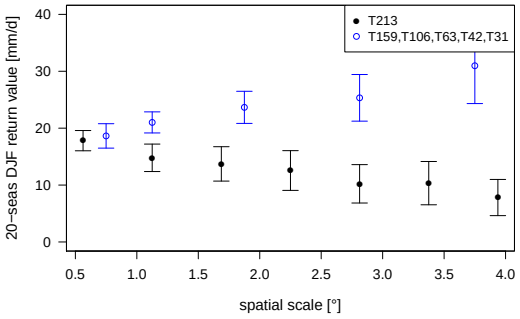

(d) Western USA DJF convective

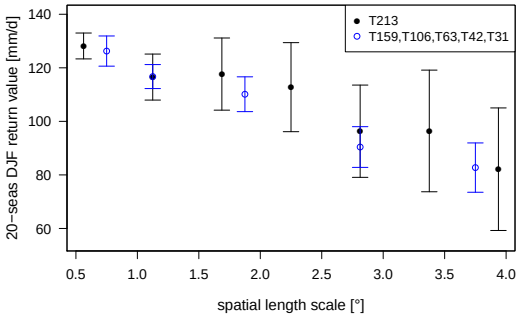

(e) Central USA DJF large scale

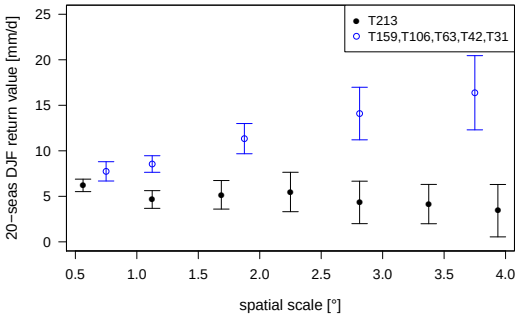

(f) Central USA DJF convective

Figure B.16: Area-averaged large scale (a, c, e) and convective precipitation (b, d, f) 20 season return values over southern Europe in JJA (a, b), the western USA in DJF (c, d) and the central USA in DJF (e, f) estimated from ECHAM5 model output in the resolutions $T213_{1\times1}$ - $T213_{7\times7}$, T159, T106, T63, T42 and T31 against spatial length scale of ECHAM5 in the resolutions $T213_{1\times1}$ - $T213_{7\times7}$, T159, T106, T63, T42 and T31. The error bars are the 95 % confidence interval of the area average. Note the different scales of the y-axes.

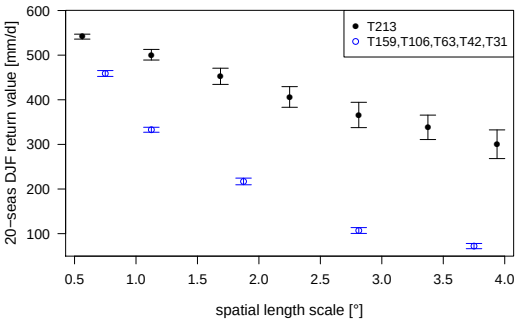

(a) Amazon region DJF large scale

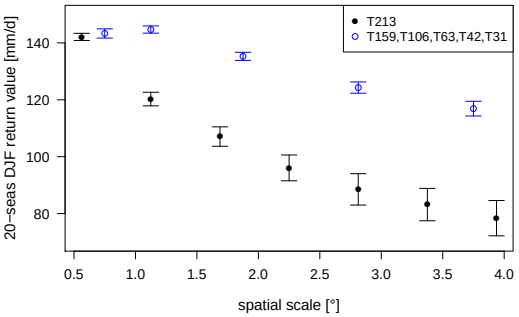

(b) Amazon region DJF convective

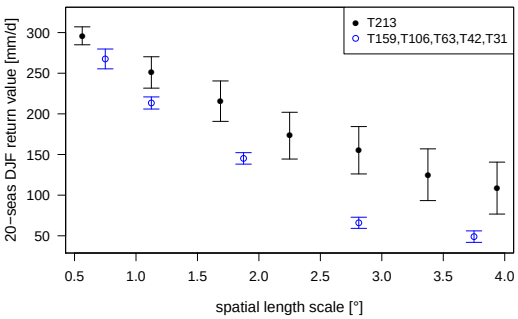

(c) Southwestern South America DJF large scale

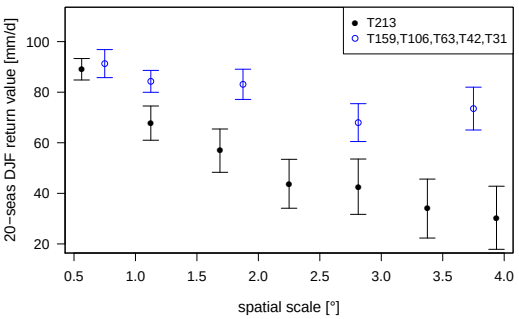

(d) Southwestern South America DJF convective

Figure B.17: Area-averaged large scale (a, c) and convective precipitation (b, d) 20 season return values over the Amazon region (a, b) and southwestern South America (c, d) in DJF estimated from ECHAM5 model output in the resolutions T213$_{1\times1}$ - T213$_{7\times7}$, T159, T106, T63, T42 and T31 against spatial length scale of ECHAM5 in the resolutions $\mathrm{T213}_{1\times1}$ - $\mathrm{T213}_{7\times7}$, T159, T106, T63, T42 and T31. The error bars are the 95 % confidence interval of the area average. Note the different scales of the y-axes.

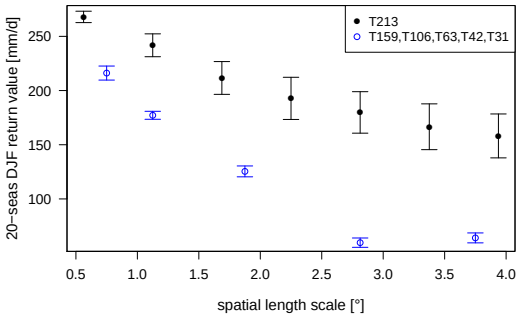

(a) Central Africa DJF large scale

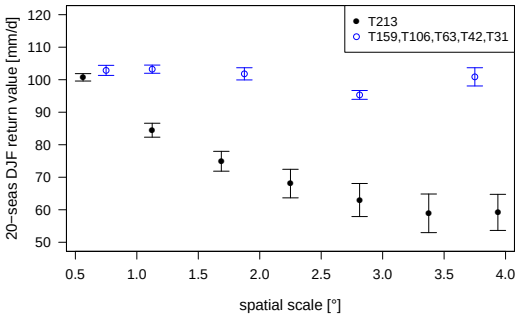

(b) Central Africa DJF convective

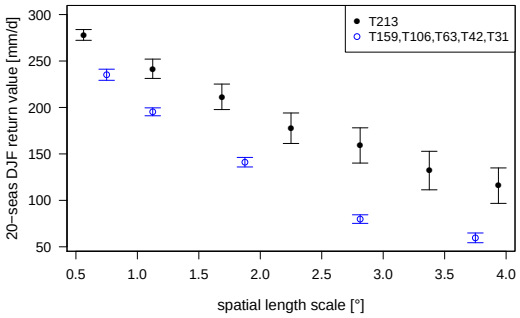

(c) Southern Africa DJF large scale

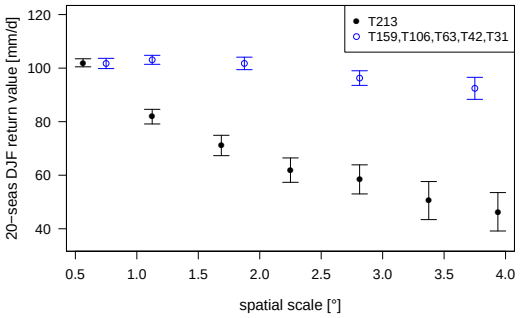

(d) Southern Africa DJF convective

Figure B.18: Area-averaged large scale (a, c) and convective precipitation (b, d) 20 season return values over central Africa (a, b) and southern Africa (c, d) in DJF estimated from ECHAM5 model output in the resolutions $T213_{1\times1}$ - $T213_{7\times7}$, T159, T106, T63, T42 and T31 against spatial length scale of ECHAM5 in the resolutions $T213_{1\times1}$ - $T213_{7\times7}$, T159, T106, T63, T42 and T31. The error bars are the 95 % confidence interval of the area average. Note the different scales of the y-axes.

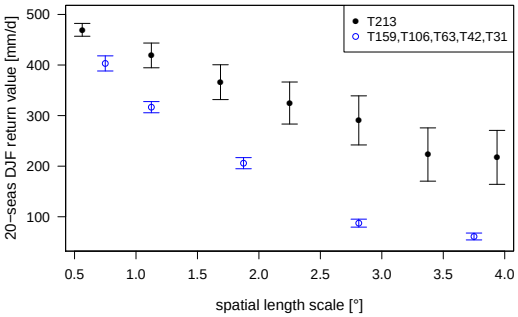

(a) Peru-Bolivia-Ecuador DJF large scale

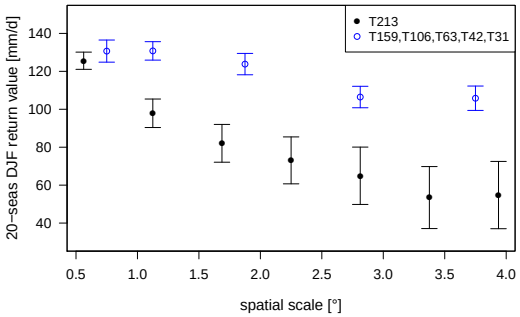

(b) Peru-Bolivia-Ecuador DJF convective

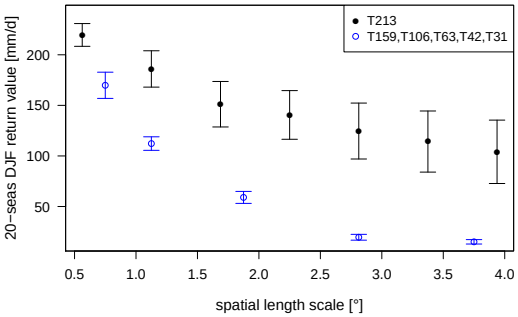

(c) Northern South America-southern Central America DJF large scale

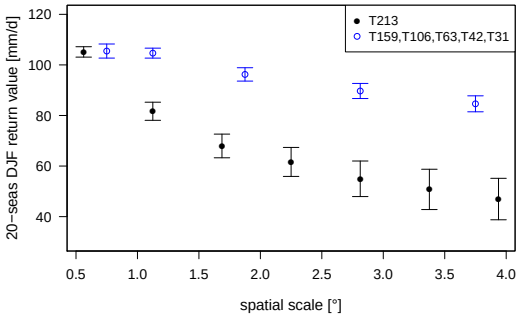

(d) Northern South America-southern Central America DJF convective

Figure B.19: Area-averaged large scale (a, c) and convective precipitation (b, d) 20 season return values over Peru-Bolivia-Ecuador (a, b) and northern South America-southern Central America (c, d) in DJF estimated from ECHAM5 model output in the resolutions $T213_{1\times1}$ - $T213_{7\times7}$, T159, T106, T63, T42 and T31 against spatial length scale of ECHAM5 in the resolutions $T213_{1\times1}$ - $T213_{7\times7}$, T159, T106, T63, T42 and T31. The error bars are the 95 % confidence interval of the area average. Note the different scales of the y-axes.

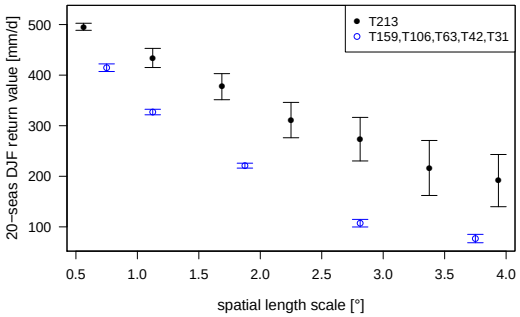

(a) Southeastern South America DJF large scale

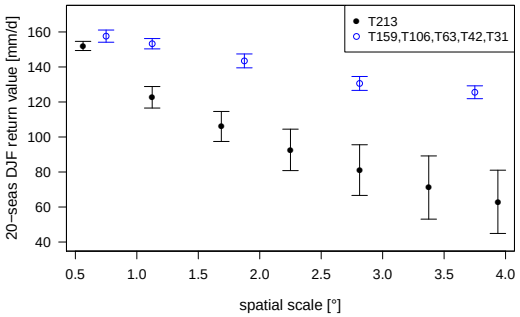

(b) Southeastern South America DJF convective

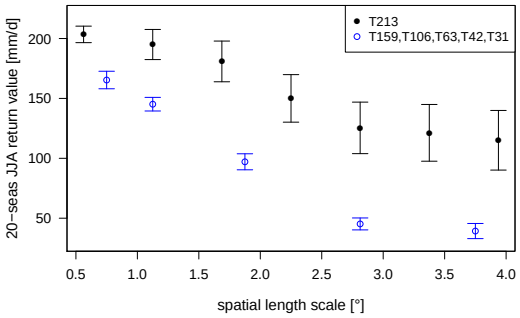

(c) Central Africa JJA large scale

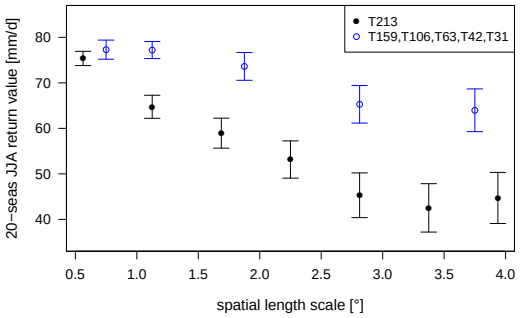

(d) Central Africa JJA convective

Figure B.20: Area-averaged large scale (a, c) and convective precipitation (b, d) 20 season return values over southeastern South America in DJF (a, b) and central Africa in JJA (c, d) estimated from ECHAM5 model output in the resolutions $T213_{1\times1}$ - $T213_{7\times7}$, T159, T106, T63, T42 and T31 against spatial length scale of ECHAM5 in the resolutions $T213_{1\times1}$ - $T213_{7\times7}$, T159, T106, T63, T42 and T31. The error bars are the 95 % confidence interval of the area average. Note the different scales of the y-axes.

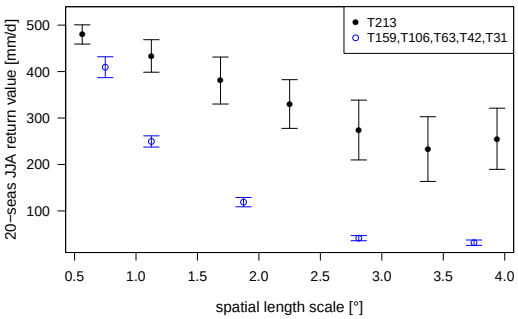

(a) Northern Peru-Ecuador-Colombia JJA large scale

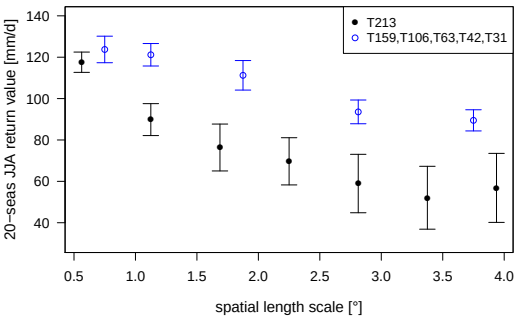

(b) Northern Peru-Ecuador-Colombia JJA convective

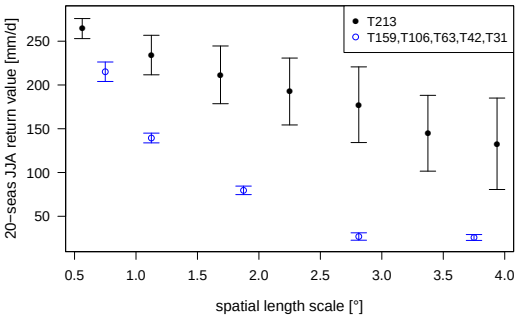

(c) Northeastern South America JJA large scale

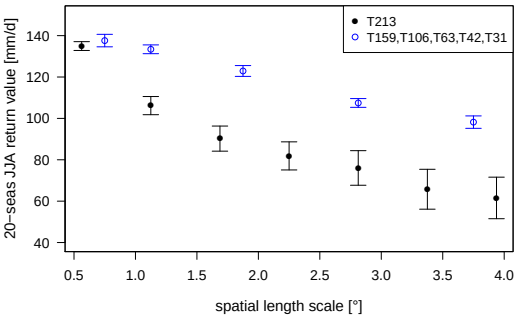

(d) Northeastern South America JJA convective

Figure B.21: Area-averaged large scale (a, c) and convective precipitation (b, d) 20 season return values over northern Peru-Ecuador-Colombia (a, b) and northeastern South America (c, d) in JJA estimated from ECHAM5 model output in the resolutions T213$_{1\times1}$ - T213$_{7\times7}$, T159, T106, T63, T42 and T31 against spatial length scale of ECHAM5 in the resolutions $\mathrm{T213}_{1\times1}$ - $\mathrm{T213}_{7\times7}$, T159, T106, T63, T42 and T31. The error bars are the 95 % confidence interval of the area average. Note the different scales of the y-axes.

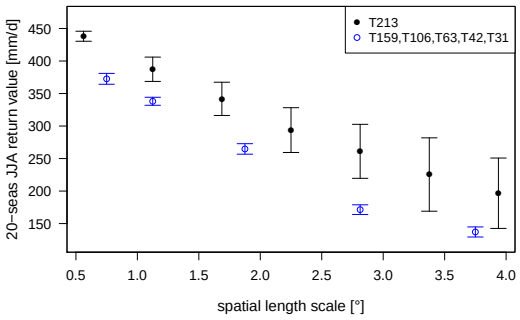

(a) Southeastern South America JJA large scale

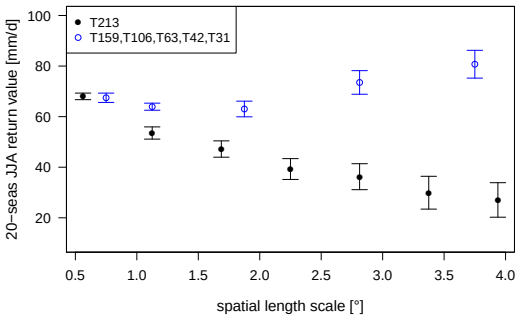

(b) Southeastern South America JJA convective

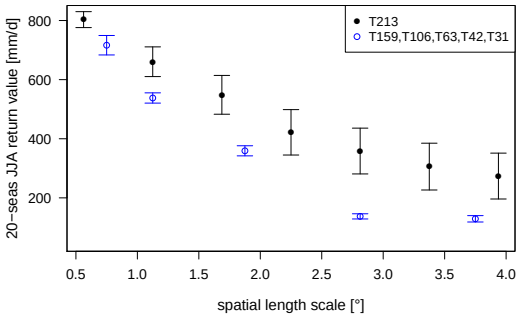

(c) India JJA large scale

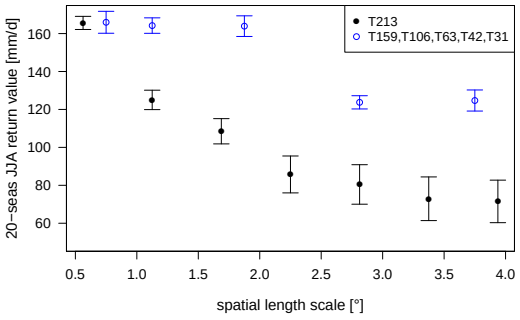

(d) India JJA convective

Figure B.22: Area-averaged large scale (a, c) and convective precipitation (b, d) 20 season return values over southeastern South America (a, b) and India (c, d) in JJA estimated from ECHAM5 model output in the resolutions T213$_{1\times1}$ - T213$_{7\times7}$, T159, T106, T63, T42 and T31 against spatial length scale of ECHAM5 in the resolutions $\mathrm{T213}_{1\times1}$ - $\mathrm{T213}_{7\times7}$, T159, T106, T63, T42 and T31. The error bars are the 95 % confidence interval of the area average. Note the different scales of the y-axes.

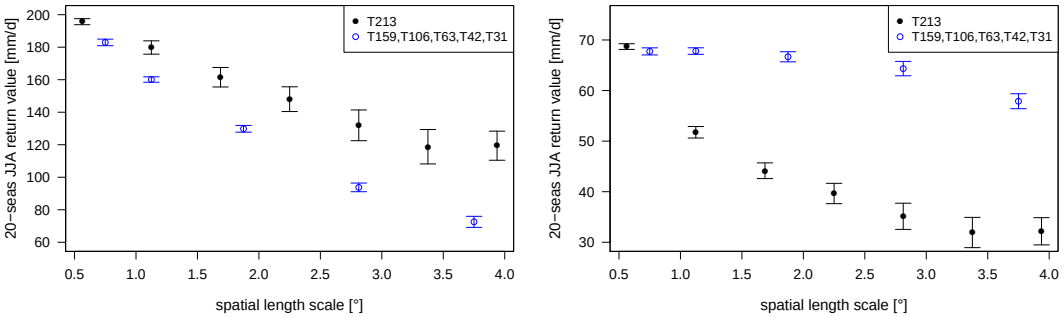

(a) Western Siberia JJA large scale

(b) Western Siberia JJA convective

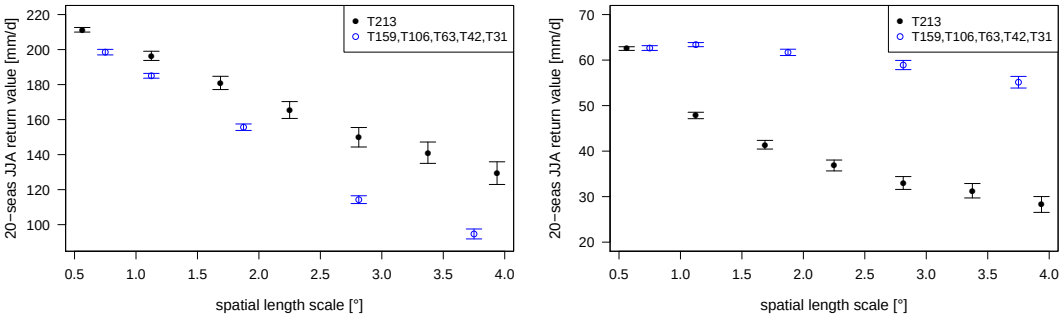

(c) Russia JJA large scale

(d) Russia JJA convective

Figure B.23: Area-averaged large scale (a, c) and convective precipitation (b, d) 20 season return values over western Siberia (a, b) and Russia (c, d) in JJA estimated from ECHAM5 model output in the resolutions T213$_{1\times1}$ - T213$_{7\times7}$, T159, T106, T63, T42 and T31 against spatial length scale of ECHAM5 in the resolutions $\mathrm{T213}_{1\times1}$ - $\mathrm{T213}_{7\times7}$, T159, T106, T63, T42 and T31. The error bars are the 95 % confidence interval of the area average. Note the different scales of the y-axes.

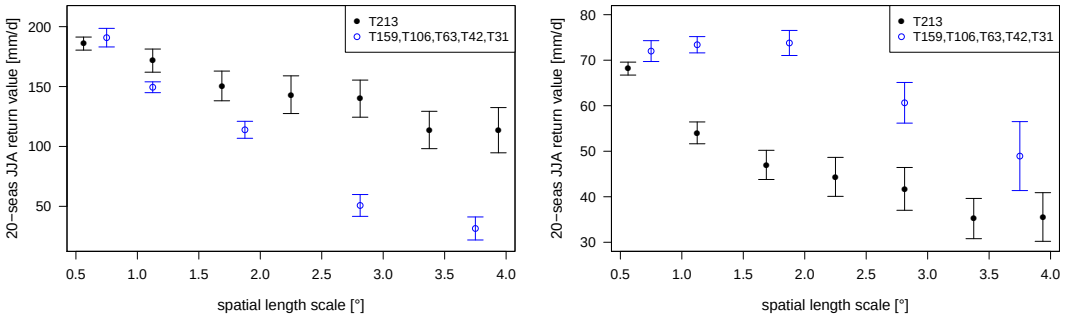

(a) Central USA JJA large scale

(b) Central USA JJA convective

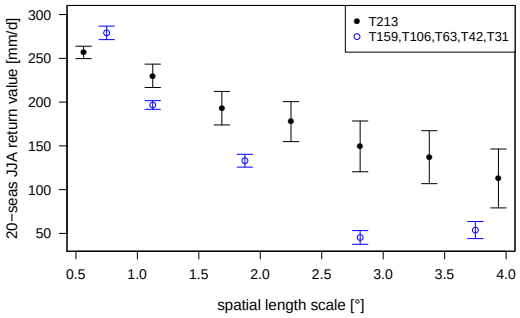

(c) Southeastern USA JJA large scale

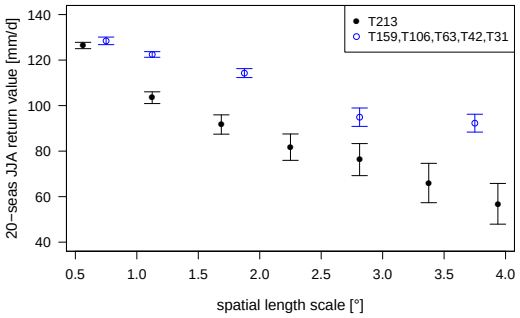

(d) Southeastern USA JJA convective

Figure B.24: Area-averaged large scale (a, c) and convective precipitation (b, d) 20 season return values over the central USA (a, b) and the southeastern USA (c, d) in JJA estimated from ECHAM5 model output in the resolutions T213$_{1\times1}$ - T213$_{7\times7}$, T159, T106, T63, T42 and T31 against spatial length scale of ECHAM5 in the resolutions $\mathrm{T213}_{1\times1}$ - $\mathrm{T213}_{7\times7}$, T159, T106, T63, T42 and T31. The error bars are the 95 % confidence interval of the area average. Note the different scales of the y-axes.

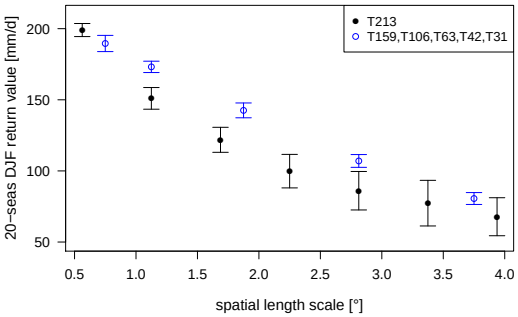

(a) Southern Europe DJF large scale

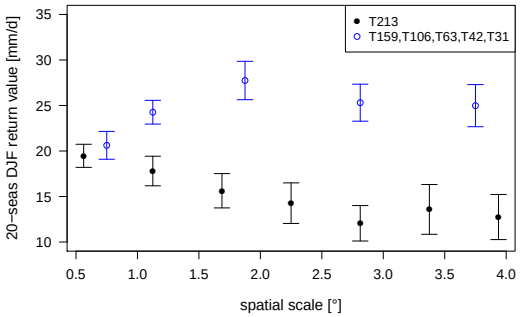

(b) Southern Europe DJF convective

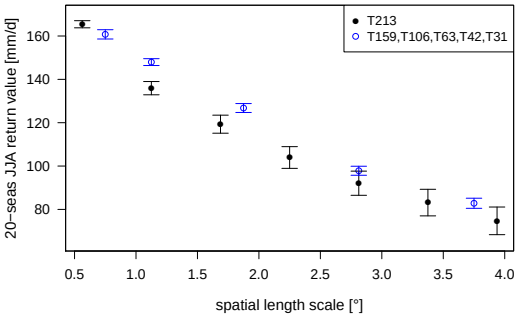

(c) Canada-Alaska-Greenland JJA large scale

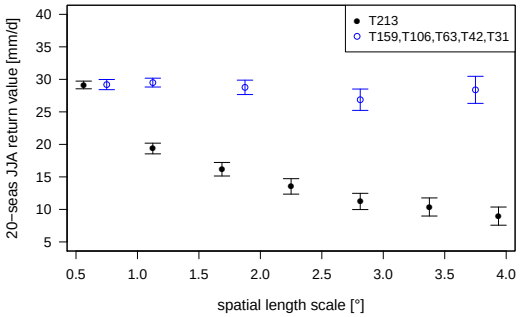

(d) Canada-Alaska-Greenland JJA convective

Figure B.25: Area-averaged large scale (a, c) and convective precipitation (b, d) 20 season return values over southern Europe in DJF (a, b) and Canada-Alaska-Greenland in JJA (c, d) in DJF estimated from ECHAM5 model output in the resolutions $T213_{1\times1}$ - $T213_{7\times7}$, T159, T106, T63, T42 and T31 against spatial length scale of ECHAM5 in the resolutions $T213_{1\times1}$ - $T213_{7\times7}$, T159, T106, T63, T42 and T31. The error bars are the 95 % confidence interval of the area average. Note the different scales of the y-axes.

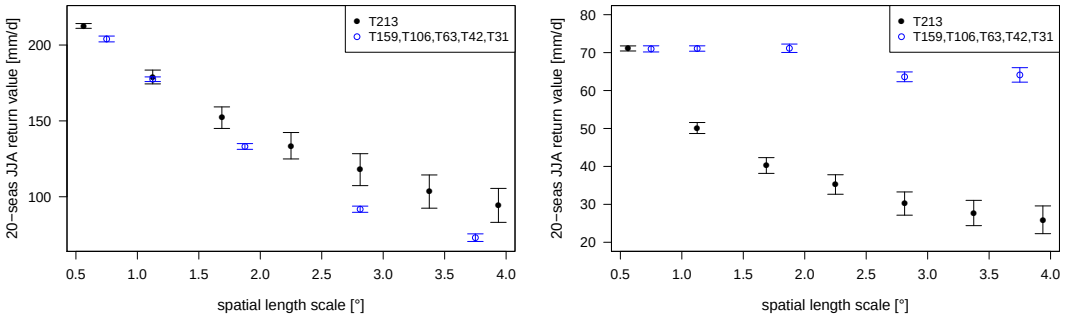

(a) Northern Europe JJA large scale

(b) Northern Europe JJA convective

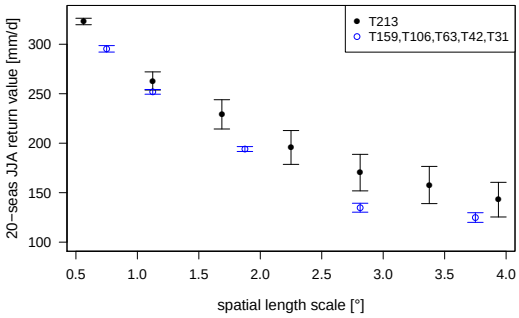

(c) Northeastern USA JJA large scale

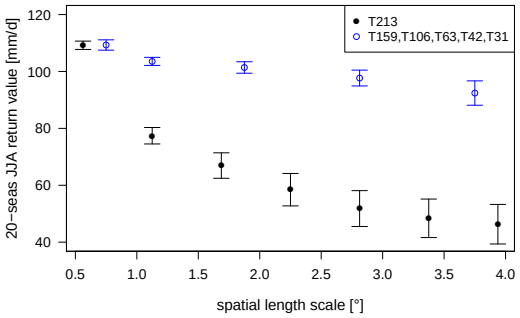

(d) Northeastern USA JJA convective

Figure B.26: Area-averaged large scale (a, c) and convective precipitation (b, d) 20 season return values over northern Europe (a, b) and the northeastern USA (c, d) in JJA estimated from ECHAM5 model output in the resolutions T213$_{1\times1}$ - T213$_{7\times7}$, T159, T106, T63, T42 and T31 against spatial length scale of ECHAM5 in the resolutions $\mathrm{T213}_{1\times1}$ - $\mathrm{T213}_{7\times7}$, T159, T106, T63, T42 and T31. The error bars are the 95 % confidence interval of the area average. Note the different scales of the y-axes.

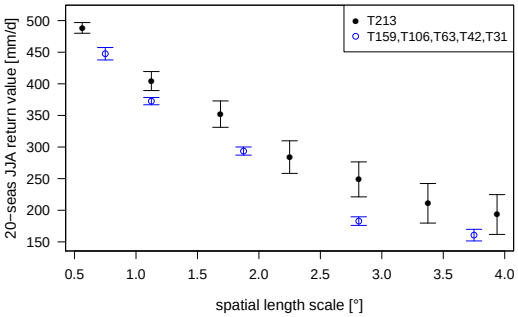

(a) Eastern Asia JJA large scale

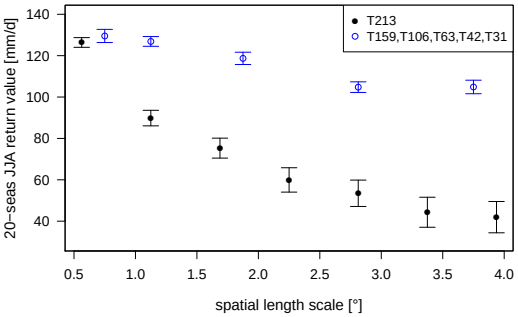

(b) Eastern Asia JJA convective

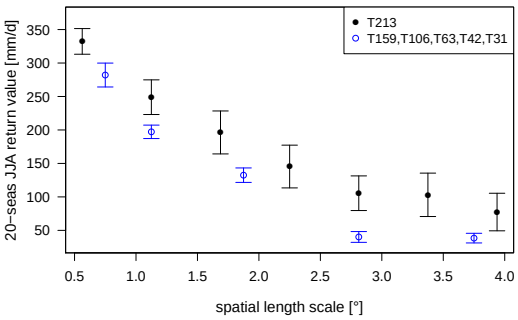

(c) Central America JJA large scale

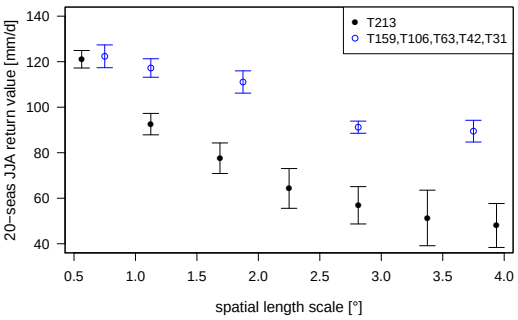

(d) Central America JJA convective

Figure B.27: Area-averaged large scale (a, c) and convective precipitation (b, d) 20 season return values over eastern Asia (a, b) and Central America (c, d) in JJA estimated from ECHAM5 model output in the resolutions $T213_{1\times1}$ - $T213_{7\times7}$, T159, T106, T63, T42 and T31 against spatial length scale of ECHAM5 in the resolutions $T213_{1\times1}$ - $T213_{7\times7}$, T159, T106, T63, T42 and T31. The error bars are the 95 % confidence interval of the area average. Note the different scales of the y-axes.

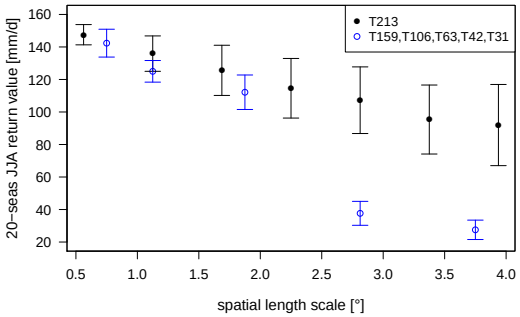

(a) Southern Peru-Bolivia-central Amazon region JJA large scale

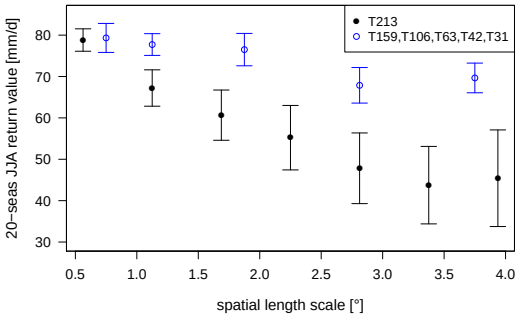

(b) Southern Peru-Bolivia-central Amazon region JJA convective

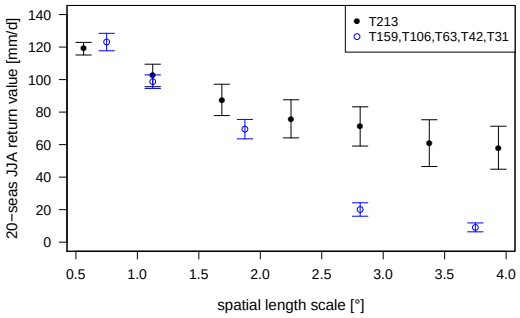

(c) Western USA JJA large scale

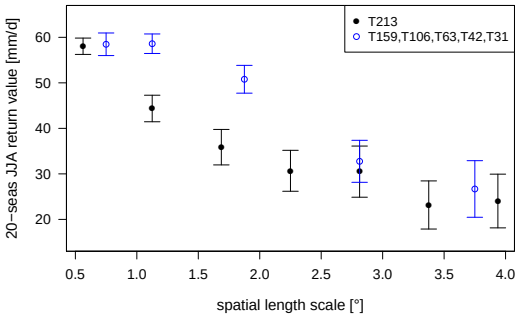

(d) Western USA JJA convective

Figure B.28: Area-averaged large scale (a, c) and convective precipitation (b, d) 20 season return values over southern Peru-Bolivia-central Amazon region (a, b) and the western USA (c, d) in JJA estimated from ECHAM5 model output in the resolutions $T213_{1\times1}$ - $T213_{7\times7}$, T159, T106, T63, T42 and T31 against spatial length scale of ECHAM5 in the resolutions $T213_{1\times1}$ - $T213_{7\times7}$, T159, T106, T63, T42 and T31. The error bars are the 95 % confidence interval of the area average. Note the different scales of the y-axes.

B.3 Ensemble Members

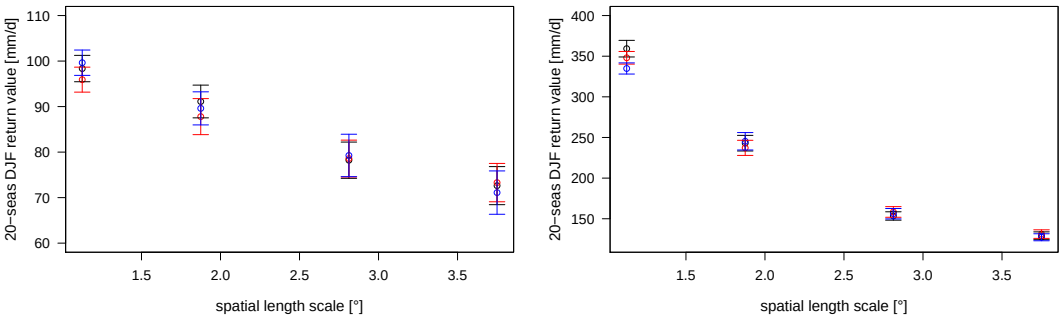

(a) Northern Europe **(b)** Amazon region

Figure B.29: Area-averaged total precipitation 20 season return values over northern Europe (a) and the Amazon region (b) in DJF estimated from three ensemble members of the resolutions T106, T63, T42 and T31 from ECHAM5 model output against spatial length scale. The error bars are the 95 % confidence interval of the area average. Note the different scales of the y-axes.